UBXD1 and YOD1:
p97 cofactors involved in
autophagic mitochondrial quality control

Inauguraldissertation

zur Erlangung der Würde eines Doktors der Philopsophie

vorgelegt der Philosophisch-Naturwissenschaftlichen Fakultät

der Universität Basel von

Ana Catarina De Pinho Ferreira Bento

aus Porto/Portugal

Basel, 2018

Genehmigt von der Philosophisch-Naturwissenschaftlichen Fakultät

auf Antrag von Prof. T. Mrsic-Flogel

Prof. C. Handschin

PD A. Neutzner

Basel, den 27.02.2018

Prof. Dr. Martin Spiess

Dekan

Contents

1 Summary

Diminished mitochondrial function impacts on cellular metabolism but also critically influences life and also health span. Mitochondrial dysfunction due to accumulating mitochondrial damage is considered one of the main factors of aging and aging-related disease such as Alzheimer's disease and other neurodegenerative disorders. Mitochondrial quality control is essential to prevent dysfunction and associated deleterious outcomes. Multi-tiered molecular machinery is in place to remove and degrade superfluous or damaged proteins to maintain mitochondrial proteostasis, cull mitochondrial subunits beyond repair or remove entire mitochondrial networks through apoptosis. Besides proteolytic pathways, autophagic removal is an important part of mitochondrial quality control. Severe damage to mitochondria exceeding the repair capacity of proteolytic systems, but below the apoptotic threshold, leads to the removal of mitochondrial units through mitochondria-specific autophagy or mitophagy under control of the kinase PINK1 and the ubiquitin ligase Parkin. Following recognition of damaged mitochondrial subunits by PINK1, Parkin is recruited causing the ubiquitination of mitochondrial proteins. This results in the recruitment of autophagy cargo adaptors leading to the engulfment of the damaged mitochondria and its subsequent degradation in the lysosome. Among the proteins recruited during mitophagy is the AAA-ATPase VCP/p97. As ubiquitously expressed protein, p97 acts in a plethora of cellular functions involving ubiquitination, including cell cycle control, transcriptional regulation as well as proteostasis. In addition, p97 was recently connected to ubiquitin-mediated degradation of mitochondrial proteins, Parkin-dependent mitophagy and deubiquitinating enzymes. These multiple diverse functions of p97 suggest tight spatial and temporal control of its activity, which is brought upon by the interaction with various cofactors promoting substrate recognition and processing by p97.

In this *in vitro* study the connection of p97 to mitochondrial quality control with focus on mitophagy was studied. In a first step, p97 cofactors were screened using subcellular localization analysis for their ability to translocate to mitochondria under mitophagic

conditions. From this screen, UBXD1, SAKS1, and Erasin were found to alter their locations following mitophagic induction implicating these proteins in the autophagic clearance of mitochondria. Further analysis suggested a role for UBXD1 as recruitment factor for p97 to damaged mitochondria. It was shown that UBXD1 recognizes depolarized mitochondria via its C-terminal UBX domain and translocates to mitochondria in a Parkin-dependent manner. Once translocated, UBXD1 recruits p97 to mitochondria via a bipartite binding motif consisting of its N-terminal VIM and PUB domains. Recruitment of p97 by UBXD1 only depends on the presence of UBXD1 on mitochondria without the need for further mitochondrial signals. Following translocation of UBXD1 to CCCP-depolarized mitochondria and p97 recruitment, formation of autolysosomes is strongly enhanced and autophagic degradation of mitochondria is significantly accelerated. Diminished levels of UBXD1 result in decreased mitophagic flux.

In a next step, a potential role in mitophagy for the deubiquitinating enzyme YOD1 was studied. YOD1 was previously reported to facilitate together with p97 and UBXD1 lyosphagy and ERAD. Alternative transcript analysis revealed a differential role for YOD1. Under mitophagic conditions, the shorter YOD1.2 was translocating to mitochondrial while the longer YOD1.1 remained in the cytosol. In addition, ecotopic expression of UBXD1 greatly enhanced mitochondrial translocation of YOD1.2. Under these conditions, UBXD1 and YOD1.2 translocate to depolarized mitochondria in a mutually exclusive manner with YOD1.2 seemingly to displace UBXD1.

In summary, the work presented here suggests a novel role for UBXD1 as sensor for mitochondria undergoing mitophagy and mitochondrial recruitment factor for p97 during mitophagy. Furthermore, UBXD1 potentially initiates a multi-step cascade involving YOD1.2 ultimately aiding the mitophagic quality control of damaged mitochondria.

2 Aims of the thesis

- Identification of p97 cofactors potentially involved in mitophagy
  - Cloning of p97 cofactors into mammalian expression vectors
  - Subcellular localization under normal and mitophagic conditions
- Characterization of p97 cofactor UBXD1
  - Parkin dependency of UBXD1 mitochondrial translocation
  - Structure-function relationship for mitochondrial translocation
  - Structure-function relationship for p97 recruitment to mitochondria
  - Mitophagic flux under elevated/diminished levels of UBXD1
- Analysis of potential mitophagic role for YOD1
  - Subcellular localization of YOD1 during mitophagy
  - Structure-function relationship for mitochondrial translocation
  - Interplay between YOD1 and UBXD1 under mitophagic conditions

3 Introduction

3.1 Mitochondria

3.1.1 Mitochondrial structure and function

Mitochondria are multifunctional organelles in eukaryotic cells. Although mostly recognized as powerhouses because of their respiratory energy conversion, mitochondria perform various other essential functions. Mitochondria provide iron–sulfur cluster assembly, integrate anabolic and catabolic processes, including amino acid and lipid metabolism, and participate in cellular ion homeostasis and signalling pathways [1, 2, 3]. Their involvement in cellular metabolism makes mitochondria crucial even for eukaryotes that inhabit anaerobic environments, with only one recent example of the evolutionary loss of this organelle [4]. The perturbation of mitochondrial function results in cellular stress and often has devastating effects, including mitochondrion-related diseases in humans [3]. Mitochondria possess well-defined boundaries that are provided by two membranes that outline the organelle [5]. These membranes, external or outer mitochondrial membrane (OMM) and internal or inner mitochondrial membrane (IMM), surround two distinct aqueous subcompartments: the mitochondrial intermembrane space (IMS) and the mitochondrial matrix. The IMM is further divided into an inner boundary membrane that is adjacent to the OMM and is separated by crista junctions from invaginations that protrude into the matrix, called cristae. Mitochondria are organized into a dynamic network that is shaped by frequent fusion and fission processes [6, 7, 8].

To perform their functions, mitochondria need a set of proteins to build the mitochondrial proteome. The best-characterized proteomes of yeast and human mitochondria comprise approximately 1000–1500 different proteins, but the annotation of mitochondrial proteins is an ongoing process [8, 9]. Mitochondria have their own genome and transcription and translation machinery [10, 11]. However, only a very limited number of mitochondrial proteins, peptides and ribonucleic acids (RNAs) are synthesized inside the organelle. The majority of mitochondrial components is produced outside of mitochondria and imported

using sophisticated import machinery.

Given the overarching importance of mitochondria, impaired mitochondrial homeostasis and function has been linked to multiple human diseases including cancer and neurodegeneration, but also aging. Their important role, but also their susceptibility to damage, is mirrored in a multi-layered quality control system keeping mitochondria in shape [12]. Mitochondrial maintenance and quality control are an concerted effort of protein degradation either through specialized mitochondrial proteases or the UPS, lysosomal degradation triggered through autophagy, and also programmed cell death. The goal of this study was to further elucidate mitochondrial quality control at the intersection between ubiquitin-mediated protein degradation and autophagy.

3.1.1.1 Structural properties of mitochondria Structurally, mitochondria are highly compartmentalized organelles [13]. As shown in Figure 1, mitochondria contain two lipid bi-layers, an OMM and an IMM, leading to the IMS, topologically equivalent to the cytoplasm, and the matrix, an internal space that contains enzymes important for fatty acid oxidation as well as for the Krebs tricaboxylic acid cycle (TCA). The matrix also hosts mitochondrial DNA (mtDNA) and is the site of mitochondrial protein synthesis[14, 15]. The IMM is highly impermeable, and by folding in a convoluted manner, forms the cristae, a large surface area where the respiratory chain (RC) complexes I–V are located [16]. The IMS is part of the proton gradient necessary for adenosine triphosphate (ATP) generation across the IMM [17], where an increased concentration of protons in the IMS compared to the matrix is established during mitochondrial respiration (see 3.1.1.2). The inner boundary membrane as part of the IMM forms a double membrane layer with the OMM. It houses translocase of the inner membrane (TIM) complex, which facilitates protein transport across the IMM into the matrix [18]. The protein complexes of the electron transport chain (ETC) are largely localized to the cristal region of the IMM. The invaginations or cristae of this cristal membrane contain the majority of the mitochondrial cytochrome c pool [19].

The OMM acts as a diffusion barrier [20], while permitting size-restrictive passage across

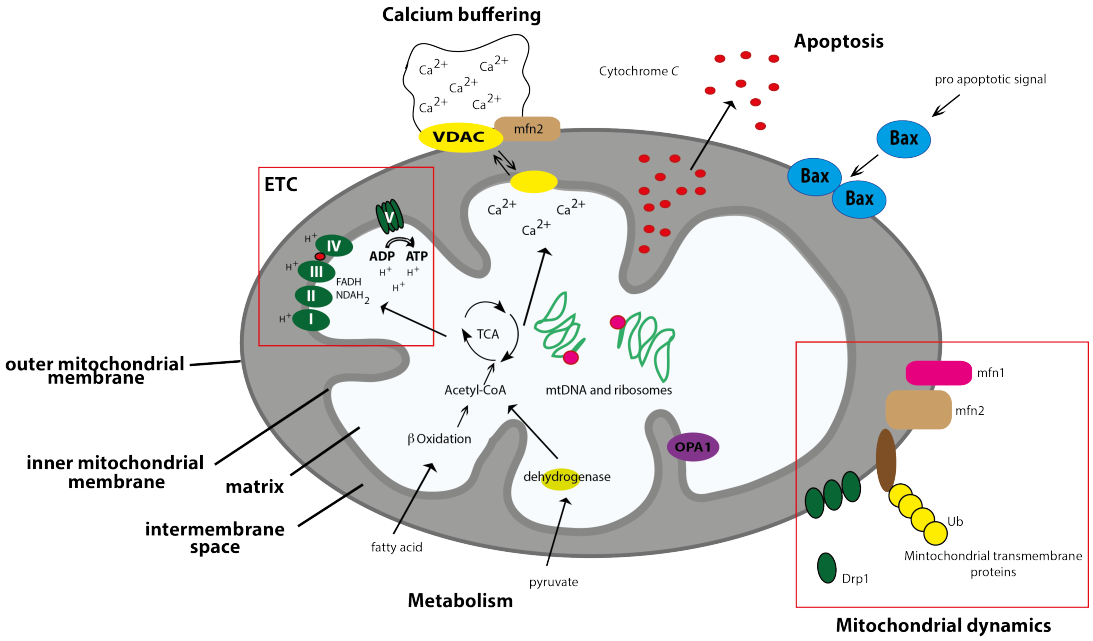

Figure 1: Mitochondrial compartments. Shown is a scheme of a mitochondrion with annotations for the different mitochondrial compartments. Mitochondria are double membrane-bound organelles with an outer and inner mitochondrial membrane (IMM). The mitochondrial matrix is the inner most part of mitochondria harboring mtDNA and also the enzymatic machinery for the tricarboxylic acid cycle (TCA cycle). The IMM is highly folded forming so called cristae in order to expand the membrane surface for the components of the electron transport chains (ETC). The ETC is generating the mitochondrial membrane potential ultimately used for the production of ATP by complex V. Ion transporters such a voltage-dependent anion channel (VDAC) are involved in Ca2+ buffering. Cytochrome c is a small protein localized in intermembrane space as part of the ETC.

the membrane through porins and receptor-mediated traffic via the translocase of the outer membrane (TOM) complex [21, 22]. Mitochondria-associated membranes (MAM) [23] are sites of connection of the OMM to the endoplasmic reticulum (ER) and are involved in both Ca_2^+ [24] and inflammasome signalling [25]. Additionally, the OMM is lipids source for the formation of the isolation membrane during autophagy [26].

3.1.1.2 Mitochondrial energy production The structure, function, and organization of the respiratory chain have been under investigation since Otto Warburg discovered Atmungsferment, the enzymatic basis for cellular respiration [27]. Mitochondria are the site of OXPHOS and generate as much as 90 % of all ATP used by cells via a chemiosmotic mechanism. Mitochondria generate the energetic potential via the respiratory complexes I to IV [28]: complex I (CI or reduced nicotinamide adenine dinucleotide

(NADH):ubiquinone oxidoreductase), complex II (CII or succinate:ubiquinone oxidoreductase), complex III (CIII or ubiquinol:cytochrome-c oxidoreductase), and complex IV (CIV or cytochrome-c oxidase). Together with complex V (CV or FO F1 -ATP-synthase) they form what is usually called the OXPHOS system (Figure 2). The entry point for mitochondrial metabolism consists of electron donors. These donors are generated during the metabolization of glucose by the TCA and though ß-oxidation of fatty acids. Complex I, Complex III, and Complex IV generate proton motive force across the IMM and their actions are facilitated by Complex II and electron transfer cofactors (i.e., ubiquinone and cytochrome-c). Proton translocation back to the mitochondrial matrix drives Complex V, which is coupled to ATP synthesis. Most of the ATP produced by Complex V is exchanged against cytosolic adenosine diphosphate (ADP) through a specific adenine nucleotide carrier to supply the rest of the cell with energy and to maintain the ADP phosphorylation capacity of mitochondria [29].

3.1.1.3 Mitochondria are highly dynamic organelles Mitochondria are highly dynamic organelles forming an organellar network shaped by the balanced fission and fusion of mitochondrial tubules. The integrity of the mitochondrial network relies on the ability of individual subunits to establish new connections with or break away from the network. Fusion of individual mitochondrial subunits with the network allows for the exchange of mitochondrial DNA, proteins, lipids and metabolites, for example to alleviate localized imbalances of these components or dilute impaired components across the mitochondrial network. In this manner, the mitochondrial network can act as a buffer against a build-up of damage in individual subunits. Fission on the other hand allows for easier transport of mitochondria across the cell. At the same time, subunits irreaparably damaged for example due to accumulating oxidative stress can be separated from the network and degraded, without further compromising the integrity of the mitochondrial network. Both fusion and fission rely on their own sets of mitochondrial proteins.
Mammalian fusion proteins are mitofusin 1 (Mfn1) and mitofusin 2 (Mfn2) [30] on the OMM as well as Opa1 [31] on the IMM. Mitofusins are thought to facilitate fusion of

the OMM by tethering opposing membranes, either through heterodimerization of Mfn1 and Mfn2 [32] or Mfn2 homodimers [33]. Fusion of the IMM is performed by Opa1 [34]. Fission of mammalian mitochondria is driven by dynamin-related protein 1 (Drp1) [35], mitochondrial fission factor (Mff) [36], mitochondrial dynamics proteins (MiD) 49 and 51 [37] and mitochondrial fission 1 protein (fis1) [38]. Mitochondrial fission relies on an inhibition of fusion proteins and recruitment of cytosolic Drp1 to the OMM [39] where it may interact with Fis1 [40], although the importance of fis1 has recently been called into question and may be cell type specific [36, 41]. Both Mff as well as MiD49 and MiD51 on the other hand have been shown as essential for a successful fission event to take place [42, 37]. After recruitment of Drp1 to the OMM, Drp1 forms oligomeric rings encompassing the future fission site [35]. These rings are able to constrict by hydrolyzing GTP, which eventually leads to scission of the OMM. The importance for balanced fission and fusion of mitochondria is highlighted by the diseases connected to dysregulation of mitochondrial morphology. Lack of proper mitochondrial fusion due to mutations in fusion factors Mnf2 and OPA1 cause neurodegenerative diseases Charcot-Marie-Tooth 2A and autosomal dominant optic atrophy, respectively [43]. Lack of mitochondrial fission due to mutations in Drp1 are linked to birth defects [44] and optic nerve degeneration [45].

3.1.2 Mitochondrial damage

3.1.2.1 Generation of reactive oxygen species Mitochondria and oxidative phosphorylation open up a highly efficient source of chemical energy for cells (3.1.1.2). However, chemical reactions involving singlet oxygen come with the price of generating highly reactive oxygen derivatives, which if left unchecked, wreak havoc on the cell [46]. The term reactive oxygen species (ROS) is used to describe a variety of molecules and free radicals derived from molecular oxygen. Molecular oxygen in the ground state is a bi-radical, containing two unpaired electrons in the outer shell (also known as a triplet state). Since the two single electrons have the same spin, oxygen can only react with one electron at

a time and therefore it is not very reactive with the two electrons in a chemical bond. On the other hand, if one of the two unpaired electrons is excited and changes its spin, the resulting singlet oxygen becomes a potent oxidant as the two electrons with opposing spins can quickly react with other pairs of electrons, especially double bonds [47].

ETC-linked ROS production was first reported a half century ago. It was observed that antimycin A-treated, isolated mitochondria are producing hydrogen peroxide [48]. Further studies identified the mitochondrial components responsible for ROS production, including complex I, complex III, and other mitochondria-localized redox systems.

Complex I is the largest and first enzymatic complex of the ETC. It is essential for cellular energy production, providing about 40 % of the proton motive force required for ATP synthesis. It oxidizes NADH to NAD+ and donates the released electrons to the electron carrier coenzyme Q10 (CoQ10, also known as ubiquinone), linking this process to the translocation of four protons from the mitochondrial matrix to the IMS [49]. These electron transfers generate superoxide (O_2^-) [50]. Superoxide is normally converted to H_2O_2 by manganese superoxide dismutase (MnSOD); the former can easily diffuse across the membranes and be quickly reduced to water by mitochondrial and cytoplasmic peroxiredoxins, catalases, and glutathione peroxidases. It is estimated that 40 % of all mitochondrial disorders are related to mutations of complex I subunits [51]. Parkinson's disease (PD) is one of the typical examples. PD is characterized with a progressive loss of dopaminergic neurons and cell bodies of the substantia nigra pars compacta and nerve terminals in the striatum (see also 3.3.4). ROS are considered as one of the main pathogenesis factors based on dopamine oxidation-related metabolic pathways. Under physiological circumstance, oxidative deamination of dopamine by monoamine oxidase produces hydrogen peroxide [52]. In the pathological pathway, dopamine can be oxidized non-enzymatically by superoxide forming dopamine quinone which will be reduced by mitochondrial complex I to generate semiquinone followed by a transfer of its electron to molecular oxygen to form superoxide, completing a vicious oxidative cycle [53]. Both somatic and mitochondria DNA point mutations might cause complex I dysfunction,

thus subsequently linking ROS-mediated damage to neurodegenerative disorders such as Leber's hereditary optic neuropathy (LHON), Leigh's syndrome (LS), and mitochondrial encephalomyopathy, lactic acidosis, and stroke like episodes (MELAS) [54].

Complex II, succinate-ubiquinone oxidoreductase, commonly known as succinate dehydrogenase (SDH), is a tetrameric iron-sulfur flavoprotein of the IMM and acts as part of the TCA and respiratory chain [29]. SDH catalyzes the conversion of succinate to fumarate, yielding reducing equivalents in the form of reduced flavin adenine nucleotide ($FADH_2$). This is followed by a reduction of ubiquinone to ubiquinol [55].

Typically, complex II is excluded from the list of potential candidates for important physiological contributors of ROS [56]. It is partially due to fact that the succinate level in the tissue is low. During oxidation of succinate in isolated respiring mitochondria, electron flow can bifurcate forming direct (towards cytochrome oxidase) and reverse (toward NAD; rotenone-blocked) transport with the latter requiring energy input [57, 58]. The succinate-driven ROS generation during reverse electron transport from succinate to NAD resulting in the formation of NADH is higher when compared with that forming under direct oxidation of NAD-dependent substrates [59]. The observed relationship between ROS formation and the redox state of the couple NADH/NAD resulted in the proposition that the ROS formation is directly proportional to the level of reduction of NAD.

The role of complex II in maintaining and modulating the mitochondrial and cellular redox environment remains undetermined. It is unknown whether *in vivo* mitochondria reverse electron transfer from complex II to complex I occurs, and whether under physiological conditions the reverse electron transport could result in substantial ROS production considering that physiological concentrations of NADH would significantly attenuate O2·- production under conditions where reverse electron transport could be observed in *in vitro* model systems [60]. Complex III (ubiquinol-cytochrome c oxidoreductase) accepts reducing equivalents formed in complexes I and II and processes them by the Q-cycle operating mechanism. Operation of this cycle is initialized by ubiquinol, which releases

a proton to the IMS and donates one electron to the Riske iron-sulfur protein producing unstable semiquinone on the outer side of the IMM. The semiquinone serves as an electron donor for hemes of cytochrome bL, and then of cytochrome bH which is located close to the inner side of the membrane. Cytochrome bH reduces ubiquinone in an antimycin A-sensitive way producing ubisemiquinone followed by its further reduction with a second electron and protonation [61]. However, if the flow of electron through the complex III is stalled e.g. following application of complex III inhibitors such as antimycin A, myxothiazol, or stigmatellin, semiquinone levels are elevated resulting in more opportunities to donate single-electron to reduce oxygen [62, 63].

Aside of complex I and III as the major production site of mitochondrial ROS, also complex IV is able to generate ROS [64]. Complex IV, also called cytochrome c oxidase, is a protein- phospholidpid complex containing four redox centers (CuA, cyt. a, cyt. a3 and CuB) involved in electron transport and the conversion of oxygen to water. During this process, several -peroxyl and -ferryl intermediates are produced, which are considered as potential sources of free radicals [65, 66]. *In vitro* mitochondrial ischemia/reperfusion experiments showed significant increase of ROS production, and complex IV has been suggested to contribute around 30-35 % of total mitochondrial superoxide production [67].

While mitochondria are a major producer of ROS, these organelles are also a major sink for these toxic metabolites. Only if the antioxidant capacity of mitochondria are overwhelmed can ROS accumulate and cause significant mitochondrial as well as cellular damage. As result of aging or disease, the efficiency of the ETC is diminished causing increased production of ROS. In case of insufficient antioxidant defense, increased levels of ROS cause a further decrease of ETC efficiency leading in a vicious circle to increased ROS production. It is widely accepted that oxidative damage is at the bottom of many age-related disorders and that keeping oxidative damage to mitochondrial components in check is essential to maintain mitochondrial energy production and, thus, cellular function.

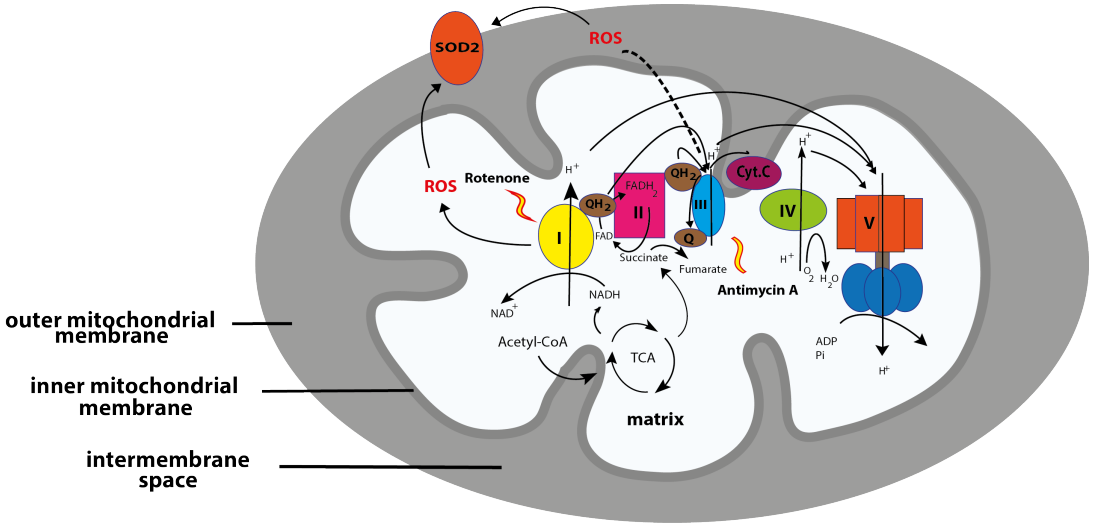

Figure 2: The ETC. The ETC is composed of five complexes (complex I - V). The substrates NADH and succinate generated by the TCA pass electrons through the ETC (I - IV) to O_2 generating H_2O, meanwhile protons (H^+) are transferred out of the matrix into the intermembrane space generating an electro-chemical potential across the IMM to store the energy. At last, H^+ flow back through complex V or F0F1-ATPase into the matrix compartment driving ATP production. As byproduct of OXPHOS, the ETC is involved in ROS production. ROS are being neutralized by local antioxidants, such as superoxide dismutase 2 (SOD2). However, overwhelming ROS production due to mitochondrial dysfunction will lead to oxidative stress. Inside the ETC, complex I and III are the two major sites of ROS production. For example, ROS production increases after inhibition of complex I by rotenone or complex III by antimycin.

3.2 Mechanisms of cellular quality control and their connection to mitochondrial maintenance

A major cause for mitochondrial dysfunction and associated disease is oxidative stress (3.1.2.1). Several mechanisms are in place to deal with oxidative stress and damaged mitochondrial components including mtDNA, lipids and proteins. Antioxidant activity is the first line of defense directly detoxifying reactive species to prevent direct damage to mitochondrial components. However, additional mechanisms are in place trying to repair damage caused by ROS escaping the antioxidant defense. These mechanisms are active on the level of the entire cell (3.2.1), the organellar level (3.2.4.2), or the level of damaged proteins (3.2.3).

3.2.1 Mitochondria and programmed cell death

Programmed cell death or apoptosis, the last line of defense in mitochondrial quality control, is a process whereby cells are induced by either intrinsic or extrinsic signals to die. Dysregulation of this process leads to several diseases ranging from neurodegenerative disease to cancer and viral infections [68]. A wide variety of neurological disorders such as Alzheimer's disease (AD) (3.3.3), PD (3.3.4), amyotrophic lateral sclerosis (ALS) and others are characterized by a loss of neuronal cells. In these diseases, inappropriate apoptosis results in the untimely death of neurons causing ultimately dysfunction of the central nervous system [69]. On the other hand, cancer cells are able to survive due to their decreased ability to undergo apoptosis in response to cytotoxic conditions [70]. Thus, apoptosis is an essential process for the removal of damaged or harmful cells, so that the organism as a whole can survive [71]. As opposed to death-receptor induced apoptosis, intrinsic programmed cell death is initiated by the release of apoptotic factors such as cytochrome c from the mitochondria to the cytosol. The release of these apoptotic factors requires mitochondrial outer membrane permeabilization (MOMP) modulated by various pro- and anti-apoptotic proteins [72]. It was found that cytochrome c, a 15kD redox carrier protein, responsible for the electron transfer between complex III and IV in the electron respiratory chain, is released during MOMP subsequently leading to caspase activation [73]. Thus, mitochondria are an important hub for integrating different intrinsic apoptotic signals and are involved in important cellular life-death decisions which upon dysregulation can lead to the development of cancer or neurodegeneration.

3.2.2 The UPS

The UPS constitutes one of the principal pathways for cellular protein homeostasis. The UPS plays a key role in regulating many crucial processes including cell cycle progression, DNA repair, apoptosis and gene transcription by mediating the elimination of relatively short-lived regulatory proteins when they are no longer needed. In addition to modulating cellular activities, it also controls the degradation of unfolded or misfolded proteins

to prevent cellular damage [74].

For substrate recognition, the UPS relies on tagging substrates with the 76 amino acid-short protein modifier ubiquitin. Upon ubiquitination, substrate proteins are targeted by the 26S proteasome for degradation into peptide fragments followed by further degradation into their component amino acids by cytoplasmic peptidases. This process occurs in the cytoplasm and nucleoplasm of the cell [75]. The 26S proteasome is a multimeric complex consisting of about 31 different proteins. It is comprised of two different subcomplexes, the 19S cap complex and the 20S proteolytic core [76]. The 19S cap is responsible for regulating access to the 20S core recognizing ubiquitinated substrates, removing and recycling their ubiquitin chains by complex component deubiquitinating enzymes [77, 78]. Next, bound proteins are unfolded and fed into the barrel-shaped 20S proteolytic core for degradation [79]. Once inside the 20S proteolytic core, substrate proteins are sequentially cleaved into small peptides by three different proteolytic activities [80, 81]. In addition to the 19S cap complex, proteasome activity and function is regulated through binding with a variety of proteins, such as chaperones or cofactors, which regulate subcellular localization and substrate specificity. Sec61 e.g. targets the 26S proteasome to the ER membrane [82, 83].

3.2.2.1 The machinery of ubiquitination

3.2.2.1.1 Ubiquitin activating, ubiquitin conjugating and ubiquitin ligating enzymes Ubiquitination is a covalent, post-translational protein modification where a small 76 amino acid ubiquitin (Ub) moiety via the C-terminal carboxyl is covalently conjugated onto a lysine residue of a target protein (Figure 3). This is accomplished through the joint action of three families of enzymes [84]. In a first step, the E1 ubiquitin-activating enzyms binds individual ubiquitin molecules in an ATP-dependent manner via a high-energy thioester linkage between the ubiquitin carboxy terminus and a cysteine side chain on the E1 enzyme. This activated ubiquitin is subsequently transfered onto a E2 ubiquitin-conjugating enzyme again in a thioester linkage. An ubiquitin ligase or

E3 enzyme then binds both the E2-ubiquitin complex and a substrate protein facilitating ubiqutin transfer [85]. This substrate can either be a target protein or any of the seven lysine residues of ubiquitin leading to the formation of poly-ubiquitin chains [86]. While there is only one ubiquitin-activating enzyme, about 50 E2 enzymes and hundreds of E3 enzymes are found in the human genome [87]. This allows for multiple combinations of E1, E2 and E3 enzymes conferring very selective substrate specificity for ubiquitination [88]. Depending on the type of ubiquitin ligase, binding of the E2 complex and the substrate occur either simultaneously or sequentially [89]. There are two main groups of E3 ligases classified according to their catalytic domain. Homologous to the E6AP C-Terminus (HECT) ubiquitin ligases generate Ub-thiolester-intermediate prior to establishing an isopeptidic bond between the C-terminus of ubiquitin and an amino group on the substrate protein, while really interesting new gene (RING)-finger E3 ligases facilitate the transfer of activated ubiquitin directly from E2 to the substrate[90] without forming an E3-ubiquitin intermediate.

Depending on ubiquitin conjugating and ligating enzymes involved, the outcome of ubiquitination can be manifold. Substrate proteins might be mono-ubiquitinated, multiply mono-ubiquitinated, or poly-ubiquitinated with ubiquitin chains of different configuration with the most common form being lysine 48 linked ubiquitin chains. For ubiquitin-dependent degradation by the 26S proteasome a minimum of four Lys48 linked ubiquitin moieties seems to be required [91]. More recently, polyubiquitin chains involving Lys6, Lys11, Lys27 and Lys29 [92, 93] and heterogeneous chains involving Lys11, Lys48 and Lys63 linkages [94] have also been implicated in proteasomal targeting [95].

3.2.2.2 Determining the fate of ubiquitinated proteins

3.2.2.2.1 DUBs Next to the complex system of ubiquitinating enzymes, a class of dDUBs facilitates the removal of ubiquitin chains. These DUBs are able to hydrolyze all types of polyubiquitin chains [96]. The 19S lid of the 26S proteasome contains DUB activity [97, 98]. The removal of poly-Ub chains by DUBs associated with the protea-

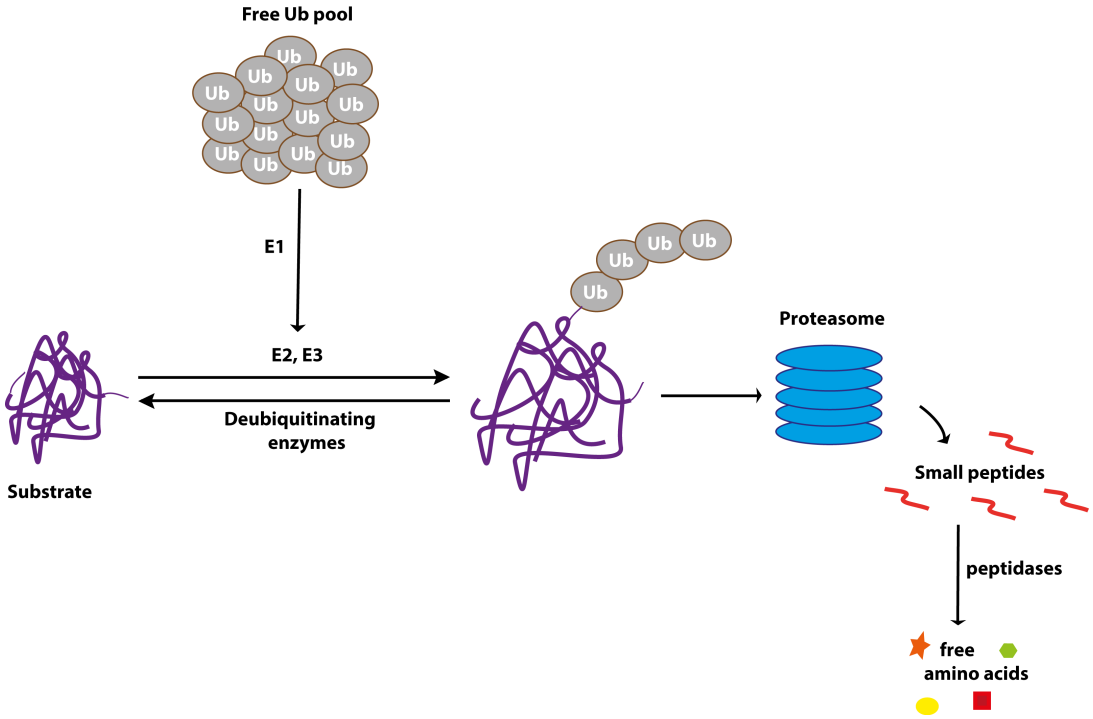

Figure 3: The UPS. Substrate proteins are recognized by E3 ubiquitin ligases and are subsequently conjugated with ubiquitin chains. These chains serve as recruitment signals for subsequent trafficking to the 26S proteasome for degradation into peptides and component amino acids.

somal lid precedes the threading of unfolded proteins through a narrow pore into the proteolytic chamber of the core 20S proteasome [99, 100, 101]. The removal of ubiquitin prior to degradation also recycles this essential modifier and replenishes the cellular pool of free ubiquitin. It follows that DUB activity can have distinct outcomes for proteasomal turnover of proteins: some DUBs facilitate degradation, whereas others may stabilize proteins destined for degradation [102].

In addition to their important role in ubiquitin recycling, DUBs also regulate the fate of subcellular proteins makes them a prominent diagnostic and therapeutic target for research [103]. Multiple studies have clearly illustrated the auto-ubiquitylation of E3 ligase and their subsequent interaction with DUBs [104]. DUBs have been classified into five families [105]. Papain-like cysteine proteases with the ubiquitin-specific proteases (USP), the ubiquitin C-terminal hydrolasess (UCHs), the ovarian tumor domain proteases (OTUs), the Josephin domain proteases, and zinc-dependent metalloproteases containing a JAB1/MPN/Mov34 (JAMM) [106].

The OTU family of DUBs has emerged as regulators of important signaling cascades. A20 [107], OTUD7B/Cezanne [108] and OTULIN [109] regulate NF-κB signaling, OTUD5/DUBA regulates interferon signaling [110], OTUD2/YOD1 and VCPIP regulate p97-mediated processes [111], while OTUB1 is involved in the DNA damage response [112]. The astonishing variety of different types of DUBs might be explained by the complexity of ubiquitin modification. DUBs must display various layers of specificity. They must distinguish not only between ubiquitin and ubiquitin-like modifications but also between the eight ubiquitin linkage types. Moreover, chain topology and length may also affect DUB activity [96]. In sum, DUBs are what phosphatases are to kinases and are an integral part of the ubiquitination machinery and fulfill important regulatory functions.

3.2.2.2.2 P97 – a key component of the UPS P97, also called valosin containing protein (VCP), or CDC48 in yeast is a member of the ATPase associated with diverse cellular activities (AAA ATPase) family of proteins [113, 114, 115]. P97 is highly conserved and expressed in mammals, with around 1 % of total cellular protein being P97 [116]. It is involved in a wide variety of regulatory functions, which are conferred through cofactors, in the cytosol [117], the plasma membrane [118], the nucleus [119], and various organelles, such as the endoplasmic reticulum, [116], mitochondria [120], golgi [121], lysosomes [118], autophagosomes [122] and peroxisomes [123, 124]. These functions of P97 include cell cycle regulation [125], control of membrane fusion [126, 127], DNA damage response [119], and various aspects of the UPS [128, 129, 115].

Structure of p97

Initially identified as a homohexameric particle by negative stain electron microscopy, p97 was shown to possess ATPase activity that is dependent on its oligomeric state and the presence of Mg_2^+ [130, 131]. Subsequently, the crystal structure of the N-domain and first ATPase domain (ND1) was solved by crystallography [132, 133, 134]. The hexamer displays a mushroom-like shape where two rings of ATPase domains stack on top of each other and the N-domain is co-planar to the D1 ATPase domain in ADP-bound p97 and in an 'up' conformation in the ATP-bound state [135]. The D1 and D2 ATPase domains

both fold into typical AAA domains with an α/β-subdomain followed by a helical subdomain. Of the 12 ATPase domains in a p97 hexamer, the D1 domains are primarily involved for oligomerization, while the D2 domains play a larger role in ATP hydrolysis for force generation [136, 137]. There is some evidence that the D1–D2 linker is required for activity. While D1 domain alone displays negligible ATPase activity, a slightly longer protein containing the 20 aa D1–D2 linker possesses ATPase activity roughly half of full-length p97 [138, 136, 139]. ATP hydrolysis is also regulated by inter-subunit interactions between the D2 domain and the C-terminal tail of the neighboring protein [140, 141].

P97 processes ubiquitinated client proteins

P97 together with its cofactors recognizes and processes ubiquitinated client proteins [123]. One of the ubiquitin mediated pathways with a well-established role for p97 is ER associated degradation (ERAD) [116, 142]. ERAD governs the retrotranslocation of misfolded and superfluous proteins, of both luminal and membrane-bound, from the ER to the cytosol. First, ERAD consists of a recruitment step from the ER-lumen to the ER-membrane. This is followed by ubiquitination of the substrate protein in the ER membrane through specialized, ER-membrane anchored E3 ubiquitin ligases. P97 cofactors on the ER-membrane then recruit P97 [143], which then extracts the misfolded proteins through ATP hydrolysis from the ER-membrane [144]. After extraction, these proteins may undergo further processing by cofactors, for example removal of sugars from glycoproteins [145], ubiquitin chain elongation [146], or ubiquitin removal by DUBs [147]. Ultimately, retrotranslocation ends with degradation of the substrate by the proteasome, although DUBs can divert certain substrates from proteasomal degradation through deubiquitination [122].

P97 can also act as part of a positive feedback loop through recruitment of an E4 ubiquitin chain elongation factor, where oligo-ubiquitinated substrates are poly-ubiquitinated before proteasomal degradation [148]. Transfer of ubiquitinated substrate proteins to the proteasome is also regulated. P97 cofactors UFD2 and RAD23 promote the transfer of ubiquitinated substrates to the proteasome [148], while the cofactor UFD3 acts in an

antagonistic manner [149]. Similar to its segregase activity, P97 aids in the unfolding of its substrates, which facilitates processing by the proteasome [150, 151]. The central role of p97 for the UPS is especially evident after inhibition of P97, which leads to the accumulation of ubiquitin conjugates in the cytosol [152, 153].

P97 adapter proteins and cofactors

A large collection of p97-interacting proteins has been identified. These proteins either function as adaptors that link p97 to a specific subcellular compartment or substrate, or serve as cofactors helping to process substrates. Binding of and competition between p97 cofactors regulates p97 activity. Although a few proteins such as PLAA/Ufd3, PNGase, HOIP, and Ufd2 bind p97 at the short C-terminal tail [149, 154, 155, 98, 156, 157], the vast majority of p97-interacting proteins bind N-domain [158]. Representative N-domain-interacting proteins include Ufd1, Npl4, p47, ataxin3, and FAF1. Binding of cofactors is mediated by a small group of conserved protein-protein interaction motives. Sequence analyses identified several frequently occurring p97-interaction patterns such as the UBX motif [159], the VCP interacting motif (VIM) [160], VCP-binding motif (VBM) [161] and SHP box [162].

The UBX domain is an 80-residue module structurally homologous to ubiquitin and found in a several p97 cofactors. The VCP-interacting motif (VIM) is a linear sequence motif (RX5AAX2R) found in a number of p97 cofactors or adaptors including gp78 [163], SVIP (small VCP-inhibiting protein) [164] and VIMP (VCP-interacting membrane protein) [165]. The VBM domain features a highly polarizing linear sequence motif (RRRRXXYY) found in ataxin-3, Ufd2 and Hrd1 [161]. The SHP box is a short amino acid stretch enriched in hydrophobic residues, which can be found in p47 [166], Ufd1-Npl4 [167] and Derlin-1 [168, 169, 165]. The cofactors can be divided into two groups depending on what part of p97 they interact with. The larger group of cofactors binds the p97 N-domain, via UBX, UBX-L, VIM, VBM or SHP (binding segment 1) motif [128, 170]. A smaller group binds the very C-terminus of p97, via peptide N-glycosidase/ubiquitin-associated (PUB) (PNGase/UBA- or UBX-containing proteins) and PUL (PLAA, Ufd3p

and Lub1p) domains.

3.2.2.2.3 UBX domain containing cofactors UBX-domain containing proteins represent the largest family of p97 cofactors with 13 members identified in the human genome. The UBX domain has a tridimensional structure similar to ubiquitin [171] and interacts with the p97 N-terminus [159]. UBX proteins can be further classified into two main groups based on their domain composition: UBA-UBX and UBX-only proteins. UBA-UBX proteins (p47, UBXD7, UBXD8, FAF1, and SAKS1) contain an additional ubiquitin-associated (UBA) domain at their N-terminus, which enables them to bind ubiquitinated substrates [172]. UBX-only proteins (UBXD1, UBXD2, UBXD3, UBXD4, UBXD5, ASPL, p37, VCIP135 and YOD1) lack such an UBA domain and therefore likely ability to bind polyubiquitinated proteins [173].

UBA-UBX proteins bind ubiquitinated substrates in a manner that is enhanced upon inhibition of the proteasome, suggesting that they function as ubiquitin-receptors in the ubiquitin-proteasome pathway. Furthermore, they interact with an assortment of HECT and RING-domain E3 ubiquitin-ligases, including a large number of cullin-ring ligase subunits [173]. Thus, each UBA-UBX protein is likely to target a particular subset of substrate proteins carrying an ubiquitin modification. UBX-only proteins on the other side do presumably not interact with ubiquitin and, as a consequence, the type of substrates they target is less clear. The distinctive substrate specificity of each UBX protein is the key to defining the p97 functions they mediate [174]. The family of UBX domain [175, 171] proteins appear to associate with p97 via their UBX domains [176], and UBX proteins are therefore generally considered to function as p97 adaptors. The approximately 80 amino acid long UBX domain displays a remarkably similar structure to that of ubiquitin [171]. A loop region in the p47 UBX domain lacking in ubiquitin, appears to be specific for interaction with a hydrophobic binding pocket in the N-terminal part of p97 [177]. Another group of proteins, containing the so-called PUB [178] or PUG [179] domain, was also shown to mediate interaction with p97 [180]. UBX and PUB domains do not bind to p97 in a mutually exclusive manner [180], and accordingly the PUB binding

site maps downstream of the UBX binding site [157]. The structure of the PNGase PUB domain was recently solved [180], revealing a hydrophobic groove which binds p97, an association which is occluded upon tyrosine phosphorylation of p97 [157]. Interestingly, many of the UBX family of adaptors have no identified ubiquitin-association domain, and no other functional domain to suggest a function. The diversity within the UBX family suggests an array of potential effects on cellular processes and it is of high interest to determine the function of other known p97 adaptors.

3.2.2.2.4 Non-UBX domain containing cofactors While the UBX domain may constitute the major p97 interaction domain, the bulk of the functional work deciphering the specific roles of p97 cofactors has been done with the non UBX containing interactors. These p97 cofactors can be further divided into two subgroups, adapters and accessory proteins. Adapters are required for substrate binding, while accessory proteins may use p97 as a docking site to perform a specific enzymatic function on the already associated substrate. The majority of non-UBX p97 interactors have been shown to perform a variety of key roles in mediating ERAD. Arguably the two best studied and most important p97 adapters, Npl4 (nuclear protein localization 4) and Ufd1 (ubiquitin fusion degradation 1), form a heterodimer crucial for binding p97 in a 1:1 ratio [167]. Npl4-Ufd1 function as essential substrate recruiting factors binding to ubiquitinated substrates at the ER membrane linking p97's physical conformational change upon ATP hydrolysis to the translocation of these proteins into the cytosol [145, 152, 181, 182]. p97 interacting proteins consist not only of adapters, but also accessory proteins that use p97 as a docking site to target for their specific functions. They are called substrate-processing cofactors. They include the deglycosylase, PNGase I, the E3 ubiquitin ligases Hrd1, gp78, and Ufd2, and the deubiquitinase Ataxin-3. PNGase I contains a PUB domain responsible for maintaining the interaction with p97's carboxy-terminal tail [157]. The E3 ubiquitin ligases, Hrd1, gp78 and Ufd2 have all been identified as being tied to substrate ubiquitination in ERAD.

3.2.2.2.5 UBXD1 Human UBXD1 has recently been shown to be an abundant and stable protein that localizes to the nucleus, cytosol, microsomal pellet, and centrosomes in HeLa cells [175]. Interestingly, UBXD1 contains from the N- to the C-terminus a valosin-containing protein (VCP) interacting motif (VIM), a peptide N-glycosidase/ubiquitin-associated (PUB), as well as an ubiquitin regulatory X (UBX) domain. Unlike other UBX domain containing proteins which bind to p97 via their UBX domain, UBXD1 interacts with p97 via its VIM and PUB domain [183]. This is due to the absence of a phenylalanine-proline-arginine conserved motif in between β-strands 3 and 4 within the p97 interaction site of UBXD1 [175].

Recently, insights into the function of UBXD1 became available. Initial work suggests that UBXD1 plays a role in ERAD through moderate defects in the clearance of an ERAD substrate, CFTRΔF508 upon UBXD1 overexpression [184]. In addition, UBXD1 was shown to co-purify with a known member of the ERAD pathway, the E3 ubiquitin ligase Hrd1 one of two main ubiquitin ligases involved in ubiquitinating ERAD substrates. The authors theorize that this interaction is likely indirect, instead mediated by p97 [175]. Recent work, however, has provided some convincing evidence that UBXD1 does play an important role in directing p97's function, not only in ERAD but also in endolysosomal sorting. UBXD1 and p97, have been implicated to be key mediators in the internalization and post-endocytic trafficking to the lysosome of membrane protein Caveolin-1 [185]. Furthermore, UBXD1 is of clinical relevance, as p97 mutations linked to inclusion body myopathy associated with Paget's disease of the bone and frontotemporal dementia (IBMPFD) and ALS are defective at interacting with UBXD1 [185].

UBXD1 is of particular interest to study due to the lack of a clear ubiquitin binding domain, in addition to the unique differences within its UBX domain (lack of phenylalanine-proline-arginine motif essential for p97 interaction). Additionally, it is one of a few adaptors that have been shown to bind both at the N-terminal and C-terminal domains of p97. Work presented here will show pro-mitophagic function for UBXD1, which acts as a mitochondrial recruitment factor for p97 during Parkin-dependent autophagic removal

of damaged mitochondria.

3.2.2.2.6 YOD1 – a DUB linked to UBXD1 and p97 YOD1/OtuD2/DUBA8 is a ubiquitin-specific protease containing a UBX domain, considered a hallmark of p97-associated proteins [159]. YOD1 is the closest homolog of *S. cerevisiae* Otu1, which associates with Cdc48 to regulate the processing of the ER-membrane embedded transcription factor Spt23, a crucial component of the OLE pathway [98]. Although highly conserved, the function of YOD1 is not clear in higher eukaryotes. The human genome lacks a homolog of Spt23, suggesting that YOD1 participates in other, presumably conserved, cellular processes. YOD1 comprises three domains, an N-terminal UBX domain, a central otubain domain, and a C-terminal C2H2-type zinc finger domain [111]. Recently, YOD1 was suggested to act together with UBXD1 and p97 in the autophagic removal of ruptured lysosomes by selectively removing K48-linked ubiquitin chains from lysosomes thereby improving recognition by the autophagic machinery [186].

3.2.3 UPS-mediated protein degradation on mitochondria

3.2.3.1 Outer mitochondrial membrane associated degradation Recognition and elimination of misfolded proteins are essential cellular processes. More than thirty percent of the cellular proteins are targeted to the secretory pathway. They fold in the lumen or membrane of the endoplasmic reticulum from where they are sorted to their final destination. The folding process, as well as any refolding after cell stress, depends on chaperone activity. In case, proteins are unable to acquire their native conformation, chaperones with different substrate specificity and activity guide them to elimination. For most misfolded proteins of the ER this requires retrotranslocation to the cytosol and polyubiquitylation of the misfolded protein through (ERAD). Thereafter ubiquitinated proteins are guided to the proteasome for degradation [187]. Similar to the ER, mitochondria were recently linked to UPS in form of outer mitochondrial membrane associated degradation (OMMAD) [188] (Figure 4). Interestingly proteasome inhibitors can increase

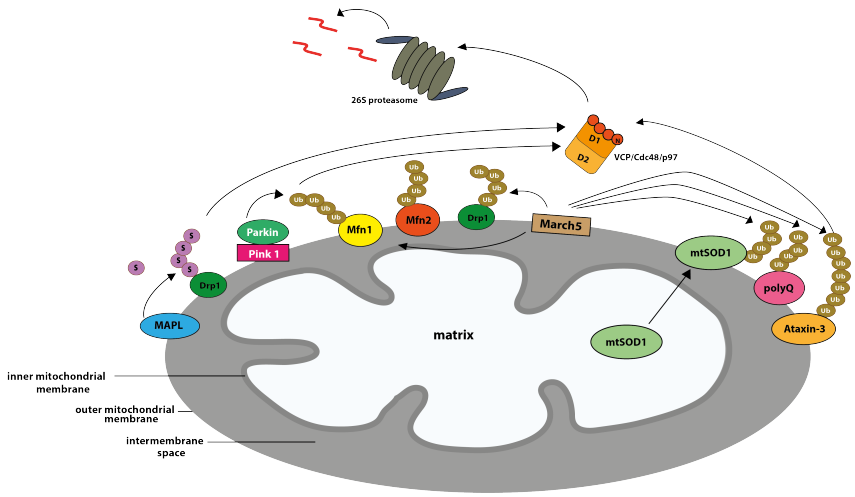

Figure 4: Outer mitochondrial membrane associated degradation or OMMAD refers to the protein quality control machinery localized on the outer mitochondrial membrane, in which multiple ubiquitin ligases namely MARCH5, IBRDC2, RNF185, MULAN/MAPL and Parkin are involved. OMMAD is not only restricted to protein quality control. Other mitochondrial functions such as morphology and mitophagy are influenced by OMMAD.

the levels of ubiquitinated mitochondrial proteins, indicating the role that proteasomes play for mitochondrial protein degradation. In this way, OMM proteins such as Mfn1, Mfn2 and Mcl-1 were found to be polyubiquitinated and degraded by the proteasome. Also, several specific E3 ligases were found to localize to the OMM and were shown to be involved in the ubiquitylation of mitochondrial proteins, including MULAN, Parkin, MARCH5, RNF185, and IBRDC2 [189, 190, 191] (Table 1). Among many others, RING-E3 ligases Parkin, MULAN and MARCH5 are widely studied together with their potential mitochondrial substrates (mitofusins, Drp1, Mutated SOD1, ETC) (1). Interestingly and analogous to ERAD, p97 is also involved in promoting extraction of polyubiquitinated proteins from the mitochondrial membrane and transport to the cytosolic proteasome [192]. Described by many studies, several mitochondrial dynamics regulators as mitofusins and Drp1 are the target of ubiquitination [193]. Thus, by affecting mitochondrial fission and fusion machinery, the UPS is certainly connected to mitochondrial dynamics, therefore participating in mitochondrial maintenance. The UPS is also through the ubiquitin E3 ligase Parkin, which serves to initiate mitophagy (3.2.4.2), connected to autophagic mitochondrial quality control [194].

Ubiquitin ligase	Localization	Mitochondrial Substrates
Parkin	cytosol, mitochondria	Mcl-1, Mfn1/2, Drp1
Mulan/MAPL	mitochondria	Omi/HtrA2, Drp1
MARCH5	mitochondria	Drp1, Mfn1/2, MuSOD1, ataxin-3, polyQ
IBRDC2	cytosol, mitochondria	Bax

Table 1: Overview of mitochondrial ubiquitin ligases, their localization and known and potential substrates. Please note Mulan/MAPL is described as ubiquitin as well as SUMO ligating enzyme.

3.2.4 Autophagy

3.2.4.1 General autophagy Autophagy is a major pathway for endo-lysosomal degradation of cellular cargo sequestered within double-membrane organelles called autophagosomes. Upon induction of autophagy, autophagosomes form *de novo* and initially appear as small membrane structures referred to as isolation membranes or phagophores. The isolation membranes expand, gradually enclosing a part of the cytoplasm, and eventually close to give rise to autophagosomes. Subsequently, the outer membrane of the autophagosome fuses with the lysosomal membrane, and autophagosome inner membrane and autophagosome cargo are degraded by lysosomal hydrolases. When induced by starvation, autophagy is largely nonselective with regard to the cargo enclosed in autophagosomes and serves mainly to replenish intracellular metabolite stores. In addition to unspecific autophagy, targeted autophagic processes are known. Damaged or superfluous organelles such as lysosomes, peroxisomes or mitochondria are degraded in a targeted fashion through lysophagy [195], pexophagy [196] or mitophagy [197].

The formation of autophagosomes is generally thought to require the action of conserved machinery that includes the ULK1/Atg1 complex, the class III phosphatidylinositol 3-kinase complex 1, ATG9, WD-repeat protein interacting with phosphoinositides (WIPI), and the ATG12 and LC3/GABARAP conjugation systems. All of these components localize to the isolation membrane at some stage of autophagosome formation. In addition to these conserved core components, other factors such as cargo receptors are required for selective autophagy [197]. Autophagy represents a highly conserved process for the

lysosomal degradation of cytoplasmatic long-lived proteins and organelles. It can result in final decomposition of proteins contributing to a certain form of programmed cell death (autophagic cell death), but it may also serve as a survival mechanism through intracellular clearance of toxic or damaged proteins and organelles or, in times of starvation, through protein recycling and maintenance of intermediary metabolism [198].

3.2.4.2 Mitochondria-selective autophagy Mitochondria-selective autophagy or mitophagy is a specialized form of autophagy for to the elimination of dysfunctional mitochondria, and is a crucial quality control mechanism to ensure mitochondrial network's integrity and functionality. Besides the removal of dysfunctional mitochondria, mitophagy is also responsible for mitochondrial degradation during erythrocyte maturation, and it contributes to maternal inheritance of mitochondrial DNA, by eliminating the sperm-derived mitochondria [199]. In mammals, two major mitophagic pathways can be distinguished - Parkin-dependent as well as Parkin-independent mitophagy. In Parkin-dependent mitophagy, damaged or dysfunctional mitochondria are removed by the concerted action of the PTEN induced putative kinase 1 (PINK1) and of the E3 ubiquitin ligase Parkin (see also 3.3.4). PINK1 and Parkin accumulate on damaged mitochondria, flagging these organelles with Parkin-dependent ubiquitination of outer membrane proteins, thus allowing their autophagic degradation [200]. In the PINK1/Parkin independent pathway, different protein regulators, such as BNIP3L [201], FUNDC1 [202], or Autophagy And Beclin 1 Regulator 1 (AMBRA1) [203] contribute to the flagging and recognition of mitochondria. Efficient mitophagy relies on the engulfment of the damaged organelles by a forming autophagosome, without affecting the entire mitochondrial network. For this reason, mitochondrial network fragmentation is observed prior to mitophagy, which thus results to be strictly connected with mitochondria dynamics and the machineries controlling the balance between fusion and fission of the organelles. In fact, not only the main pro-fission protein Drp1 is modulated through post-translational modifications such as SUMOylation, but also proteins favoring the fusion and transport of the organelles such as Mfn2 or Miro, are selectively degraded in order to promote

mitophagy [204]. Interestingly, proteomic studies have shown proteins on the IMM to be eliminated at rates similar to the turnover of whole mitochondria through mitophagy [205]. At the same time, proteins of the OMM and mitochondrial matrix redistribute much faster through fission and fusion events through the mitochondrial network than proteins of the IMM [206]. These observations suggest that protein degradation on the IMM may mainly be a product of mitophagy.

3.3 Mitochondria and neurodegeneration

Mitochondria have a fundamental role in eukaryotic metabolic processes by generating ATP to maintain cellular functions. Dysfunctional mitochondria deprive cells of energy, produce cytotoxic ROS, and release proapoptotic mediators to initiate cell death. The mitochondrial quality-control pathways that evolved to maintain the integrity of mitochondria therefore have key roles in the normal function of cells [2, 207]. Many neurodegenerative disorders are age related, which is also the most important risk factors for such diseases like AD, PD, and ALS. And interestingly, mitochondrial function declines with aging. It is assumed that mitochondria accumulate mtDNA mutations and, thus, non-functional proteins during the lifespan of the organism, thus contributing to the process of aging as well as neurodegeneration due to insufficient ATP production. In addition, mitochondria are the trigger of intracellular apoptosis responsible for the final loss of neuron cell numbers [208]. Also, extensive literature point at oxidative stress as the key perpetrator for neurodegeneration further linking mitochondria to the demise of neurons as the main source of ROS [209]. As oxidative stress causes mitochondrial dysfunction and as failing mitochondria producing even more ROS [210], a vicious cycle progresses in which more oxidative stress induces more structural and metabolic damages - nucleic acid breakdown, enzymatic proteins inactivation, lipid peroxidation - resulting in even more severe mitochondrial dysfunctions [211]. Thus, mitochondrial dysfunction is the center of many neurodegenerative disorders. Not only deficiencies in mitochondrial respiration are responsible for neuron loss and cell death, mitochondrial quality control, mitochondrial

dynamic and apoptosis all play important roles in the survival of neurons.

3.3.1 Dysfunction of p97 and neurodegeneration

Given the crucial role of p97 in maintaining cellular proteostasis, it is not surprising that autosomal dominant mutations in *VCP*, the gene encoding p97, lead to a rare multisystem degenerative disorder IBMPFD, also called VCP disease. IBMPFD is associated with progressive muscle weakness including heart and respiratory muscles leading to difficulty breathing and heart failure. IBMPFD also affects the bones causing chronic pain and might lead to frontotemporal dementia. Interestingly, pathogenic mutations in the N-terminal half of p97 in the interface region between N- and D1-domain suggest that communication between these two regions is important for disease pathogenesis. Disease-associated mutations do not appear to alter p97 oligomerization but have been reported to enhance basal ATP hydrolysis, which is mediated through the D2 domain [212]. However, this seems not to be an essential requirement for disease pathogenesis as not all mutations affect ATP hydrolysis [213]. Other studies have found that disease-associated mutations might affect the association of p97 with certain cofactors [214]. This suggests that disease-associated mutations in p97 do not lead to a global loss of function but, instead, to impairment of a distinct subset of p97 functions.

Pathogenic p97 mutations have been suggested to interfere with the interaction between p97 and UBXD1 affecting ubiquitin-dependent membrane sorting at endosomes and degradation in lysosomes and implying this pathway in IBMPFD. This altered p97-UBXD1 interaction seems to weaken substrate recognition. In particular, the interaction of p97-UBXD1 with caveolin-1 (CAV1), a main component of caveolae, is affected [185]. For degradation, CAV1 is modified with mono-ubiquitin, a signal important for endosomal sorting, and transported to intraluminal vesicles in endolysosomes. UBXD1 is necessary for the endolysosomal trafficking of ubiquitinated CAV1 [215]. Mice and patients with pathogenic p97 mutations accumulate CAV1-positive endolysosomes and have reduced levels of CAV3, a muscle-specific caveolin, at the sarcolemmal membrane of skeletal mus-

cle [215, 215]. Intriguingly, autosomal dominant inherited mutations in CAV3 cause limb girdle muscular dystrophy 1C, which has phenotypic similarities to p97-associated muscle disease and also shows reduced localization of CAV3 to the sarcolemma [216]. These data suggest that p97 might have tissue-specific functions and that the selective disruption of these cellular processes (e.g. CAV1 or CAV3 sorting) leads to tissue-specific phenotypes. Endolysosomal degradation is likely to be more broadly affected in VCP disease pathogenesis as cells that express mutant p97 have enlarged late endosomes with absent intraluminal vesicles (ILVs), implicating a defect in multivesicular body (MVB) biogenesis [215].

3.3.2 Huntington's disease

Huntington's disease (HD) is an inherited neurodegenerative disorder characterized by unsteady gait and uncoordinated body movements as well as dementia in late stage disease. Early onset HD as symptomatic overlap to PD. HD is caused by mutations in Huntingtin causing expansion of CAG triplet repeats. Interestingly, diminished removal of dysfunctional mitochondria observed in HD suggested impairment in the mitophagy process. It has been proposed that mutant Huntingtin could impair the delivery of flagged dysfunctional mitochondria to onforming autophagosomes, because of its reduced interaction with the autophagy receptor SQSTM1/p62 [217], and by affecting autophagosome transport towards the lysosome [218]. Recently, it has been observed that Huntingtin is involved in selective autophagy, by serving as a scaffold for both SQSTM1/p62 and the autophagy initiation kinase ULK1 [219], re-opening the question about the role of mutant Huntingtin in these processes. A partial answer has been suggested by the observation that a reduced delivery of dysfunctional mitochondria to the autophagosome could be partially rescued when PINK1 is overexpressed, in fly and mice HD models [220]. In addition, the analysis of PINK1$^{-/-}$ mice indicates that mitophagy levels are very different in various areas of the brain [221], thus suggesting that different neuronal population could rely on or modulate different forms of Parkin-dependent/Parkin-independent mitophagy,

probably in response to different stimuli. Thus, recent insight into HD further support the importance of selective mitophagy and mitochondrial quality control to prevent neurodegeneration.

3.3.3 Alzheimer's disease

Mitochondrial dysfunction in AD is due to the accumulation of Aβpeptides on these organelles. In particular, Aβtoxicity could depend upon: i) its interaction with mitochondrial matrix proteins [222]; ii) the perturbation of the fission and fusion processes [223]; iii) the alteration of mitochondrial motility [224]; iv) the disruption of the functionality of the electron transfer chain and of the ATP/ADP exchange [223]. Accumulation of autophagic vacuoles in AD brains suggested defective autophagy as one of the pathogenic features of AD [225]. Very recently, it has been reported that although the autophagic machinery is competent in AD neurons, the flux is impaired in the final stages of the process, namely the fusion of autophagosomes with lysosomes [226]. In addition, it has been reported that Parkin overexpression in an AD mouse model results in an enhancement of the autophagic clearance of defective mitochondria, and in the prevention of mitochondrial dysfunction [227]. Taken together these observations suggest that whereas enhanced mitophagy increases the autophagic flux, defective lysosomal removal of autophagic vesicles is responsible for the aberrant accumulation of defective mitochondria in AD. Further, it has been very recently reported that N-terminal truncated Tau is able to induce aberrant Parkin recruitment, thus leading to excessive mitophagy, contributing to synaptic failure [228].

3.3.4 Parkinson's disease

PD is a neurodegenerative disorder causing characteristic movement abnormalities known as parkinsonism. The disease mainly affects the dopamin-producing neurons substantia nigra in the midbrain. Death of these neurons and the resulting lack of dopamin is responsible for the movement disorder and other symptoms such as sleep and emotional

problems. Most cases of PD are idiopathic and late onset. Rare, early onset PD is caused by autosomal recessive mutations in the *PARK2* gene, coding for the Parkin protein [229], or by mutations in the *PARK6* gene encoding the PINK1 protein [230]. PINK1 and Parkin are key factors acting on the same biological pathway, leading to the tagging and engulfment of dysfunctional mitochondria by the autophagy machinery [231]. PINK1 is a mitochondrial resident protein kinase, which is rapidly degraded after its import into healthy organelles, by the action of mitochondrial matrix protease (MMP) and the presenilins-associated rhomboid-like protein (PARL) [232]. Whereas, in dysfunctional mitochondria, characterized by a lack of mitochondrial membrane potential, PINK1 is not degraded and accumulates on the OMM [233]. OMM-localised PINK1 in turn phosphorylates cytosolic Parkin, as well as mitochondrial ubiquitin chains, thus providing signals for Parkin recruitment to the damaged organelle [234]. Indeed, Parkin mediates the ubiquitination of the OMM proteins, including Mfn1 and Mfn2, Miro, the translocase of outer mitochondrial membrane 20 (TOMM20), and VDAC. Ubiquitinated Mfn1 and Mfn2 are delivered to the proteasome for degradation, thus stimulating mitochondrial fission and mitochondrial network fragmentation [235]. Other ubiquitinated proteins are recognised by autophagy receptors, such as p62 and optineurin [236], allowing the selective engulfment of mitochondrial subunits in the forming autophagosome [237]. The mitophagy process acting through PINK1-Parkin seems to be important not only to protect neurons from the damage caused by dysfunctional mitochondria in the soma, but it has been proposed that this system could be very efficient in the removal of damaged organelles in axons of these cells [238]. Perturbation of the system in PD patients, could depend upon both mutations in the genes encoding key proteins in the system [239], but also on altered Parkin solubility, as a consequence of age or oxidative and/or nitrosative stress [240]. In addition, a number of different proteins have been identified as important for interacting with and/or being able to modify the PINK1-Parkin pathway [231]. Notably, among these are proteins able to antagonise Parkin activity, such as the anti-apoptotic members of the Bcl-2 family Bcl-X or Mcl-1, or DUBs USP30 [241]

and USP15 [242]. On the other side, Parkin activity is induced by the deubiquitinase USP8 [243], and mitophagy is induced by its interaction with AMBRA1 [244], whose localization on the OMM induces mitophagy even in the absence of Parkin [203]. The relevance of Parkin-independent mitophagy activation has yet to be addressed in PD, as other ubiquitin ligases have been identified as able to mark mitochondria for removal. In fact, it has been proposed that PINK1-generated phospho-ubiquitin on mitochondria is the main signal for mitophagy and that Parkin acts as an amplifier in the system [245]. Parkin-mediated mitophagy is likely a rare event *in vivo* and acts only on severely damaged mitochondria only present when other mitochondrial quality control mechanism are insufficient or overwhelmed [246]. The importance of Parkin-mediated mitophagy to idiopathic PD is still not completely understood and other regulators of mitophagy might be involved in the onset and progression of neurodegenerative diseases [247]. However, the importance of mitochondrial quality control on all levels for neuronal survival and prevention of neurodegeneration is strongly supported by the elucidation of mechanism leading to PD.

4 Material and Methods

4.1 Materials

4.1.1 Equipment

Equipment	Manufacturer
CyAn ADP Analyzer	Beckman Coulter (Nyon, CH)
Easyject Plus Electroporator	Equibio Ltd (Belgium)
Odyssey CLx Imaging System	Li-Cor (DMP AG, Fehraltorf, CH)
Thermomixer comfort	VWR (Eppendorf, Basel, CH)
TProfessional TRIO Thermocycler	Analytik Jena (Reinach, CH)
Trans-Blot SD Semi-Dry Transfer Cell	Bio-Rad (Cressier, CH)
Nanodrop	Thermo Scientific (Waltham, USA)
Scale PM1200	Mettler Toledo (Zurich, CH)
Sterile filter 0.2 µM	Roth (Karlsruhe, D)
Thermomixer	Eppendorf (Hamburg, D)
Transfer-blot Semi-Dry Transfer cell	Biorad (Berkley, USA)
VisiScope	Visitron Systems (Puchheim, D)
Water bath	Memmert (Buchenbach, D)
Water purification system	Millipore (Billercia, USA)

Table 2: Equipment used during this study.

4.1.2 Reagents

Item	Order number	Supplier
1 Kb plus DNA ladder	10787018	TFS (Reinach, CH)
1,4-Dithiothreitol	6908	Carl Roth (Arlesheim, CH)
Acetic acid (glacial) 100 %	1000631000	Merck Millipore (Zug, CH)
Aceton	650501	Sigma-Aldrich (Buchs, CH)
Adenine	A3159	Sigma-Aldrich (Buchs, CH)
Agarose	2267.4	Carl Roth (Arlesheim, CH)
Amersham Protran 0.45 NC	10600002	GE Healthcare (Glattbrugg, CH)
Ammoniumperoxidsulfate	9592.3	Carl Roth (Arlesheim, CH)
Ampicillin sodium salt	K029.1	Carl Roth (Arlesheim, CH)
Aureobasidin A	630466	Sigma-Aldrich (Buchs, CH)
BCA protein assay kit	23225	TFS (Reinach, CH)
Bovine serum albumin Fraction V	8076.4	Carl Roth (Arlesheim, CH)
Bromophenol blue	1610404	Bio-Rad (Cressier, CH)
Calcium chloride dihydrate	C7902	Sigma-Aldrich (Buchs, CH)

CCCP	C2759	Sigma-Aldrich (Buchs, CH)
D-(-)-Mannitol	4175.1	Carl Roth (Arlesheim, CH)
D-(+)-Glucose	G7528	Sigma-Aldrich (Buchs, CH)
D-(+)-Saccharose	6421.1	Carl Roth (Arlesheim, CH)
dam-/dcm- E. coli	C2925l	NEB (Bioconcept, CH)
DAPI	6335.1	Carl Roth (Arlesheim, CH)
Digitonin	HN76.3	Carl Roth (Arlesheim, CH)
Dimethyl sulfoxide	D8418	Sigma-Aldrich (Buchs, CH)
DMEM	D5671	Sigma-Aldrich (Buchs, CH)
ECL Plus Substrate	32132	TFS (Reinach, CH)
EDTA	CN06.1	Carl Roth (Arlesheim, CH)
Ethidium bromide	1410433	Bio-Rad (Cressier, CH)
FBS	F7524	Sigma-Aldrich (Buchs, CH)
Fugene 6	E2691	Promega (Dübendorf, CH)
Medical X-ray Super RX-N	47410 19284	FujiFilm (Lucerna-Chem, CH)
Gel Cassettes	NC2015	TFS (Reinach, CH)
GenElute kit	G1N70-1KT	Sigma-Aldrich (Buchs, CH)
Gene Pulser Cuvettes	165-2086	Bio-Rad (Cressier, CH)
Glycerol	3783.1	Carl Roth (Arlesheim, CH)
Glycine	3790.3	Carl Roth (Arlesheim, CH)
HeLa cell line		LGC Standards (Wesel, D)
Hepes	H3375	Sigma-Aldrich (Buchs, CH)
Histidine		Sigma-Aldrich (Buchs, CH)
Hydrochloric acid	9277.1	Carl Roth (Arlesheim, CH)
Hypodermic Needles 25G	NN-2516R	Terumo (Spreitenbach, D)
Kanamycin sulfate	T832.2	Carl Roth (Arlesheim, CH)
Leucine	L8912	Sigma-Aldrich (Buchs, CH)
L-glutamine	G7513	Sigma-Aldrich (Buchs, CH)
LB broth	X968.3	Carl Roth (Arlesheim, CH)
Leupeptin	L2884	Sigma-Aldrich (Buchs, CH)
Magnesium sulfate	M7506	Sigma-Aldrich (Buchs, CH)
Manganese(II) chloride	T881.1	Carl Roth (Arlesheim, CH)
Matchmaker Gold Y2H System	630489	Clontech Laboratories
Methanol	4627.5	Carl Roth (Arlesheim, CH)
MF-Millipore Membrane Filter	VMWP02500	Merck Millipore (Zug, CH)
Mounting medium	H1000	Vector Labs (ReactoLab, CH)
MOPS	M1254	Sigma-Aldrich (Buchs, CH)
NEB 5-α *E. coli*	C2987I	NEB (Bioconcept, CH)
NSC-687852	ab142195	Abcam (Lucerna-Chem, CH)
TEMED	2367.2	Carl Roth (Arlesheim, CH)
N-Ethylmaleimide	E1271	Sigma-Aldrich (Buchs, CH)
NucleoSpin Gel/PCR Clean-Up	740609.250	Macherey-Nagel (Oensingen, CH)
NucleoSpin Plasmid	470588.250	Macherey-Nagel (Oensingen, CH)
Opti-MEM	11058021	TFS (Reinach, CH)
Orange G	O3756	Sigma-Aldrich (Buchs, CH)
Paraformaldehyde	28906	TFS (Reinach, CH)
PBS, 1x	D8537	Sigma-Aldrich (Buchs, CH)

PBS, 10x	70011036	TFS (Reinach, CH
Pepstatin A	P5318	Sigma-Aldrich (Buchs, CH)
Peptone	2366.2	Carl Roth (Arlesheim, CH)
Phenylmethanesulfonyl fluoride	78830	Sigma-Aldrich (Buchs, CH)
PEI MAX 40000	24765	Polysciences (Warrington, USA)
Potassium chloride (KCl)	P9311	Sigma-Aldrich (Buchs, CH)
Protease inhibitor cocktail	05892791001	Roche, CH
ProtA/G beads	E2512	Santa Cruz (Heidelberg, D)
RIPA buffer	89901	TFS (Reinach, CH)
Rotiphorese Gel 30 (Acrylamide)	3029.1	Carl Roth (Arlesheim, CH)
Rubidium chloride	4471.1	Carl Roth (Arlesheim, CH)
Superfrost microscope slides	10143560W90	TFS (Reinach, CH)
Sodium dodecyl sulfate (SDS)	2326.2	Carl Roth (Arlesheim, CH)
Sodium Chloride (NaCl)	3957.1	Carl Roth (Arlesheim, CH)
Sodium pyruvate	S8636	Sigma-Aldrich (Buchs, CH)
TopBlock	TB232010	LuBioScience (Luzern, CH)
Tris base	4855.2	Carl Roth (Arlesheim, CH)
Triton X 100	6683.1	Carl Roth (Arlesheim, CH)
Trypsin-EDTA	T3924	Sigma-Aldrich (Buchs, CH)
Tryptophan	T0254	Sigma-Aldrich (Buchs, CH)
TWEEN 20	P9416	Sigma-Aldrich (Buchs, CH)
Whatman GB003	WHA10427826	Sigma-Aldrich (Buchs, CH)
Whatman GB005	WHA10426994	Sigma-Aldrich (Buchs, CH)
Yeast extract	2904.1	Carl Roth (Arlesheim, CH)
X-αGal	630462	Sigma-Aldrich (Buchs, CH)

Table 3: Material used during thesis. Supplier TFS - Thermo Fisher Scientific, NEB-New England Biolabs.

4.1.2.1 Antibodies

Antibody	order no.	supplier	usage
mouse anti-cytochrome c	556432	BD (Allschwil, CH)	1:1000 IF
mouse anti-GAPDH	sc-32233	Santa Cruz (Heidelberg, D)	1:6000 WB
rabbit anti-GFP	G1544	Sigma-Aldrich (Buchs, CH)	1:4000 WB
rabbit anti-GFP	ab290	Abcam (Lucerna-Chem, CH)	1:500 IF
mouse anti-p97	MA3-004	TFS (Reinach, CH)	1:1000 IF
rabbit anti-Flag	PA1-984B	TFS (Reinach, CH)	1:1000 IF,WB
rabbit anti-UBXD1	ab80659	Abcam (Lucerna-Chem, CH)	1:1000 WB
mouse anti-Flag	F1804	Sigma-Aldrich (Buchs, CH)	1:1000 IF
mouse anti-myc	M5546	Sigma-Aldrich (Buchs, CH)	1:1000 IF
goat anti-mouse-Alexa546	11003	TFS (Reinach, CH)	1:1000
goat anti-rabbit-Alexa546	11010	TFS (Reinach, CH)	1:500
goat anti-mouse-Alexa680	11010	TFS (Reinach, CH)	1:500
goat anti-Rabbit-HRP	-	TFS (Reinach, CH)	1:20000
goat anti-Mouse-HRP	-	TFS (Reinach, CH)	1:20000

Table 4: Antibodies used during this work. Antibodies were used for immunofluorescence (IF) and Western blotting (WB). Supplier TFS - Thermo Fisher Scientific

4.1.2.2 Composition of buffers and media

4.1.2.2.1 2YT medium

NaCl	10 g/l
yeast extract	10 g/l
peptone	12 g/l
$MgSO_4$	20 mM
KCl	10 mM

$MgSO_4$ and KCl were added from sterile 1 M stock solutions after autoclaving.

4.1.2.2.2 6x Orange G DNA loading dye

Tris/HCl, pH 7.5	10 mM Tris/HCl
Orange G	0.15 % (w/v)
glycerol	60 % (v/v)

4.1.2.2.3 10x Laemmli running buffer (SDS-PAGE)

Tris base	30 g/l
glycine	144 g/l
SDS	10 g/l

4.1.2.2.4 2x Laemmli sample buffer

Tris/HCl, pH 6.8	125 mM
SDS	4 % (w/v)
glycerol	20 % (v/v)
Bromophenol blue	0.04 % (w/v)
dithiothreitol	100 mM (fresh before use)

4.1.2.2.5 PBS-T

10x PBS	10 %
Tween20	0.1 %

4.1.2.2.6 SOB media

peptone	2 % (w/v)
yeast extract	0.5 % (w/v)
NaCl	10 mM
KCl	2.5 mM
$MgCl_2$	10 mM
$MgSO_4$	10 mM

4.1.2.2.7 10x TAE buffer

Tris base	400 mM
acetic acid (glacial)	200 mM
EDTA	10 mM

4.1.2.2.8 Transformation buffer 1 (TFB 1)

$MnCl_2$	30 mM
RbCl	100 mM
$CaCl_2$	10 mM
glycerol	15 % (v/v)
	pH 5.8

4.1.2.2.9 Transformation buffer 2 (TFB 2)

MOPS	10 mM
RbCl	10 mM
$CaCl_2$	75 mM
glycerol	15 % (v/v)
	pH 6.8

4.1.2.3 Enzymes and nucleic acids

Name	order number	vendor
*Bam*HI	R0136	NEB (Bioconcept, CH)
*Eco*RI	R0101	NEB (Bioconcept, CH)
*Eco*RV	R0195	NEB (Bioconcept, CH)
*Hin*dIII	R0104	NEB (Bioconcept, CH)
*Nde*I	R0111	NEB (Bioconcept, CH)
*Nhe*I	R0131	NEB (Bioconcept, CH)
*Not*I	R0189	NEB (Bioconcept, CH)
*Xho*I	R0146	NEB (Bioconcept, CH)
Phusion Polymerase	M0530	NEB (Bioconcept, CH)
T4 DNA ligase	M0202	NEB (Bioconcept, CH)
Shrimp alkaline phosphatase	M0371	NEB (Bioconcept, CH)

Table 5: DNA modifying enyzmes used during this study. Supplier NEB - New England Biolabs.

4.1.2.4 Oligonucleotides

Name	Sequence
OAN2020	TCATCTCTCGAGCTATGAAGAAATTCTTTCAGGAGTTCAAG
OAN2021	TGTACTAAGCTTTCACAAGAGCTTCTCGATGGCT
OAN2022	TCATCTGAATTCATGGATTACAAGGATGACGACGA
OAN2024	TCTATCCTCGAGTCACCGCTTGATCTCCTCTGCTGT
OAN2025	TGTACTGGATCCTGAGCCACCTGAGCCACCGTTGAACGTGTAGATCTTCA TGAT
OAN2333	GTCCGGACTCAGATCTCGAG
OAN2334	AGATGAGAATTCTCAATTGTTTTTTCTCAGCTGAATAATTTTGATAAAGG CGCCCAGGGAGAACACGCCAATAGCCAGCATGGCGAGAATCAGCAAGAGC TTCTCGATGGCTG
OAN2398	AGATGACATATGAAGAAATTCTTTCAGGAGTTCAAGG
OAN2399	TCATCTGGATCCTCACAAGAGCTTCTCGATGGC
OAN2400	AGATGACATATGAAGAAATTCTTTCAGGAGTTCAAGGC
OAN2401	TCATCTGCGGCCGCTCACAAGAGCTTCTCGATGGC
OAN2402	TCATCTGGATCCTCACCGCTTGATCTCCTCTG
OAN2403	AGATGACATATGTCGCAGGACACCATCCG
OAN2404	AGATGACATATGCGGGAGCAGAGGCTCAGG
OAN2412	GCTCGTAAGCTTATGGATTACAAGGATGACGACGATAAGTCGCAGGACAC CATCCG

OAN2413	GCTCGTAAGCTTATGGATTACAAGGATGACGACGATAAGCGGGAGCAGAG GCTCAGG
OAN2414	TCATCTGATATCTCACAAGAGCTTCTCGATGGC
OAN2415	AGATGAGCTAGCATGTCCGTCCTG
OAN2416	AGATGAAAGCTTTCAGATCTTCTTCAGAGATGAGTTTCTGCTCAGGGCCG GGATTCTCCTCCACGTCACCGCATGTTAGAAGACTTCCTCTGCCCTCCTT GTACAGCTCGTCCATGC
OAN2504	CTTGAAGCTTAGACATGGTGAGCAAGGGC
OAN2505	GGCTGGATCCTCAATTGTTTTTTCTCAGCTGAATAATTTTGATAAAGGCG CCCAGGGAGAACACGCCAATAGCCAGCATGGCGAGAATCAGCTTGTACAG CTCGTCCATG
OAN2518	AGATGAGCTAGCATGTCCGTCCTGACG
OAN2519	AGATGAAAGCTTTCAGATCTTCTTCAGAGATGAGTTTCTGCTCAGGGCCG GGATTCTCCTCCACGTCACCGCATGTTAGAAGACTTCCTCTGCCCTCACC GAGCAAAGAGTGGG
OAN2675	TCATCTCTCGAGTTATGTGGGGCCCCAGGC
OAN2272	CACCGCCTTGATGAGCCGCTCCCAA
OAN2273	AAACTTGGGAGCGGCTCATCAAGGC
OAN2569	AGATGACTCGAGATGTTTGGCCCCGCTAAAG
OAN2570	TCATCTAAGCTTCACTTCTCCAAAGTTGGTATGGC
OAN2571	AGATGACTCGAGATGGAAACATTACATATAATTTATTCAGAAGCAAAGTC TTTTACAGTGGAGGGGCTGTCCAGCCGG
OAN2656	AGATGACATATGTTTGGCCCCGCTAAAG
OAN2657	AGATGACTCGAGATGGAAACATTACATATAATTTATTCAGAAGCAAAGTC TTTTACAGTGGAGGGGCTGTCCAGCCGG
OAN2658	AGATGACATATGGAAACATTACATATAATTTATTCAGAAGC
OAN2661	TCATCTAAGCTTACGTTTAGTAAATGCAGGTGAACTTCTG
OAN2662	AGATGACTCGAGATGGAAACATTACATATAATTTATTCAGAAGCAAAG
OAN2663	AGATGACTCGAGATGGGTGCTTCTAGTTACGTCAGGGAA
OAN2664	AGATGACTCGAGATGTTCCCTGATCCAGATACACCTCC
OAN2665	AGATGACTCGAGATGACCCTGAGATGCATGGTATGTCA

Table 6: Oligonucleotides used in this study were purchased from Sigma-Aldrich.

4.1.2.5 Plasmids

Name Vector	Description Insert
pAN940 gift from Richard Youle	YFP-Parkin
pAN941 gift from Richard Youle	^{mcherry}Parkin

pGBKT7 Matchmaker (Clontech)	GAL4BD (bait)
pGADT7 Matchmaker (Clontech)	GAL4AD (prey)
pAN3198 gift from Michael Davidson	mKeima (Addgene #56018)
pAN2741 pcDNA3.1+-DYK	^{FLAG}UBXD1 UBXD1 (Genscript: OHu09321)
pAN2861 EYFP-C1 (Clontech)	YFP-UBXD1 pAN2741 PCR: OAN2020/2021
pAN2862 pcDNA3.1 *EcoRI, HindIII	^{FLAG}UBXD1DPUB pAN2741 PCR: OAN2022/2025 *EcoRI, HindIII
pAN2863 pcDNA3.1 *EcoRI, XhoI	^{FLAG}UBXD1DUBX pAN2741 PCR: OAN2022/2024 *EcoRI, XhoI
pAN3104 pAN2741*HindIII, EcoRV	^{FLAG}UBXD1DVIM pAN2741 PCR: OAN2412/14 *HindIII, EcoRV
pAN3105 pAN2741*EcoRV, HindIII	^{FLAG}UBXonly pAN2741 PCR: OAN2413/14 *HindIII, EcoRV
pAN3307 pAN2855 *EcoRI/XhoI	FLAG-VIMonly pAN2741 PCR: OAN2022/2675 *EcoRI/XhoI
pAN3080 pAN2861 *XhoI, EcoRI	YFP-UBXD1-ActA pAN2861 PCR: OAN2333/2334 *XhoI, EcoRI
pAN3187 pcDNA3 *BamHI, HindIII	YFP-ActA YFP-C1 PCR: OAN2504/2505 *BamHI, HindIII
pAN3090 pGBTK7 *NdeI, BamHI	GAL4BD-UBXD1 pAN2861 PCR: OAN2398/9 *NdeI, BamHI
pAN3091 pGBTK7 *NdeI, NotI	GAL4BD-UBXD1DPUB pAN2862 PCR: OAN2400/01 *NdeI,NotI
pAN3092 pGBTK7 *NdeI, BamHI	GAL4BD-UBXD1DUBX pAN2863 PCR : OAN2400/02 *NdeI, BamHI
pAN3093 pGBTK7 *NdeI, BamHI	GAL4BD-UBXD1DVIM pAN2861 PCR: OAN2403/2399 *NdeI, BamHI
pAN3094 pGBTK7 *NdeI, BamHI	GAL4BD-UBXonly pAN2861 PCR: OAN2404/2399 *NdeI, BamHI
pAN3103 pAN940*NheI, HindIII	mitoYFP-T2A-^{3xmyc}Parkin mitoYFP PCR: OAN2415/2416 *NheI, HindIII
pAN3216 pAN940 *NheI, HindIII	mKeima-T2A-^{3xmyc}Parkin pAN3198: OAN2518/2519 *NheI, HindIII
pX45945 gift from Feng Zhang	pSpCas9(BB)-2A-Puro (Addgene # 48139)
pAN3046 pX459 *BbsI	UBXD1-CRISPR/Cas9 Annealed OAN2272/2273
pAN3225 pCR-XL-TOPO	Homo sapiens YOD1 cDNA BC137167-seq-TCHS1003-GVO-TRI Biocat
pAN3238	YOD1isoform 1-mCherry

mCherry-N1*XhoI, HindIII	pAN3225 PCR: OAN2569/70 *XhoI, HindIII
pAN3239	YOD1isoform 2-mCherry
pmCherry-N1*XhoI, HindIII	pAN3225 PCR: OAN2571/70 *XhoI, HindIII
pAN3283	pGBTK7-YOD1-1 full length
pGBTK7 *NdeI, BamHI	pAN3238 PCR: OAN2656/57 *NdeI, BamHI
pAN3284	pGBTK7-YOD1-2 full length
pGBTK7*NdeI, BamHI	pAN3239 PCR: OAN2658/57 *NdeI, BamHI
pAN3285	pGADT7-YOD1-1 full length
pGADT7*NdeI, BamHI	pAN3238 PCR: OAN2656/57 *NdeI, BamHI
pAN3286	pGADT7-YOD1-2 full length
pGADT7 *NdeI, BamHI	pAN3239 PCR: OAN2658/57 *NdeI, BamHI
pAN3292	YOD1-1 aa 1-136-mCherry
pAN3238 *XhoI, HindIII	pAN3238 PCR: OAN2569/2661 *XhoI, HindIII
pAN3293	YOD1-2 aa 1-92-mCherry
pAN3238 *XhoI, HindIII	pAN3239 PCR: OAN2662/2661 *XhoI, HindIII
pAN3294	YOD1 aa 93-304-mCherry
pAN3238 *XhoI, HindIII	pAN3239 PCR: OAN2663/2570 *XhoI, HindIII
pAN3295	YOD1 aa 231-304-mCherry
pAN3238 *XhoI, HindIII	pAN3239 PCR: OAN2664/2570 *XhoI, HindIII
pAN3296	YOD1 aa 273-304-mCherry
pAN3238 *XhoI, HindIII	pAN3239 PCR: OAN2665/2570 *XhoI, HindIII
pAN3297	YOD1-1 - 3xFLAG
pAN3238 *BamHI, NotI	Annealed OAN2666/7
pAN3298	YOD1-2 - 3xFLAG
pAN3239 *BamHI, NotI	Annealed OAN2666/7
pAN3300	YOD1-1 - mCherry-ActA
pAN3238 *BamHI, NotI	pmCherry-N1 PCR: OAN2668/9 *BamHI, NotI
pAN3301	YOD1-2 - mCherry-ActA
pAN3239 *BamHI, NotI	pmCherry-N1 PCR: OAN2668/9 *BamHI, NotI

Table 7: Plasmids used in this study.

4.2 Methods

4.2.1 Molecular biological methods

4.2.1.1 Bacterial strains The *Escherichia coli* (*E. coli*) strains DH5α and dam$^-$/dcm$^-$ *E. coli* were used for cloning as well as amplification of plasmid DNA. Both strains were grown in Luria-Bertani media (LB) and on LB agar plates supplemented with the appropriate antibiotic for selection. Antibiotics used were ampicillin (100 µg /ml) or kanamycin (50 µg/ml).

4.2.1.2 Preparation of chemically competent *E. coli* 6 ml of 2YT medium were inoculated with either DH5αor dam-/dcm- E. coli strain and grown overnight. This culture was diluted 1:100 in 10 ml 2YT medium and grown to OD_{600} = 0.5. This new culture was diluted 1:100 in 100 ml 2YT medium, grown again until OD_{600} = 0.5 and then chilled for 10 minutes in an ice-water bath. Bacteria were spun down in a pre-cooled centrifuge at 2000 g and 4 °C for 7 minutes. The pellet was resuspended in ice-cold transformation buffer 1 and chilled in an ice-water bath for 10 minutes. Bacteria were again spun down in a pre-cooled centrifuge at 2000 g and 4 °C for 7 minutes, and the pellet was resuspended in 2 ml of ice-cold transformation buffer 2. The bacterial suspension was aliquoted on dry ice in 50 µl increments and immediately stored at -80 °C.

4.2.1.3 Preparation of electrocompetent *E. coli* DH5α or dam-/dcm- *E. coli* were grown overnight in 6 ml LB medium and used to inoculate 400 ml LB medium at 1:100. This new culture was grown until OD_{600}=0.5 and then chilled for 20 minutes in an ice-water bath. Bacteria were spun down in a pre-cooled centrifuge at 2000 g and 4 °C for 20 minutes. The bacterial pellet was resuspended in 400 ml ice-cold water and spun down again in a pre-cooled centrifuge at 2000 g and 4 °C for 10 minutes. After repetition of this washing step for a total of two washes, the bacterial pellet was resuspended in 1 ml of ice-cold LB medium containing 10 % glycerol. 50 µl aliquots were prepared on dry ice and immediately stored at -80 °C.

4.2.1.4 Polymerase chain reactions (PCR) Polymerase chain reaction is a method for exponential amplification of a defined DNA-sequence by a thermo stable DNA-polymerase [248].

component	PCR1	PCR2	PCR3	PCR4
template (< 250 ng)	1 µl	1 µl	1 µl	1 µl
oligonucleotide 1 (10 µM)	2.5 µl	2.5 µl	2.5 µl	
oligonucleotide 2 (10 µM)	2.5 µl	2.5 µl	2.5 µl	
dNTPs (2 mM each)	5 µl	5 µl	5 µl	5 µl
5x HF buffer	5 µl	5 µl	-	-
5x GC buffer	-	-	5 µl	5 µl
DMSO	-	1.5 µl	-	1.5 µl
Phusion polymerase	0.5 µl	0.5 µl	0.5 µl	0.5 µl
water	ad 50 µl	ad 50 µl	ad 50 µl	ad 50 µl

Table 8: Pipetting scheme for optimization of DNA amplification using Phusion polymerase. For DNA cloning purposes, DNA was amplified by PCR using high fidelity Phusion polymerase. Four different conditions were tested. The condition with the most optimal DNA amplification was chosen for further processing.

	temperature	time
1x	98 °C	30 s
35x	98 °C	15 s
	annealing	30 s
	68 °C	60s/kb
1x	10 °C	∞

Table 9: Temperature profile for DNA amplification using Phusion polymerase. The annealing temperature was chosen based on the recommendation the web-based NEB tm calculator (https://tmcalculator.neb.com). PCR amplified DNA was separated from free oligonucleotides through agarose gel electrophoresis and purified using NucleoSpin Gel and PCR Clean-Up according to the manufacturer's recommendations.

4.2.1.5 DNA digestion For cloning purposes, plasmid DNA was treated with restriction enzymes. To this end, between 0.5 and 5 µg of plasmid DNA was treated with 1 to 10 U of restriction enzyme for at least 1 h at the manufacturer recommended temperature and buffer conditions. DNA obtained through PCR amplification was digested overnight to improve digestion at the 5' and 3' ends. Whenever possible and were indicated, double digestion using two or more restriction enzymes were performed according to the manufacturer's instructions. Digested DNA was purified using agarose gel electrophoresis (4.2.1.9) followed by Machery and Nagel's NucleoSpin Gel and PCR Clean-Up kit.

4.2.1.6 DNA ligation For DNA ligations, vector DNA and insert DNA obtained by DNA digestion (4.2.1.5) were mixed at a 1:3 ratio, 1 µl of T4 DNA ligase and 2 µl of the appropriate buffer (Thermo Fisher Scientific) in a total reaction volume of 20 µl were added. The ligation mix was incubated at room temperature overnight, which was followed by transformation into DH5α or dam$^-$/dcm$^-$ *E. coli* (4.2.1.7).

4.2.1.7 DNA transformation into chemically competent *E. coli* Competent DH5α or dam$^-$/dcm$^-$ *E. coli* were thawed on ice. 3 µl of DNA ligation mix (4.2.1.6) was added to 40 µl of competent bacteria and incubated for 30 minutes on ice. Heat shock was carried out by incubating the reaction mix for 45 seconds at 42 °C, immediately followed by cooling for 2 minutes on ice. The transformed bacteria were resuspended in 900 µl SOC medium and shaken at 700 rpm and 37 °C in a Thermomixer. An aliquot of the transformation mix was spread on LB plates containing an appropriate antibiotic and incubated at 37 °C overnight.

4.2.1.8 DNA plasmid isolation After DNA transformation, several *E.coli* clones grown on LB plates were picked for verification. Each clone was used to inoculate 5 ml of LB medium containing the appropriate antibiotic and incubated overnight at 37 °C and 250 rpm. Machery-Nagel's NucleoSpin Plasmid kit was used to isolate plasmid DNA. DNA digestion (4.2.1.5) with appropriate restriction enzymes followed by agarose gel electrophoresis (4.2.1.9) was performed to select correct clones. Correct clones were verified by sequence analysis (Microsynth, Basel, CH).

4.2.1.9 Agarose gel electrophoresis Agarose gels were prepared from 0.7 % (w/v) agarose diluted in 50 ml TAE buffer supplemented with 0.5 µg/ml ethidium bromide. Plasmid DNA was mixed with DNA loading dye, and gel electrophoresis was carried out at 85 V for 45 minutes. For purification of DNA fragments, NucleoSpin Gel and PCR Clean-Up kit (Machery-Nagel) was used according to manufacturer's recommendations.

4.2.1.10 Phosphatase treatment of DNA Vector DNA for ligation reactions was treated with shrimp alkaline phosphatase (SAP) to minimize vector religation. After DNA digestion of plasmid DNA (4.2.1.5) and before purification, 1 µl of TSAP with 2 µl of 10x buffer was added to the reaction mix and incubated at 37 °C for 15 minutes. SAP was inactivated by incubation at 74 °C for 15 minutes. The reaction product was purified via agarose gel electrophoresis (4.2.1.9) followed by Machery-Nagel's NucleoSpin Gel and PCR Clean-Up kit.

4.2.1.11 Yeast two hybrid In a Matchmaker GAL4-based two-hybrid assay, a bait protein is expressed as a fusion to the Gal4 DNA-binding domain (DNA-BD), while libraries of prey proteins are expressed as fusions to the Gal4 activation domain. The essay is based on the reconstitution of a functional transcription factor when two proteins or polypeptides of interest interact (Figure 5). This takes place in genetically modified yeast strains, in which the transcription of a reporter gene leads to a specific phenotype, usually growth on a selective medium or change in the color of the yeast colonies [249]. A downstream analysis in order to quantify the effects of point mutations on the strength of interaction was used. In this way, the Gal-responsive LacZ gene (b-galactosidase) integrated in Y187 was implemented as a reporter for quantitative studies of protein-protein interactions because has in this strain expresses strongly.

4.3 Biochemical methods

4.3.1 Preparation of cell lysates

Cells were harvested and cell pellets were stored on ice for immediate use or at -80 °C for several days. For lysis, pellets were resuspended in RIPA buffer supplemented with protease inhibitor cocktail and incubated on ice for 15 minutes. After incubation on ice, samples were centrifuged at 14000 g for 15 minutes. Supernatants were mixed with 2x Laemmli sample buffer supplemented with 50mM DTT and heated to 95 °C for 10 minutes.

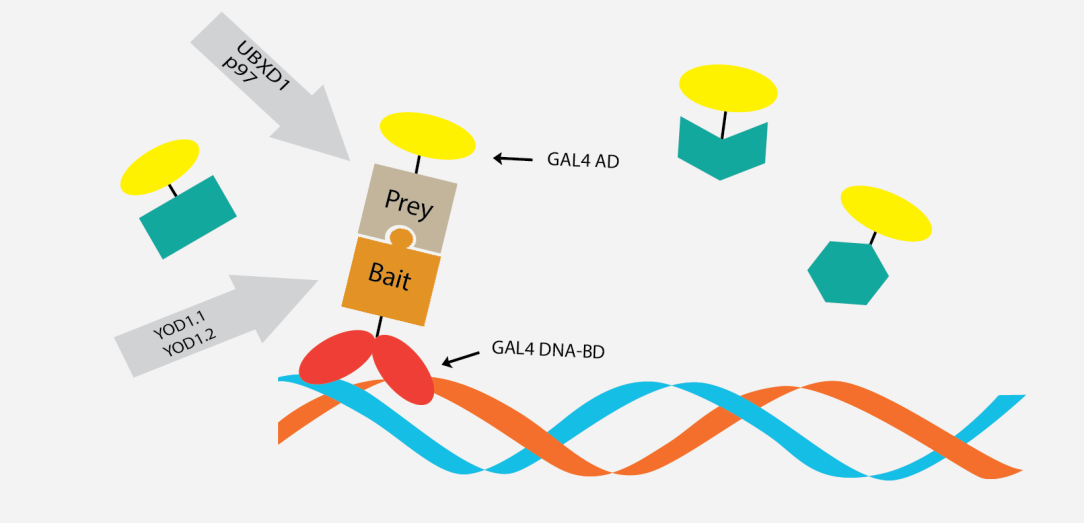

Figure 5: The yeast-two-hybrid (Y2H) principle. Two proteins are expressed separately, one (a bait protein) fused to the Gal4 DNA-binding domain (BD) for YOD1 (both isoforms) and the other (a prey protein) fused to the Gal4 transcriptional activation domain (AD) –p97 and UBXD1.

4.3.2 Measurement of protein content

During preparation of cell lysates (4.3.1), 10 µl of the supernatant obtained after centrifugation were removed and diluted 1:10 in ddH2O. This diluted sample was used to measure protein content using the Pierce BCA protein assay kit (Thermo Fisher Scientific) according to manufacturer's recommendations. Briefly, 25 µl of sample and eight BCA reference solutions were added in triplicate to a 96 well plate. 200 µl of BCA Working Reagent was added to each well, followed by incubation at 37 °C for 30 minutes. Absorption at 562 nm was measured on an ELISA reader to calculate protein content of the sample.

4.3.3 SDS PAGE

Sodium dodecyl sulfate polyacrylamide gel electrophoresis (SDS-PAGE) is a method used to distribute proteins on an acrylamide gel according to their size. Gels consisting of a 4 % (w/v) acrylamide stacking gel overlaid on a 7 %, 9 % or 12 % (w/v) acrylamide resolving gel were prepared in plastic 1.5 mm gel cassettes. Samples loaded onto the gels were separated at 120 V for 110 minutes in Laemmli running buffer.

0.5 M Tris/HCl pH 6.8	2.5 ml
10 % SDS	100 µl
30 % acrylamide	1340 µl
10 % APS	200 µl
TEMED	10 µl
ddH2O	6 ml

Table 10: Preparation of stacking gels for SDS-PAGE.

component for	7 % gels	9 % gels	12 % gels
1.5 M Tris/HCl pH 8.8	5 ml	5 ml	5 ml
10 % SDS	200 µl	200 µl	200 µl
30 % acrylamide	4.7 ml	6 ml	8 ml
10 % APS	135 µl	135 µl	135 µl
TEMED	13 µl	13 µl	13 µl
ddH2O	10 ml	8.7 ml	6.7 ml

Table 11: Preparation of gels with different resolving power for SDS-PAGE.

4.3.4 Western blotting

Western blotting is a method to transfer proteins from an SDS-PAGE gel to a nitrocellulose membrane and was performed on a Trans-Blot SD Semi-Dry Transfer Cell (Bio-Rad). After blotting, nitrocellulose membranes were blocked in PBS-T containing 3 %

(w/v) TopBlock for 1 h to reduce nonspecific antibody binding. Primary antibody was added to the membranes in PBS-T/TopBlock and incubated with gentle shaking at 4 °C overnight. After three washes in PBS-T, secondary HRP-coupled antibody diluted in PBS-T/TopBlock was added to the membrane and incubated with gentle shaking for 2 h, after which the membrane was washed three times with PBS-T. Proteins were detected using a chemiluminescent substrate.

4.3.5 Immunoprecipitation

Cells were lysed for 20 min on ice using IP Buffer consisting of 50 mM Tris-HCl, pH 7.5, 150 mM NaCl, 2 mM ethylenediaminetetraacetic acid (EDTA), 0.75 % NP40. After centrifugation (14000 g; 10 min; 4 °C) supernatant was collected and immunoprecipitation assays were performed. Supernatant was incubated with anti-myc antibody against 3xmyc-tagged p97 for 2 h at 4 °C under constant rotation following immobilization onto A/G PLUS Agarose Beads for 2h at 4 °C. After seven washing steps with IP buffer, SDS page was performed according to a standard protocol. The following antibodies were used for detection: mouse α-p97 (1:3000); rabbit α-FLAG (1:3000); mouse α-GAPDH (1:3000); anti-rabbit HRP (1:20000); anti-mouse HRP (1:20000). Immunopurified proteins were detected by Western blot.

4.3.6 Extraction of genomic DNA

Genomic DNA was extracted from cells using the GenElute Mammalian Genomic DNA Miniprep kit according to the manufacturer's recommendations.

4.4 Cell Biology Methods

4.4.1 Cell culture

All cell lines were grown in a humidified incubator at 5 % CO2 and 37 °C. HeLa cells were maintained in (Dulbecco's modified Eagle's media (DMEM)) supplemented with

10 % fetal bovine serum (FBS), 1 mM sodium pyruvate and 2 mM L-glutamine. Cells were passaged after reaching 90 % confluency by removing growth medium, washing once with PBS and incubating with Trypsin/EDTA at 37 °C until cells had detached. Trypsin/EDTA was inactivated by adding medium 1:1. The solution was centrifuged at 1000g for 3 minutes and the cell pellet was re-suspended in fresh medium. Cells were distributed into new tissue culture containers as required. For western blot experiments and flow cytometry, cells were grown in tissue culture dishes. For single cell cloning experiments, cells were grown in 96 well tissue culture plates. For immunocytochemistry, cells were grown on circular coverslips suspended in 6 well tissue culture plates. To induce mitophagy, HeLa cells were treated with 50 µM carbonyl cyanide m-chlorophenyl hydrazine (CCCP)

4.4.2 Induction of mitophagy

For measurements of mitochondrial membrane potential via flow cytometry induction of mitophagy and Parkin recruitment, cells were treated where applicable with 50 µM CCCP for 12 hours before measurement.

4.4.2.1 Transfection of mammalian cells For confocal microscopy, cells were transfected with Fugene 6. Cells were grown on circular coverslips suspended in 6 well tissue culture plates or on Nunc Lab-Tek chamber slides. After 24 h at approximately 60 % confluency, cells were transfected as follows. 3 µl Fugene 6 was added to 100 µl Opti-MEM in an Eppendorf Safe-Lock tube while minimizing direct contact of Fugene 6 to plastic surfaces. After incubation at room temperature for 5 minutes, 1 µg of plasmid DNA was added to the solution, which was incubated for another 15 minutes at room temperature. Finally, the solution was added dropwise to the cells. 24 h after transfection, cells were either fixed for immunocytochemistry. All other transfections were done using linear polyethylenimine (PEI). PEI MAX 40000 was dissolved 0.1 % (w/v) in ddH2O adjusted to pH 7 with NaOH and stored at 4 °C. Cells were grown for 24 h before

transfection with PEI [250]. PEI and plasmid DNA were added to Opti-MEM in a ratio of 2:1. The solution was incubated at room temperature for 30 minutes and added to the cells. After 4 h the medium was exchanged. Cells were grown for an additional 24 h before obtaining lysates.

4.4.2.2 Knockdown of UBXD1 using CRISPR/Cas9 CRISPR consists of two components: a guideRNA (gRNA) and a non-specific CRISPR-associated endonuclease (Cas9). The gRNA is a short synthetic RNA composed of a scaffold sequence necessary for Cas9-binding and a user-defined 20 nucleotide targeting sequence which defines the genomic target to be modified. CRISPR was originally employed to knock-out target genes in various cell types and organisms, but modifications to the Cas9 enzyme have extended the application of CRISPR to selectively activate or repress target genes, purify specific regions of DNA, and even image DNA in live cells using fluorescence microscopy. The genomic target can be any 20 nucleotide DNA sequence, provided it meets two conditions: The sequence is unique compared to the rest of the genome and the target is present immediately upstream of a protospacer adjacent motif (PAM). The PAM sequence is absolutely necessary for target binding and the exact sequence is dependent upon the species of Cas9 (5' NGG 3' for Streptococcus pyogenes Cas9) (Figure 6). Once expressed, the Cas9 protein and the gRNA form a riboprotein complex through interactions between the gRNA "scaffold" domain and surface-exposed positively-charged grooves on Cas9. Cas9 undergoes a conformational change upon gRNA binding that shifts the molecule from an inactive, non-DNA binding conformation, into an active DNA-binding conformation. The Cas9-gRNA complex will bind any genomic sequence with a PAM, but the extent to which the gRNA spacer matches the target DNA determines whether Cas9 will cut. Once the Cas9-gRNA complex binds a putative DNA target, a seed sequence at the 3' end of the gRNA targeting sequence begins to anneal to the target DNA. If the seed and target DNA sequences match, the gRNA will continue to anneal to the target DNA in a 3' to 5' direction. In this study, using CRISPR/Cas9, UBXD1 was targeted in HeLa cells and several alleles of UBXD1 were replaced with a reporter cassette coding for secreted

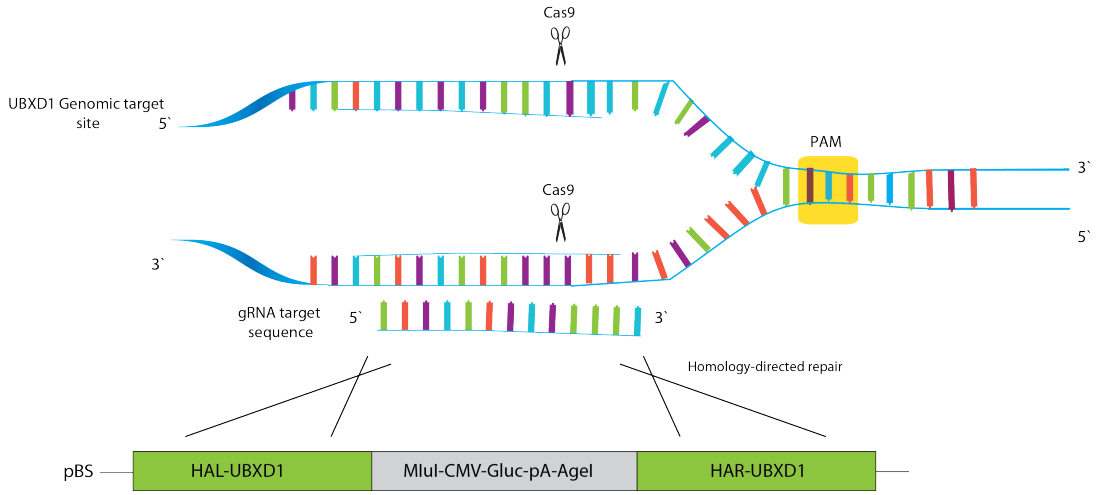

Figure 6: Schematic representation of CRISPR/Cas9 strategy for UBXD1 knockdown. Using CRISPR/Cas9, UBXD1 was targeted in HeLa cells and several alleles of UBXD1 were replaced with a reporter cassette coding for secreted Gaussia luciferase. Each gRNA needs homology arms (use 800 bp immediately CRISPR tream and downstream of the target). CMV promoter and Gluc gene were knock in for fast screening of single clones.

Gaussia luciferase. Gaussia luciferase is secreted into the cell culture media and the light output generated by the luciferase reaction can be correlated to the amount of Gaussia luciferase protein produced. In this way the activity of the promoter driving Gaussia expression was measured. PCR analysis and western blot (anti-UBXD1) were performed to confirm knockdown of UBXD1.

4.4.2.3 Immunocytochemistry Cells grown on circular coverslips suspended in 6 well tissue culture at a density of 30000 cells per well and where applicable transfected or treated were washed once in PBS. Cells were suspended in 4 % paraformaldehyde / PBS for 15 minutes at room temperature. Cells were washed again in PBS and suspended in 0.15 % Triton X 100 / PBS for 15 minutes at room temperature. Cells were re-suspended in 10 % bovine serum albumine (BSA)/PBS for 1 h. The primary antibody was added as indicated in 10 % BSA/PBS and cells were incubated at 4 °C overnight. Cells were washed three times in 10 % BSA/PBS, and the secondary antibody was added as indicated in 10 % BSA/PBS. Cells were incubated at room temperature for 2 h and finally washed three times in PBS before being mounted on Superfrost microscope slides with Vectashield mounting medium.

4.4.2.4 Confocal microscopy Confocal images were obtained on a Visitron, Spinning Disk, confocal laser scanning microscope fitted with 405 nm, 458 nm, 488 nm, 514 nm, 543 nm and 633 nm laser lines using 63x/1.40 oil DIC objective.

4.4.2.5 Image analysis Image analysis was done using the Fiji distribution of ImageJ [251].

4.4.2.6 Flow cytometric analysis of mitophagy HeLa cells were grown in 10cm culture plates and transfected with mKeima and Parkin (mKeima-T2A-^{3xmyc}Parkin) as well as UBXD1 or control vector were treated with CCCP or left untreated as indicated. 24 h after induction and treatment, cells were harvested using Trypsin/EDTA, washed with PBS and equal numbers of cells for each condition were transferred to Eppendorf Safe-Lock tubes. Cells were gated to exclude debris (FlowJo) and cells not expressing mKeima (488 nm). To quantify mitophagy, cells expressing mKeima and transfected with vector control without CCCP treatment were used to establish mKeima561nm/mKeima488nm threshold. Using R, a linear model was established based on the mean of the 99th percentile mKeima561nm for each mKeima488nm value using the R quantreg package. Cells above the mKeima561nm/mKeima488nm threshold were counted to determine percentage of cells with above control mitophagy levels.

4.4.2.7 Assessing cytochrome release HeLa cells grown in Nunc Lab-Tek chamber slides, fixed and stained with mouse anti cytochrome c and anti mouse Alexa546-labeled antibodies. Cells were assessed in a blinded manner by confocal microscopy. Apoptosis is accompanied by the release of mitochondrial cytochrome c into the cytosol. Therefore, randomly chosen YFP-positive cells were classified after their cytochrome c localization as either sharply defined mitochondrial or unspecific cytosolic.

4.4.2.8 Statistical methods All experiments were performed independently at least three times. Statistical significance was assessed by ANOVA with posthoc two-tailed Stu-

dent's t-test using Bonferroni or Holm adjustment to account for multiple comparisons. P-values > 0.05 are marked with n.s., $p < 0.05$ with *, $p < 0.01$ with **, $p < 0.001$ with ***.

5 Results

5.1 Identification of p97 cofactors involved in mitochondrial maintenance

Failing mitochondrial quality control is connected to aging and neurodegeneration [43]. Mounting evidence connects the UPS with mitochondrial maintenance [252, 253] in a process termed OMMAD. Recently, the ATPase associated with various cellular activities (AAA-ATPase) p97 was connected to OMMAD and likely constitutes the retrotranslocase for the extraction of mitochondrial proteins for proteasomal degradation in the cytosol [254, 255]. Furthermore, p97 was recently connected to the execution of mitophagy, another important mitochondrial quality control pathway [254]. As diverse p97 functions are governed by interaction with a plethora of cofactors, the mitochondrial translocation of UBX domain-containing p97 cofactors under mitophagic conditions was investigated to elucidate the cofactor requirements of p97 to perform its function at the interface between OMMAD and mitophagy.

5.1.1 Subcellular localization of p97 cofactors under mitophagic conditions

In order to identify mitochondrial cofactors of p97, a list of all known and suspected p97 cofactors was compiled (Table 12). Thirteen proteins with known or suspected connection to p97 were identified. Except for Ufd1 and Npl4, no mitochondrial function was suggested in the literature so far [256] . For all candidates except Ufd1 and Npl4, open reading frames were obtained and cloned into mammalian expression vector pcDNA3.1*-DYK leading to the expression of FLAG epitope-tagged protein. Subsequent transfection

name	Gene ID	localization	localization CCCP/Parkin
UBXN8	7993	ER	ER
UBXN7	26043	Nucleus	Nucleus
UBXN9	79058	Cytosol	Cytosol
Derlin-1	79139	ER	ER
UBXD5	91544	ER	ER
VIMP	55829	ER	ER
UBXD3	127733	Cytosol	Cytosol
UBXD4	165324	Cytosol	Cytosol
UBXD1	80700	Cytosol	mitochondrial
SAKS1 (UBXN1)	51035	Cytosol	mitochondrial
Erasin (UBXN4)	23190	ER	mitochondrial

Table 12: **UBX-domain containing p97 cofactors analyzed for mitochondrial localization.** Eleven p97 cofactors were cloned as FLAG fusion proteins and their subcellular localization under normal and mitophagic conditions (co-transfection with Parkin and CCCP treatment) was determined.

of these expression constructs into HeLa cells together with ^{mcherry}Parkin followed by staining for FLAG-tagged p97 cofactors revealed in the absence of the mitophagic inducer CCCP staining patterns typical for cytosolic, nuclear or ER localization (Table 12, Figure 7). Upon addition of CCCP for 6 h three of the eleven p97 cofactors analyzed displayed co-localization with ^{mcherry}Parkin. As CCCP induces the translocation of Parkin to mitochondria, this was indicative for a potential mitochondrial translocation of UBXD1, SAKS1 and Erasin under mitophagic conditions.

5.1.2 Localization of p97 cofactors UBXD1, SAKS1, and Erasin

To confirm the suspected mitochondrial translocation of UBXD1, SAKS1, and Erasin under mitophagic conditions, subcellular colocalization studies between FLAG-tagged UBXD1, SASK1, and Erasin and mitochondria-targeted mitoDsRed were performed (Figure 8). While all three cofactors did not colocalize with mitoDsRed in the absence of CCCP, following induction of mitophagy by addition of CCCP UBXD1, SAKS1, and Erasin displayed overlap with mitoDsRed in YFP-Parkin expressing cells. This data strongly suggested an involvement of UBXD1, SAKS1, and Erasin together with their effector p97 in mitophagy.

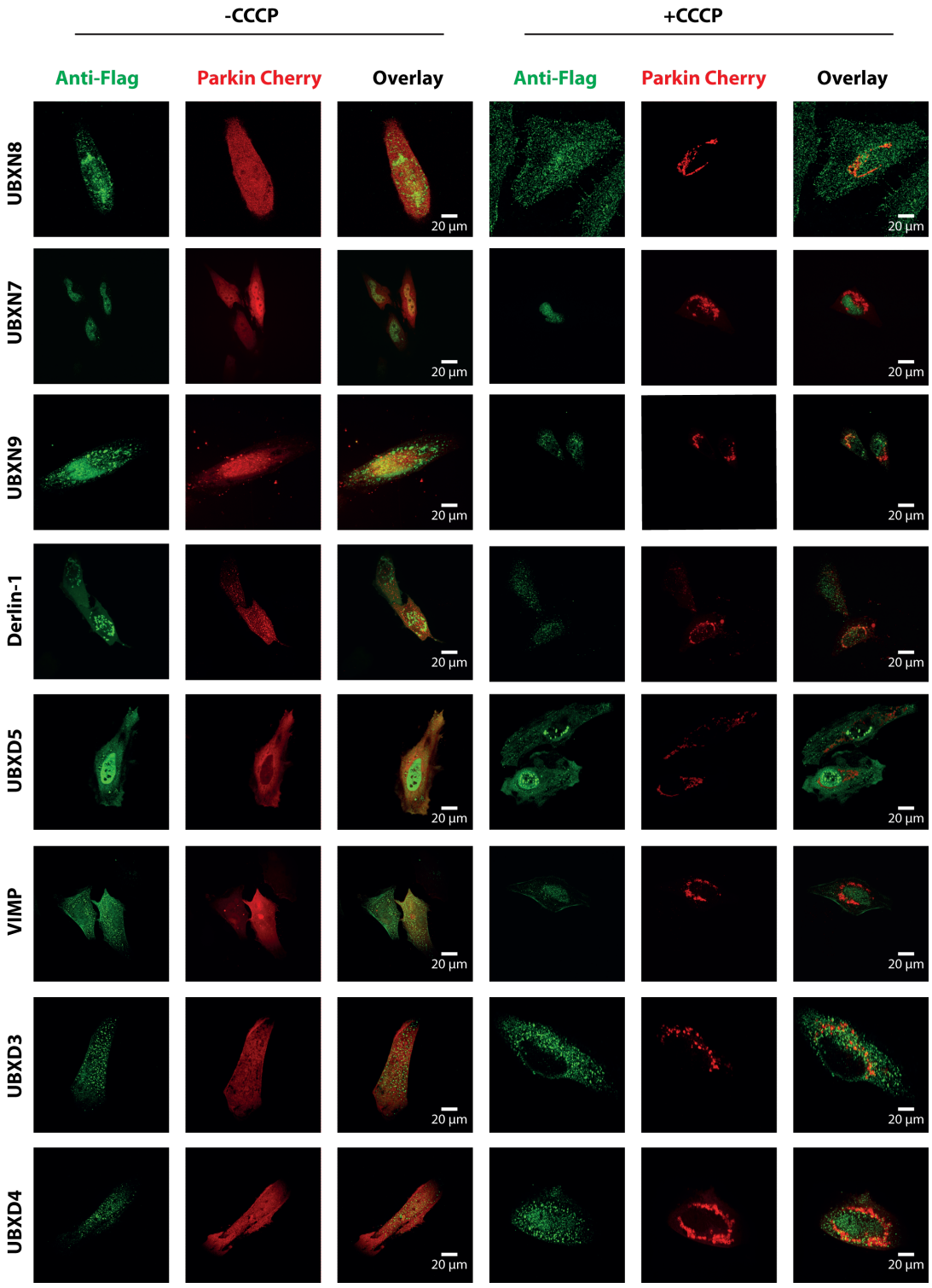

Figure 7: HeLa cells were transfected with eleven known p97 cofactors constructs for mitochondrial matrix-targeted Parkin Cherry (red) expression, treated for 6 h with 50 µM CCCP to induce mitophagy or left untreated as control. Fixed cells were stained using anti-FLAG antibodies (green) and imaged by confocal microscopy. Please note the no localization of any of these twelve candidate proteins on mitochondria upon CCCP treatment.

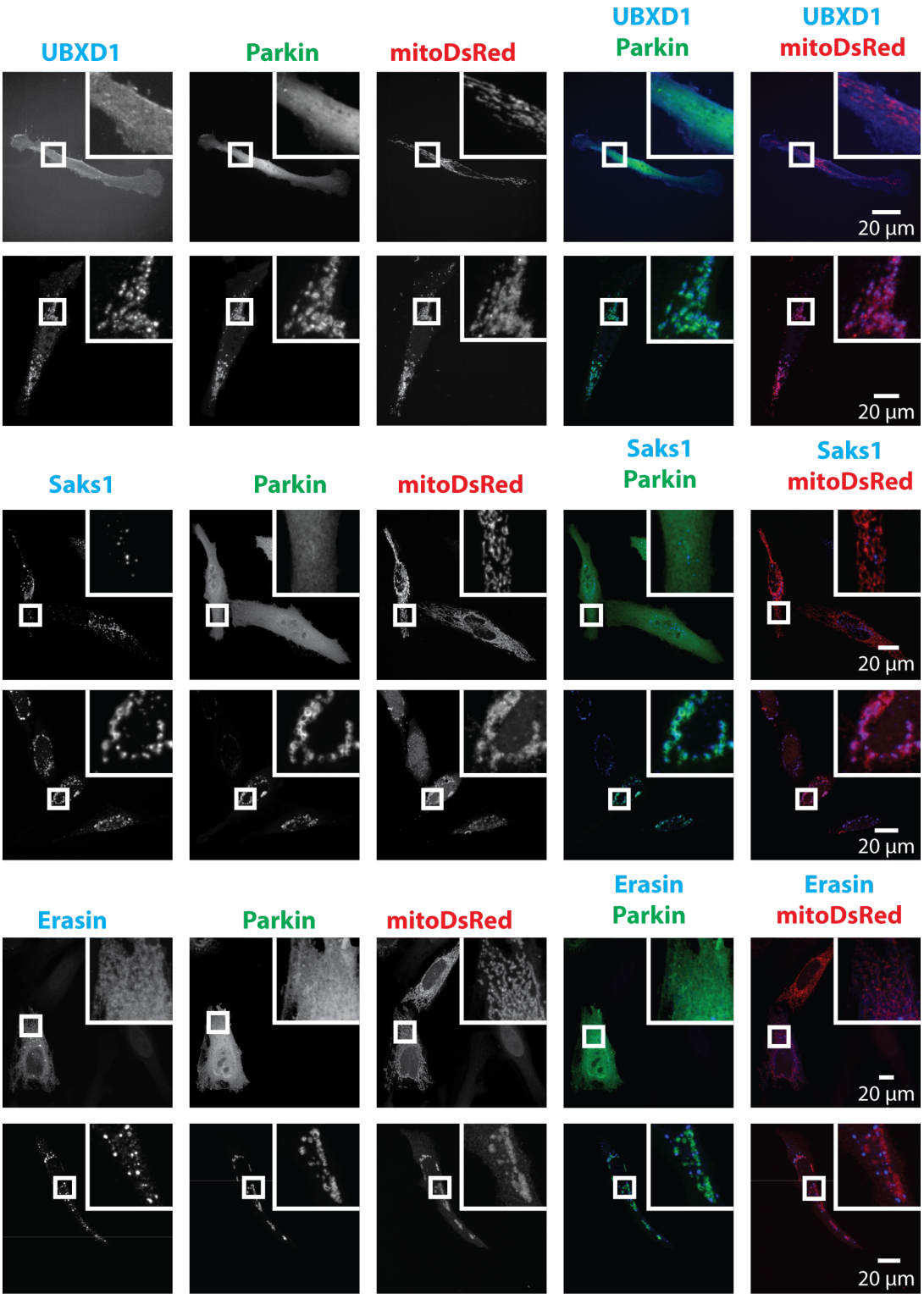

Figure 8: HeLa cells were transfected with expression constructs for mitochondrial matrix-targeted mitoDsRed (red), YFP-Parkin (green), FLAG-tagged UBXD1, SAKS1 or Erasin, treated for 6 h with 50 µM CCCP to induce mitophagy or left untreated as control. Fixed cells were stained using anti-FLAG antibodies (blue) and imaged by confocal microscopy. Please note the localization of these three p97 cofactors together with Parkin towards mitochondria upon CCCP treatment.

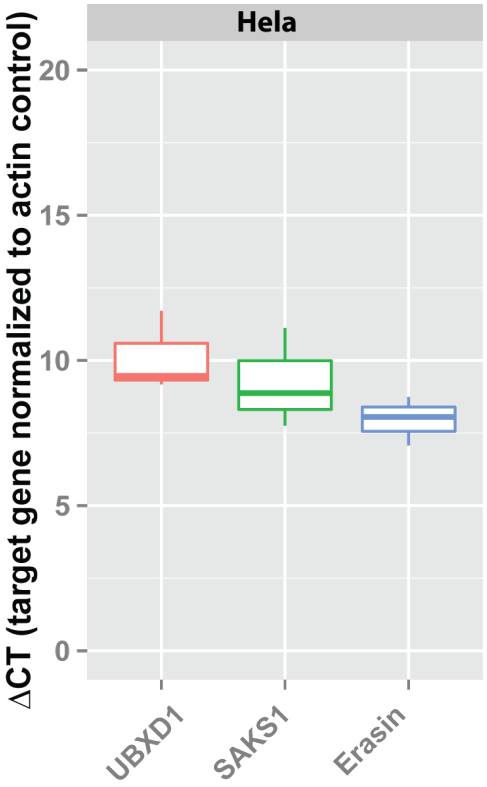

Figure 9: Expression of mitochondrial p97 cofactors UBXD1, SAKS1, and Erasin in HeLa cells. HeLa cells were harvested and total RNA was extracted. Levels of UBXD1, SAKS1, Erasin and β-actin were determined by qRT-PCR. Shown are boxplots (three biological with three technical replicates) of Δct-values for the expression level of UBXD1, SAKS1 and Erasin relative to β-actin expression levels.

In order to better assess HeLa cells as a model for studying mitochondrial cofactors of p97, the expression of UBXD1, SAKS1 and Erasin were analyzed by quantitative RT-PCR. As shown in Figure 9, all three p97 cofactors are expressed in HeLa cells.

5.2 Combined expression of mitochondria-targeted YFP and Parkin using T2A peptide fusion

HeLa cells do not express Parkin, thus, studying Parkin-mediated mitophagy necessitates the ectopic expression of this ubiquitin ligase. In this study, the simultaneous ectopic expression of more than one gene was necessary. To this end, a gene fusion between mitochondria-targeted YFP and ^{3xmyc}Parkin separated by a T2A sequence was generated. Upon translation of the fusion gene, the ribosome co-translationally cleaves the T2A pep-

tide resulting in the production of two polypetides from one mRNA [257, 258]. To assess whether mitoYFP-T2A-^{3xmyc}Parkin was indeed cotranslationally processes, HeLa cells were transfected with an expression plasmid for mitoYFP-T2A-^{3xmyc}Parkin treated with CCCP or left untreated and stained using anti-myc antibodies. As shown in Figure 10, in the absence of CCCP mitoYFP displays a clearly mitochondrial pattern, while Parkin resides in the cytosol. Upon addition of CCCP, Parkin translocates to mitochondria as expected. Thus, mitoYFP-T2A-^{3xmyc}Parkin is processed cotranslationally and Parkin shows translocation to depolarized mitochondria.

5.3 Assessing the impact of CCCP treatment on cellular viability

CCCP causes the depolarization of mitochondria through proton shuttling across the IMM while circumventing F0F1-ATPase. To establish that CCCP does not induce unwanted cell death possibly confounding results, HeLa cells were transfected with mitoYPF-T2A-^{3xmyc}Parkin and treated with 0, 10, 25, and 50 µM CCCP for 12 and 24 h. Under these conditions, no release of cytochrome c was observed (Figure 11). Thus, the employed CCCP concentrations to induce mitochondrial depolarization and mitophagy did not cause apoptotic cell death.

5.4 Dependency of UBXD1 translocation on CCCP concentration

The p97 cofactor UBXD1 translocates to mitochondria under mitophagic conditions. To further characterize this shift in subcellular localization, UBXD1 translocation in Parkin expressing cells was assessed in cells treated with increasing concentrations of CCCP. As shown in Figure 12, treatment of cells expressing mitoYFP-T2A-^{3xmyc}Parkin together with ^{FLAG}UBXD1 revealed translocation of UBXD1 at all analyzed CCCP concentrations. Interestingly, increasing CCCP concentrations caused increasingly efficient translocation of UBXD1 to mitochondria.

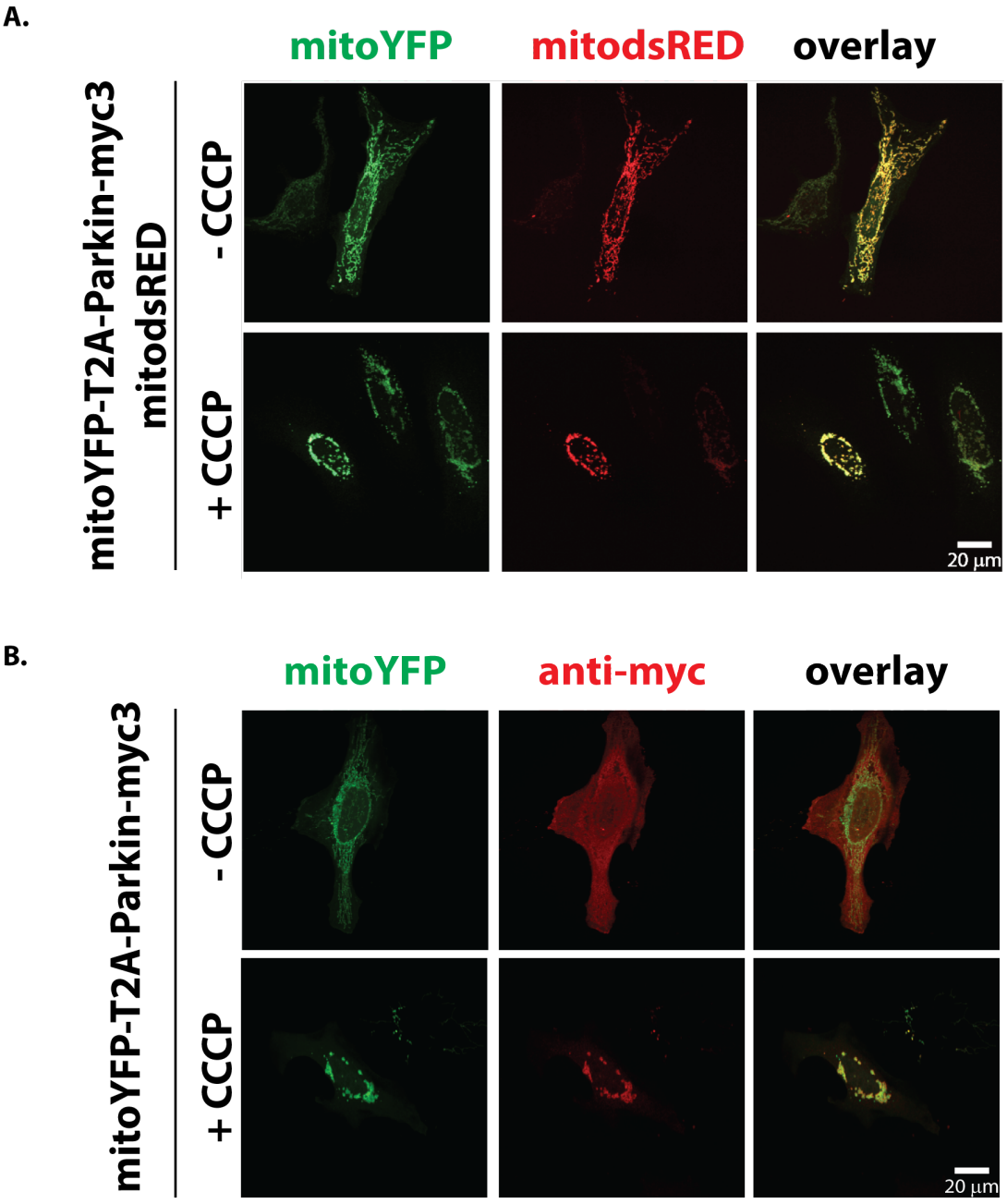

Figure 10: Combined expression of mitochondria-targeted YFP and Parkin. (A) HeLa cells transfected with an expression plasmid for mitodsRED and a fusion protein between mitoYFP and ^{3xmyc}Parkin separated with the cotranslationally-cleaved T2A peptide were analyzed by confocal microscopy after treatment with CCCP for 6 h or no treatment as control. Note that mitoYFP and mitodsRED colocalize and that both markers show the typical CCCP-induced mitochondrial fragmentation. (B) HeLa cells transfected with mitoYFP-T2A-^{3xmyc}Parkin were treated with CCCP for 6 h or left untreated, fixed and stained using mouse anti-myc antibodies. Please note the lack of co-localization between mitoYFP and ^{3xmyc}Parkin in the absence of CCCP and the overlap of both mitoYFP and Parkin in the presence of CCCP, confirming intended cotranslational processing of mitoYFP-T2A-^{3xmyc}Parkin.

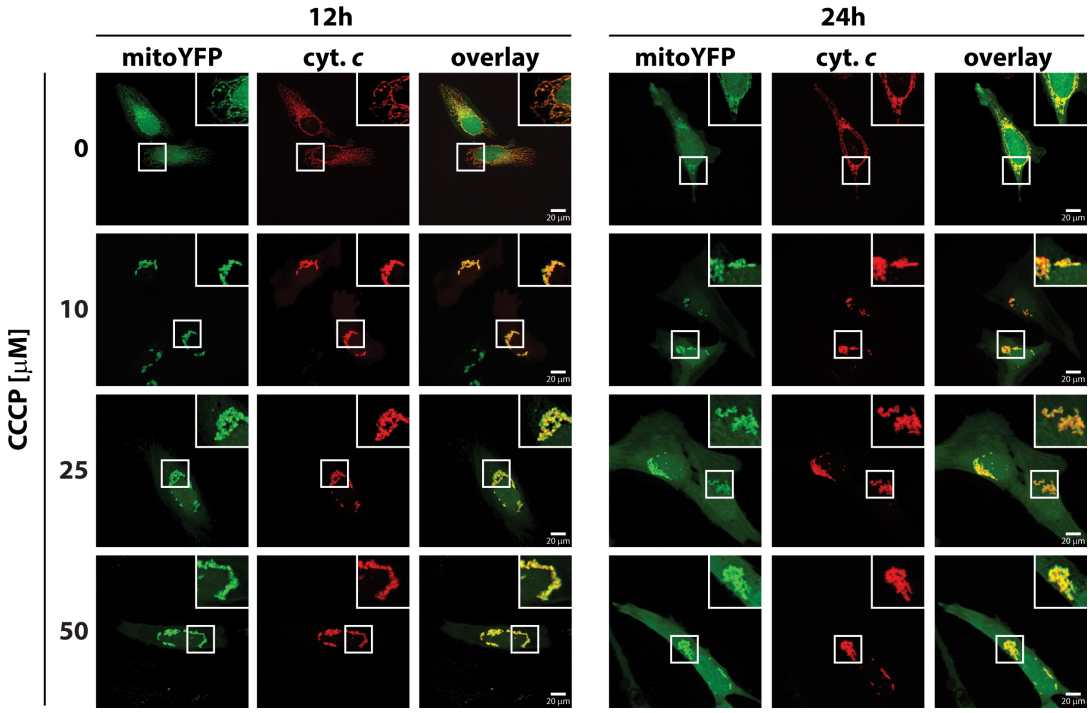

Figure 11: CCCP treatment does not induce apoptosis in HeLa cells. HeLa transfected with mitoYPF-T2A-^{3xmyc}Parkin were treated for 12 or 24 h with 0, 10, 25, or 50 µM CCCP, fixed, stained using anti-cytochrome c antibodies and analyzed by fluorescence microscopy. Shown are representative images of three independent experiments.

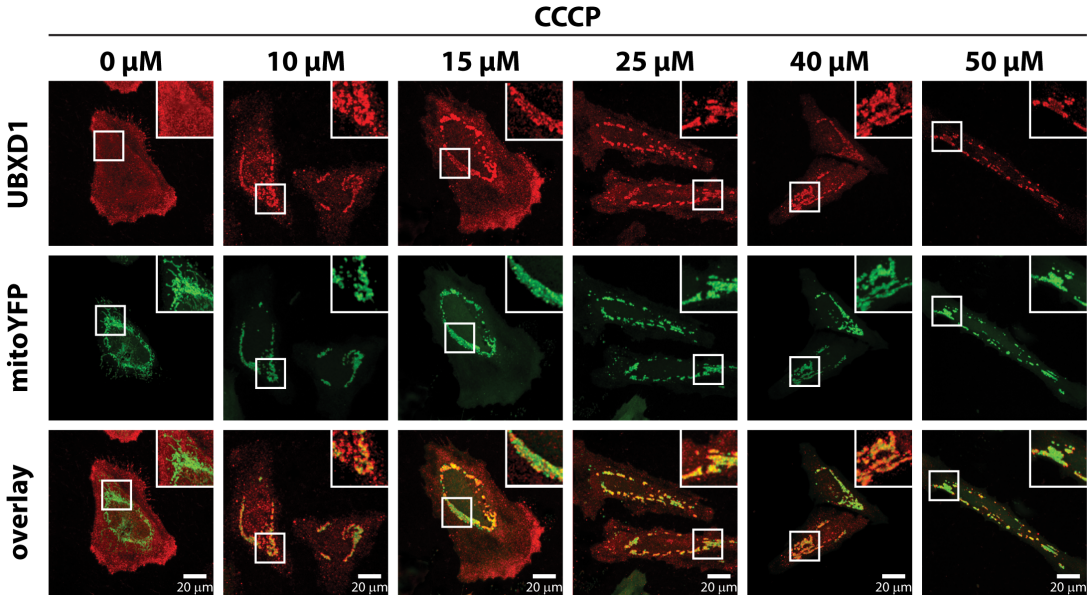

Figure 12: HeLa cells transfected with expression constructs for ^{FLAG}UBXD1 and mitoYFPT2A-^{3xmyc}Parkin were treated with 10, 15, 25, 40, or 50 µM CCCP for 6 h or left untreated as control. Cells were fixed, stained using mouse anti-FLAG antibodies to detect UBXD1 and analyzed by confocal microscopy.

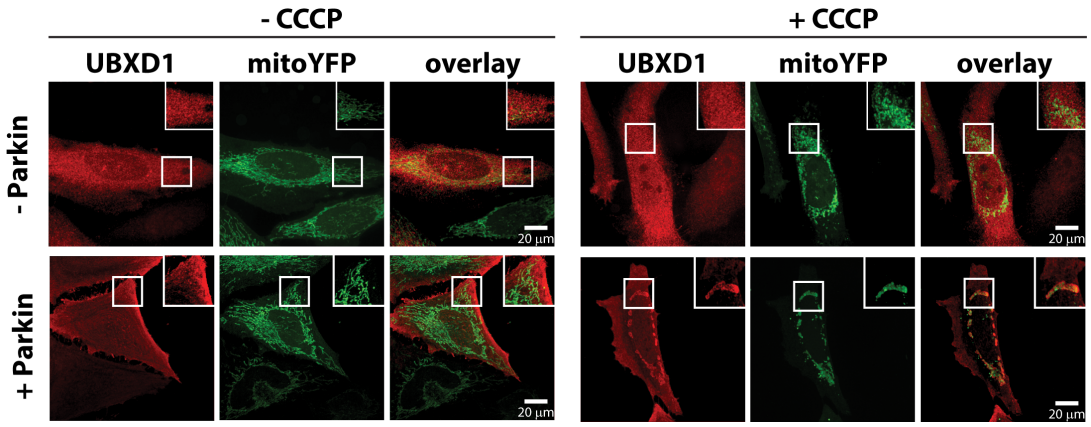

Figure 13: UBXD1 translocates to depolarized mitochondria in a Parkin-dependent manner. HeLa cells transfected with expression constructs for ^{FLAG}UBXD1, mitoYFP, and Parkin or vector control were treated with 50 µM CCCP for 6 h of left untreated as control.

5.5 UBXD1 translocates to depolarized mitochondria in a Parkin-dependent manner

To assess the Parkin-dependency of mitochondrial translocation of UBXD1, cells expressing ^{FLAG}UBXD1 in the presence or absence of Parkin were treated with 50 µM CCCP or left untreated. As shown in Figure 13, in the absence of Parkin and CCCP, ^{FLAG}UBXD1 displays cytosolic localization and does not colocalize with the mitochondrial marker mitoYFP. However, in the presence of Parkin and following mitochondrial depolarization, a proportion of UBXD1 translocates to mitochondria. These findings suggest that UBXD1 is able to recognize a signal which becomes apparent on depolarized mitochondria after Parkin recruitment.

5.6 Mutational analysis of UBXD1

Cofactors of p97 are characterized by their modular structure consisting of protein domains with known functions mediating interaction with p97 and ubiquitinated proteins. To further characterize the connection of UBXD1 to mitochondria, FLAG-tagged UBXD1 mutants lacking the VIM (UBXD1ΔVIM), PUB (UBXD1ΔPUB), UBX (UBXD1ΔUBX), PUB and UBX (VIMonly) or VIM and PUB domain (UBXonly) were generated (Figure 14).

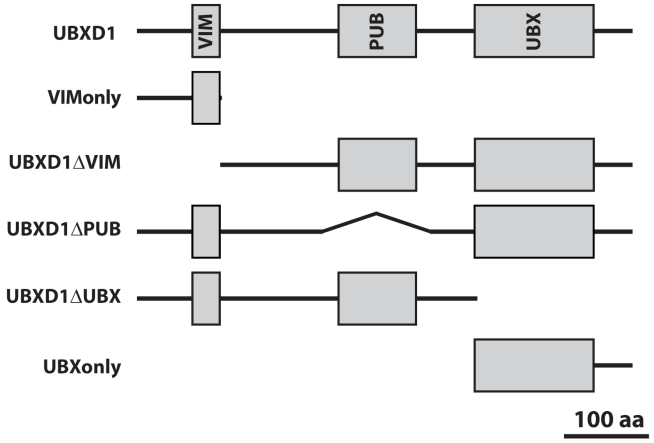

Figure 14: Schematic domain organization of wildtype UBXD1 and mutants used in this study. UBXD1 contains with VIM, PUB and UBX three protein-protein interaction domains. Shown are drawn to scale schematic representation of UBXD1 truncation mutants.

5.6.1 Protein-protein interaction domains in UBXD1

HeLa cells transiently coexpressing ^{FLAG}UBXD1 or mutants of ^{FLAG}UBXD1 together with mitoYFP-T2A-^{3xmyc}Parkin were treated with CCCP or left untreated. As shown in Figure 15A, ^{FLAG}UBXD1 lacking VIM, PUB or both domains was still capable of mitochondrial translocation, similar to wildtype ^{FLAG}UBXD1. Strikingly, ^{FLAG}UBXD1 without the UBX domain lacked mitochondrial localization even under mitophagic conditions. To quantify UBXD1 mitochondrial translocation, the ratio of ^{FLAG}UBXD1 on mitochondria to non-mitochondrial ^{FLAG}UBXD1 was determined (Figure 15B). In line with the findings shown in Figure 15A, a significant difference ($p < 0.001$) in the mitochondrial to total ^{FLAG}UBXD1 ratio (expressed as median ± median absolute deviation) between control cells and cells treated with CCCP was found for wildtype ^{FLAG}UBXD1 (no CCCP: 1.11 ± 0.24; plus CCCP: 1.63 ± 0.4), ^{FLAG}UBXD1ΔPUB (no CCCP: 1.09± 0.1; plus CCCP: 1.92 ± 0.93), ^{FLAG}UBXD1ΔVIM (no CCCP: 1.04 ± 0.21; plus CCCP: 1.34± 0.47) and ^{FLAG}UBXonly (no CCCP: 1.12 ± 0.16; plus CCCP: 1.58 ± 0.61), but not for ^{FLAG}UBXD1ΔUBX (no CCCP: 0.99 ± 0.22; plus CCCP: 1.04±0.21). These data point to an UBX domain-dependent targeting of UBXD1 to mitochondria under mitophagic conditions, while VIM and PUB domains, whether separate or in concert, are

not sufficient to mediate mitochondrial translocation.

5.7 UBXD1 mediates mitochondrial recruitment of p97

As shown in Figure 15, the UBX domain of UBXD1 determines translocation to mitochondria under mitophagic conditions. Interestingly, the UBX domain is generally considered to confer binding to p97. However, UBXD1 is particular in this regard as it has a complex interaction mode with p97 likely involving its VIM and PUB domains [158]. To assess whether translocation of UBXD1 to mitochondria might also cause recruitment of p97, mitochondrial translocation of p97 was studied.

5.7.1 UBXD1 recruits p97 to mitochondria under mitophagic conditions

Analyzing the distribution of endogenous p97 in cells co-expressing ^{FLAG}UBXD1 and mitoYFP-T2A-^{3xmyc}Parkin in the presence or absence of CCCP, a strong redistribution of p97 from the cytosol to mitochondria upon addition of CCCP compared to controls was found (Figure 16A). Quantitative image analysis (Figure 16B) confirmed a significant ($p<0.0001$) accumulation of endogenous p97 on mitochondria in cells with ectopic expression of ^{FLAG}UBXD1 under mitophagic conditions (plus ^{FLAG}UBXD1/plus CCCP: 2.01 ± 0.7) compared to control cells either with undisturbed mitochondrial membrane potential (plus ^{FLAG}UBXD1/no CCCP: 1.15 ± 0.24) or lacking ectopic UBXD1 expression (no ^{FLAG}UBXD1/plus CCCP: 1.25 ± 0.31; no ^{FLAG}UBXD1/no CCCP: 1.21 ± 0.18). These data are consistent with UBXD1 acting as p97 mitochondrial recruitment factor under mitophagic conditions.

5.7.2 The UBX domain of UBXD1 is essential for mitochondrial translocation of p97

To further explore the potential role of UBXD1 in targeting p97 to mitochondria, redistribution of endogenous p97 following expression of ^{FLAG}UBXD1 mutants was analyzed.

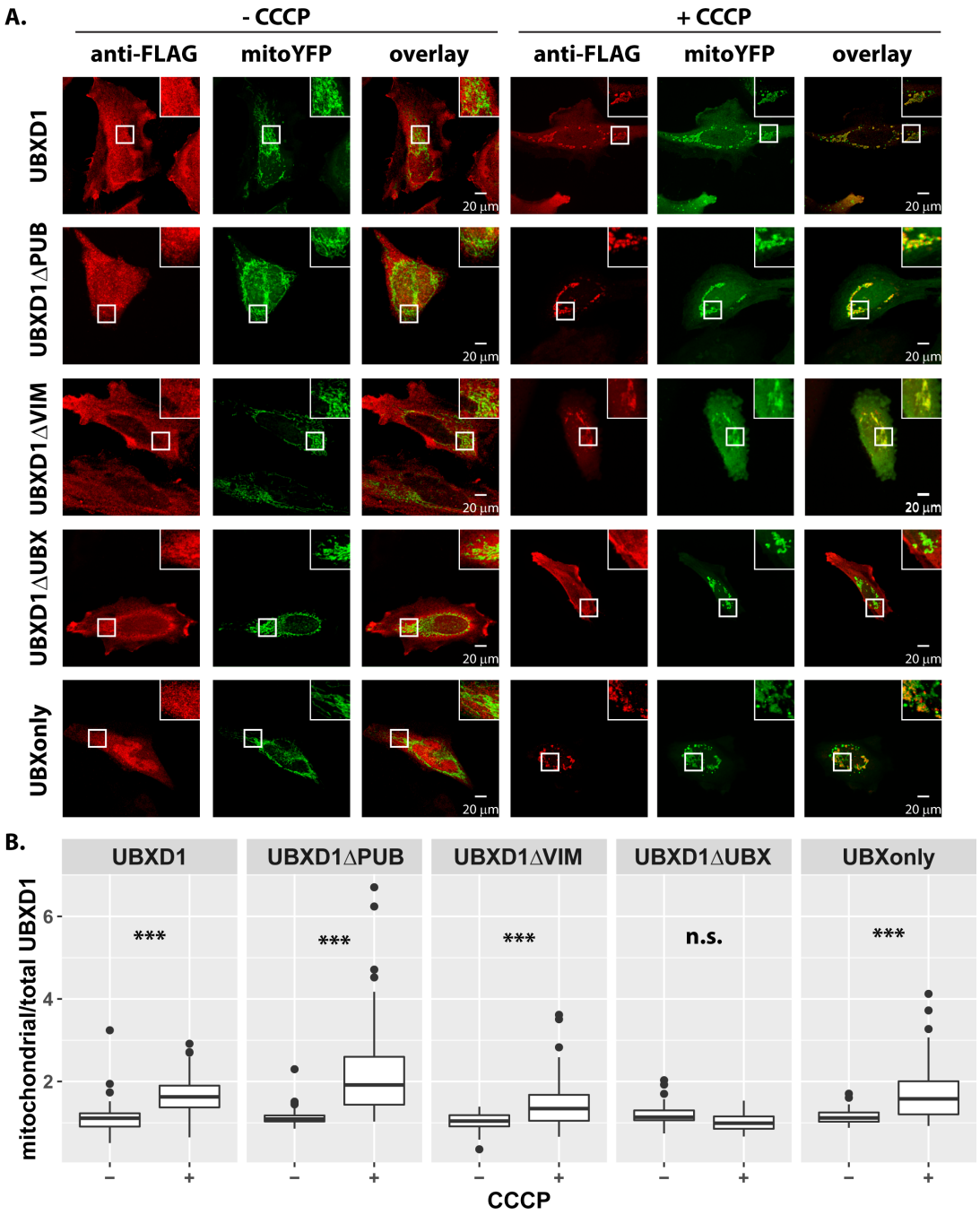

Figure 15: VIM and PUB, but not the UBX domain of UBXD1 are dispensable for mitochondrial translocation during mitophagy. (A) HeLa cells transfected with mitoYFP-T2A-^{3xmyc}Parkin and ^{FLAG}UBXD1, ^{FLAG}UBXD1ΔPUB, ^{FLAG}UBXD1ΔVIM, ^{FLAG}UBXD1ΔUBX, or ^{FLAG}UBXonly expression constructs were treated with CCCP 6 h or left untreated as control, stained using mouse anti-FLAG antibodies and analyzed by confocal microscopy. (B) The ratio of mitochondrial to total ^{FLAG}UBXD1 or various ^{FLAG}UBXD1 variants as measure for mitochondrial translocation was quantified by image analysis of confocal pictures obtain from cells treated as in A. Shown are box plots of three independent experiments with at least 15 cells per experiment and condition. Statistical significance was assessed by ANOVA followed by Student's t-test using Bonferroni correction to account for multiple comparisons. *** denotes p-values < 0.001, n.s. - no significant difference.

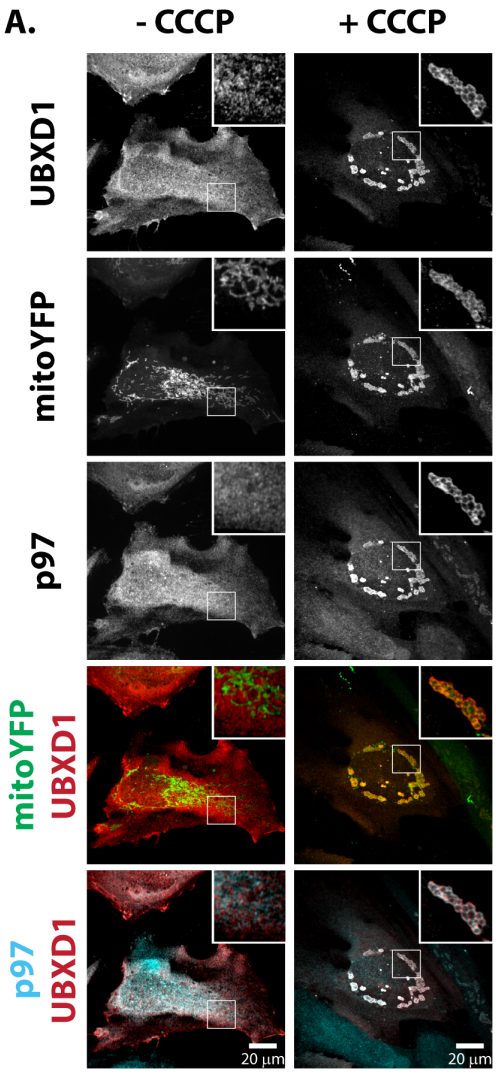

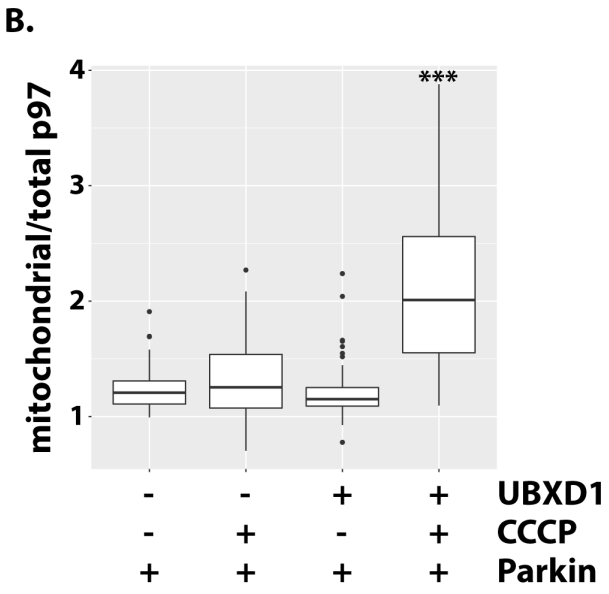

Figure 16: UBXD1 recruits p97 to mitochondria under mitophagic conditions. (A) HeLa cells transfected with expression plasmids for ^{FLAG}UBXD1 and mitoYFP-T2A-^{3xmyc}Parkin were treated with CCCP for 6 h or left untreated as control. Cells were fixed, stained using rabbit anti-FLAG and mouse anti-p97 antibodies and analyzed by confocal microscopy. (B) HeLa cells transfected with expression plasmids for ^{FLAG}UBXD1 or vector control and mitoYFP-T2A-^{3xmyc}Parkin were treated as in A. To quantify p97 redistribution to mitochondria, the ratio of mitochondrial p97 to total p97 was determined by image analysis of confocal images. Shown are box plots of three independent experiments with at least 15 cells per experiment and condition. Statistical significance was assessed by ANOVA followed by Student's t-test using Bonferroni correction to account for multiple comparisons. *** denotes p-values < 0.001.

HeLa cells expressing mitoYFP-T2A-^{3xmyc}Parkin together with wildtype ^{FLAG}UBXD1 or ^{FLAG}UBXD1 mutants were treated with CCCP or left untreated as control, and ratios of mitochondrial p97 to total p97 (p97m/p97t) and mitochondrial ^{FLAG}UBXD1 to total ^{FLAG}UBXD1 (^{FLAG}UBXD1m/ ^{FLAG}UBXD1t) were determined (Figure 17). Confirming the previous findings, ^{FLAG}UBXD1 translocated to mitochondria under mitophagic conditions via its UBX domain, while VIM and PUB domains did not contribute to mitochondrial targeting. As for p97 recruitment, confocal microscopy and determination of p97m/p97t revealed significant mitochondrial enrichment of endogenous p97 under mitophagic conditions compared to controls expressing ^{FLAG}UBXD1 (no CCCP: 1.18 $\pm$ 0.14; plus CCCP: 1.65 $\pm$ 0.29), ^{FLAG}UBXD1ΔPUB (no CCCP: 1.25 $\pm$ 0.14; plus CCCP: 1.62$\pm$0.47), and ^{FLAG}UBXD1ΔVIM (no CCCP: 1.23 $\pm$ 0.16; plus CCCP: 1.61 $\pm$0.47), but not in ^{FLAG}UBXD1ΔUBX (no CCCP: 1.18 $\pm$0.17; plus CCCP: 1.10 $\pm$ 0.21) or ^{FLAG}UBXonly (no CCCP: 1.15 $\pm$ 0.07; plus CCCP: 0.99 $\pm$ 0.1) expressing cells (Figure 17). These data are consistent with UBXD1 binding to depolarized, Parkin-containing mitochondria via its UBX and recruiting p97 through its VIM and PUB domain.

5.7.3 VIM domain characterization

Analysis of UBXD1ΔVIM translocation (Figure 17) suggested a potential involvement of the VIM domain in mitochondrial binding. To address this question, mitochondrial translocation and p97 recruitment activity of the VIM domain (VIMonly) was analyzed. HeLa cells expressing VIMonly and mitoYFP-T2A-^{3xmyc}Parkin treated with CCCP or left untreated showed neither translocation of VIMonly nor of p97 to mitochondria (Figure 18). These data are consistent with p97 recruitment to mitochondria via the VIM or PUB domain upon binding of the UBX domain of UBXD1 to mitochondria. Thus, a direct physical interaction between the VIM or PUB, but not the UBX domain of UBXD1 and p97 would be expected.

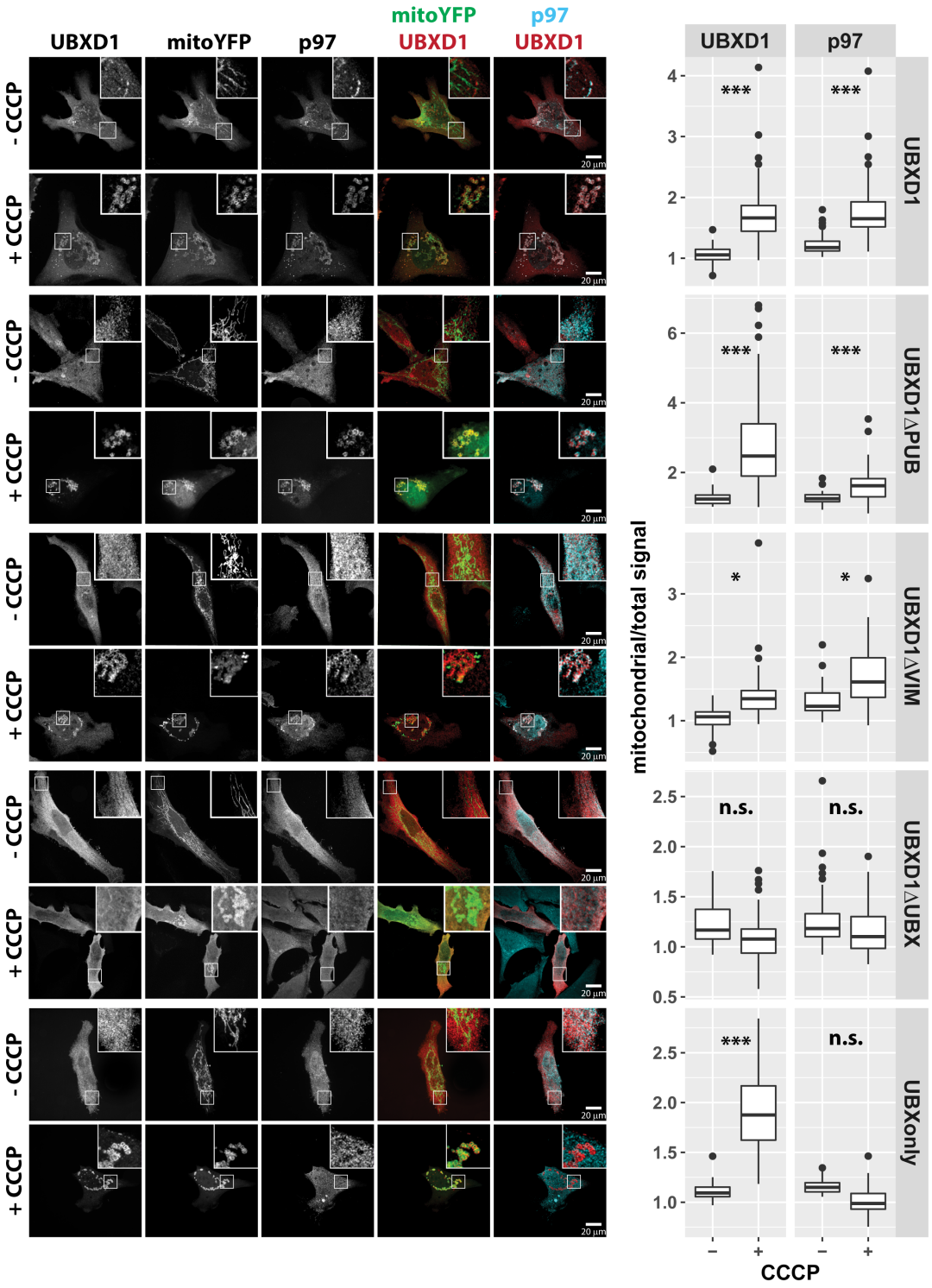

Figure 17: The UBX domain of UBXD1 is essential for mitochondrial translocation of p97. HeLa cells transfected with expression plasmids for ^{FLAG}UBXD1 or variants of ^{FLAG}UBXD1 and mitoYFP-T2A-^{3xmyc}Parkin were treated with CCCP for 6 h or left untreated as control. Fixed cells were stained using rabbit anti-FLAG and mouse anti-p97 antibodies and analyzed by confocal microscopy. The box plots represent three independent experiments with at least 15 cells/experiment/condition. Statistical significance was assessed by ANOVA followed by Student's t-test using Bonferroni correction to account for multiple comparisons. ** denotes p-values < 0.01, *** p-values < 0.001, n.s. – no significant difference.

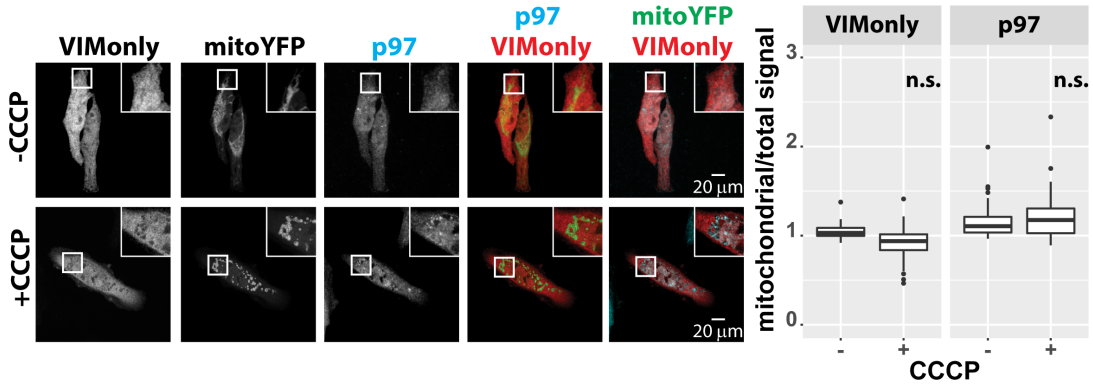

Figure 18: The VIM domain of UBXD1 is not involved in mitochondrial translocation and p97 recruitment. HeLa cells transfected with expression plasmid for FLAG-VIMonly and mitoYFP-T2A-^{3xmyc}Parkin were treated with CCCP for 6 h or left untreated as control. Fixed cells were stained using rabbit anti-FLAG and mouse anti-p97 antibodies and analyzed by confocal microscopy. The box plots represent three independent experiments with at least 15 cells/experiment/condition. Statistical significance was assessed by ANOVA followed by Student's t-test using Bonferroni correction to account for multiple comparisons. n.s. – no significant difference.

5.7.4 Mitochondrial UBXD1 is sufficient for p97 recruitment

To assess whether UBXD1 alone is sufficient to cause translocation of p97 to mitochondria, full-length ^{YFP}UBXD1 or YFP as control were targeted to the OMM through a C-terminal ActA tail anchor. ActA is a surface protein of 639 amino acids, anchored to the bacterial membrane *Listeria monocytogenes* inducing actin nucleation on the bacterial surface. The continuous process of actin filament elongation provides the driving force for bacterial propulsion in infected cells or cytoplasmic extracts [259]. ActA, when expressed in mammalian cells, is targeted to mitochondria via its C-terminal hydrophobic tail [260].

As shown in Figure 19A , ActA tail targeted ^{YFP}UBXD1 as well as YFP to mitochondria in the absence of ectopic Parkin expression or addition of CCCP. No significant difference in mitochondrial targeting between ^{YFP}UBXD1-ActA and YFP-ActA was observed (mitochondrial/total YFP – YFP-ActA: 2.09 $\pm$ 0.56, YFP-UBXD1-ActA: 1.77 $\pm$ 0.35 - Figure 19B). Interestingly, whereas endogenous p97 significantly redistributed to mitochondria in cells expressing YFP-UBXD1-ActA, p97 did not show this localization pattern in cells expressing YFP-ActA (mitochondrial/total p97, YFP-ActA: 1.13 $\pm$ 0.08, YFP-UBXD1-ActA: 1.3 $\pm$ 0.17, p = 0.0003). This observation suggests that the presence of UBXD1

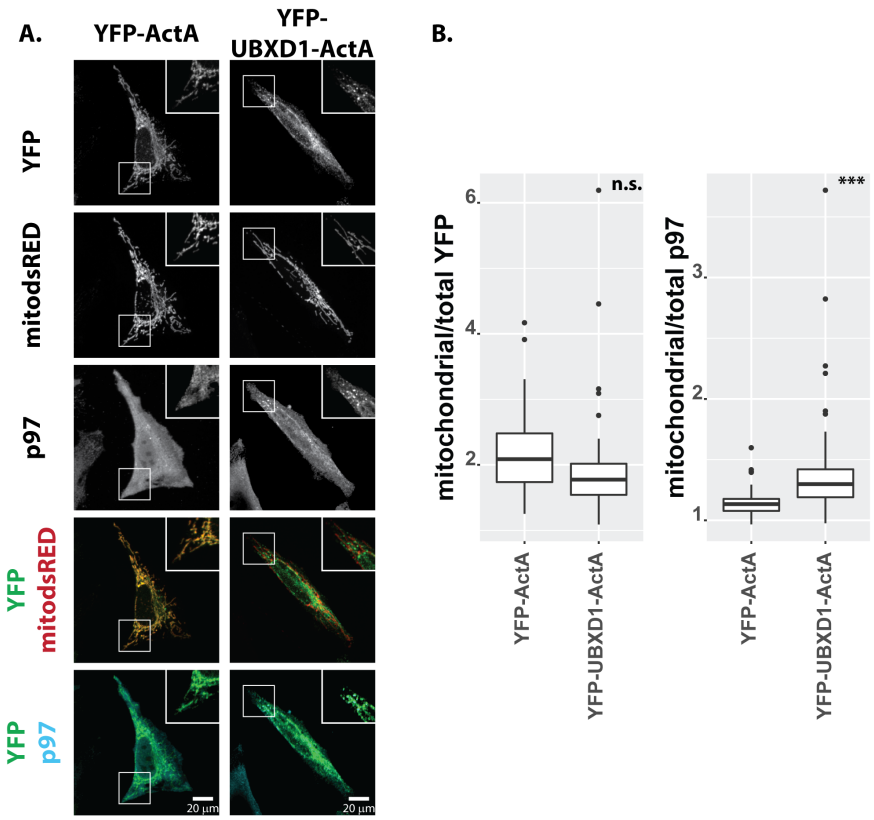

Figure 19: Induction of mitochondrial recruitment by ActA tail. HeLa cells transfected with expression plasmids for mitochondria-targeted dsRED (mitodsRED) and YFP-UBXD1 or YFP fused to the mitochondrial membrane targeting signal ActA were fixed, stained using mouse anti-p97 antibodies, and analyzed by confocal microscopy. (A) Shown are representative images out of three independent experiments. (B) The box plots represent three independent experiments with at least 15 cells/experiment/condition. Statistical significance was assessed by by Student's t-test. *** denotes $p < 0.001$, n.s. – no significant difference.

on mitochondria is sufficient for the recruitment of p97 to this organelle.

5.7.5 Physical interaction of UBXD1 with p97

To elucidate the molecular basis underlying the UBXD1-mediated mitochondrial recruitment of p97, we analyzed the contribution of all UBXD1 domains to a potential direct physical interaction between UBXD1 and p97. First, co-immunopurification and, second, direct yeast two hybrid interaction analyses were performed.

5.7.5.1 Immunopurification of p97 Co-Immunoprecipitation experiments of p97 from cells co-expressing UBXD1, UBXD1ΔVIM, UBXD1ΔPUB, UBXonly, or

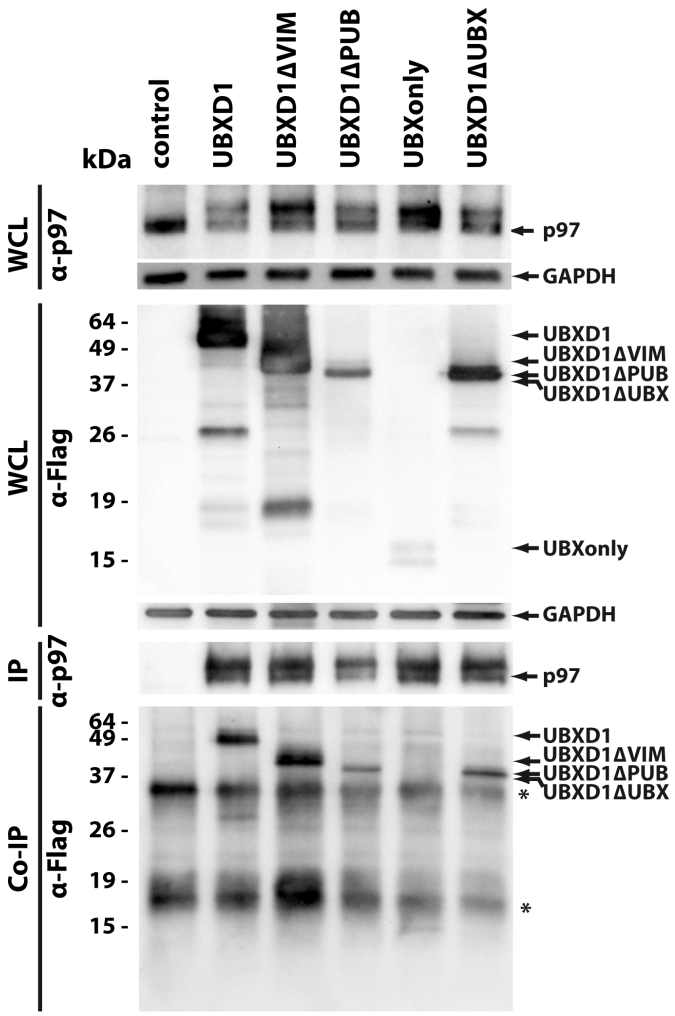

Figure 20: Physical interaction of UBXD1 with p97. Lysates of HeLa cells expressing 3x-myc epitope-tagged p97 together with ^{FLAG}UBXD1, ^{FLAG}UBXD1ΔVIM, ^{FLAG}UBXD1ΔPUB, ^{FLAG}UBXonly or ^{FLAG}UBXD1ΔUBX were incubated with mouse anti-myc antibodies and protein A/G beads. Immunopurified (IP) ^{3xmyc}p97 and co-purifying ^{FLAG}UBXD1 variants were analyzed by Western blotting. Detection of GAPDH in whole cell lysates (WCLs) served as loading control. Shown are representative blots from three independent experiments.

UBXD1ΔUBX revealed co-purification of UBXD1, UBXD1ΔVIM, UBXD1ΔPUB, and or UBXD1ΔUBX but not UBXonly with p97 (Figure 20). This data is consistent with UBXD1 interacting with p97 via its VIM and PUB, but not its UBX domain.

5.7.5.2 Yeast two hybrid system To further confirm and quantify the observed interaction pattern between UBXD1 and p97 (Figure 20), yeast two hybrid analysis was performed. This essay is based on the reconstitution of a functional transcription factor when two proteins or polypeptides of interest interact. This takes place in genetically modified yeast strains, in which the transcription of a reporter gene leads to a specific phenotype, usually growth on a selective medium or change in the color of the yeast colonies. The protein, which is fused to DNA-binding domain, was named the bait and the protein which was fused to the activating domain was called the prey [249].

As shown in Figure 21, a serial dilution of yeast strains containing Gal4BD-UBXD1 or Gal4BD-UBXD1 mutants as bait and Gal4AD-p97 as prey or GAL4AD vector as prey control on media selective for interaction (drop-out) revealed growth of strains containing Gal4AD-p97 and Gal4BD-UBXD1, or Gal4BD-UBXD1ΔVIM, or Gal4BD-UBXD1ΔPUB or Gal4BD-UBXD1ΔUBX. In contrast, no growth was detected for yeast strains containing empty pGBKT7 bait or Gal4BD-UBXonly. A serial dilution growth assay on media not selective for bait-prey interaction served as control. These data confirm a direct physical interaction between p97 and UBXD1 via its VIM and also the PUB domain of UBXD1. To elucidate to which extent VIM and PUB domain of UBXD1 contribute to the observed interaction between p97 and UBXD1, we performed a quantitative yeast two-hybrid interaction assay (Figure 21B). We found no significant difference (p=0.13) in the interaction strength expressed as percentage of wildtype GAL4BD-UBXD1 between GAL4AD-p97/GAL4BD-UBXD1ΔVIM (8.1 ± 2.8 %) and GAL4AD-p97/GAL4BD-UBXD1ΔPUB (13.8 ± 3.8 %). Interestingly, the interaction strength between GAL4AD-p97 and GAL4BD-UBXD1ΔUBX containing both PUB and VIM domain is 29.2 ± 7.1 % of wildtype GAL4BD-UBXD1. Thus, both VIM and PUB domain seem to contribute about equally to the physical interaction, and without obvious cooperativity.

5.8 UBXD1 promotes mitophagy induction

Efficient mitophagy relies on the engulfment of the damaged organelles into the forming autophagosome, without affecting the entire mitochondrial network [261]. Mitochondrial network fragmentation is observed prior to mitophagy, allowing the efficient uptake of small, depolarized mitochondrial subunits into autophagosomes for lysosomal degradation. This mitochondrial fragmentation is triggered by the Parkin-mediated ubiquitination and the p97-dependent retrotranslocation and proteasomal degradation of the mitofusin Mfn2 [255]. Based on the UBXD1-dependent recruitment of p97, UBXD1 might be a critical step for mitophagy onset and/or progression.

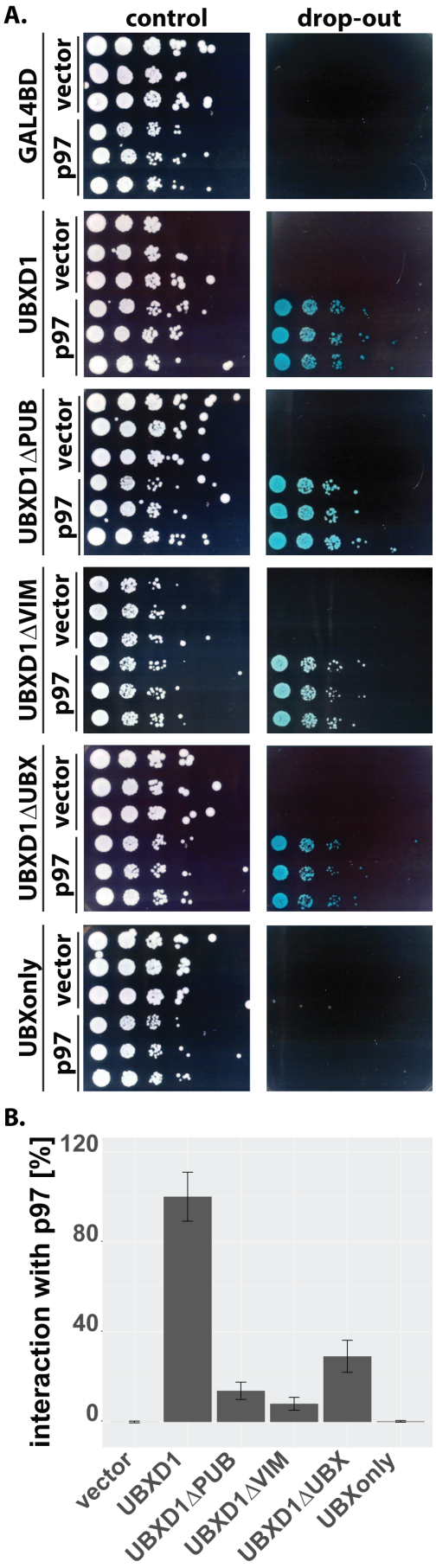

Figure 21: Physical interaction of UBXD1 with p97. Cells of yeast strain Y2HGold were transformed with expression constructs for fusion proteins between UBXD1 and the GAL4 DNA binding domain and p97 and the GAL4 activation domain. Transformation with pGADT7 (empty vector with GAL4 activation domain – labeled vector) or pGBKT7 (empty vector with GAL4 DNA binding domain – GAL4BD) served as control. Yeast strains were serially diluted onto plates selecting for expression plasmids (control) and plates selecting for yeast two-hybrid interaction (drop-out). (B) Strength of yeast two-hybrid interaction between UBXD1 or variants of UBXD1 and p97 were quantified using a para-nitrophenyl-alpha-galactoside assay. Shown is the average of three independent experiments with five independent yeast transformands per condition. Error bars represent SD.

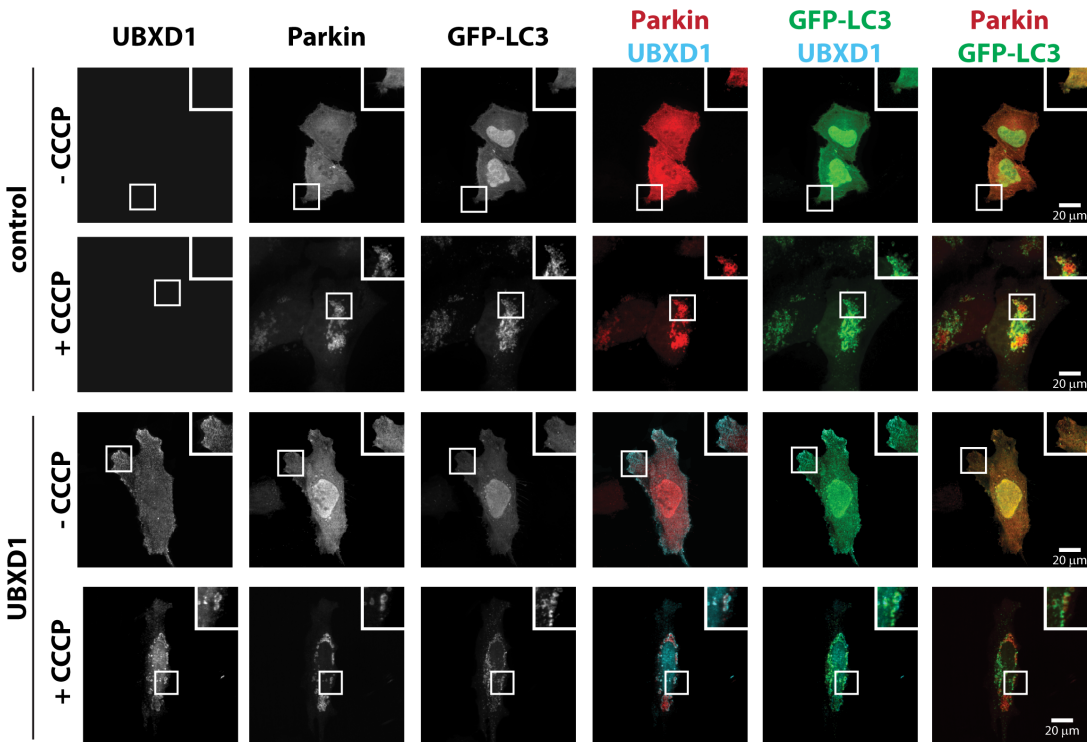

Figure 22: UBXD1 promotes mitophagy. HeLa cells transfected with expression plasmids for ^{FLAG}UBXD1 or vector control, ^{mcherry}Parkin and LC3-GFP were fixed, stained using mouse anti-FLAG antibodies, and analyzed by confocal microscopy.

5.8.1 Increased mitophagy in cells expressing UBXD1

HeLa cells co-expressing ^{FLAG}UBXD1 and LC3-GFP in the presence of ^{mcherry}Parkin were treated with CCCP for 6 h and autophagic vesicle formation was observed. As shown in Figure 22, LC3-GFP positive vesicle density near mitochondria was strongly increased in ^{FLAG}UBXD1 expressing cells compared to controls. This observation is indicative of UBXD1 acting in a pro-mitophagic fashion.

To analyze the impact of UBXD1 on mitophagy, mitophagic flux in cells ectopically expressing ^{FLAG}UBXD1 was measured. HeLa cells co-transfected with expression constructs for the pH-sensitive, mitochondria-targeted reporter mKeima fused to Parkin via the ribosome-cleaved T2A peptide (mKeima-T2A-^{3xmyc}Parkin) and UBXD1 or vector control were treated for 12 h with CCCP to induce mitophagy and analyzed flow cytometrically. The fluorescent reporter mKeima is excitable at 488 nm at pH 7 (inside mitochondria) and 561 nm at pH 4 as encountered inside autolysosomes. Thus, the ratio

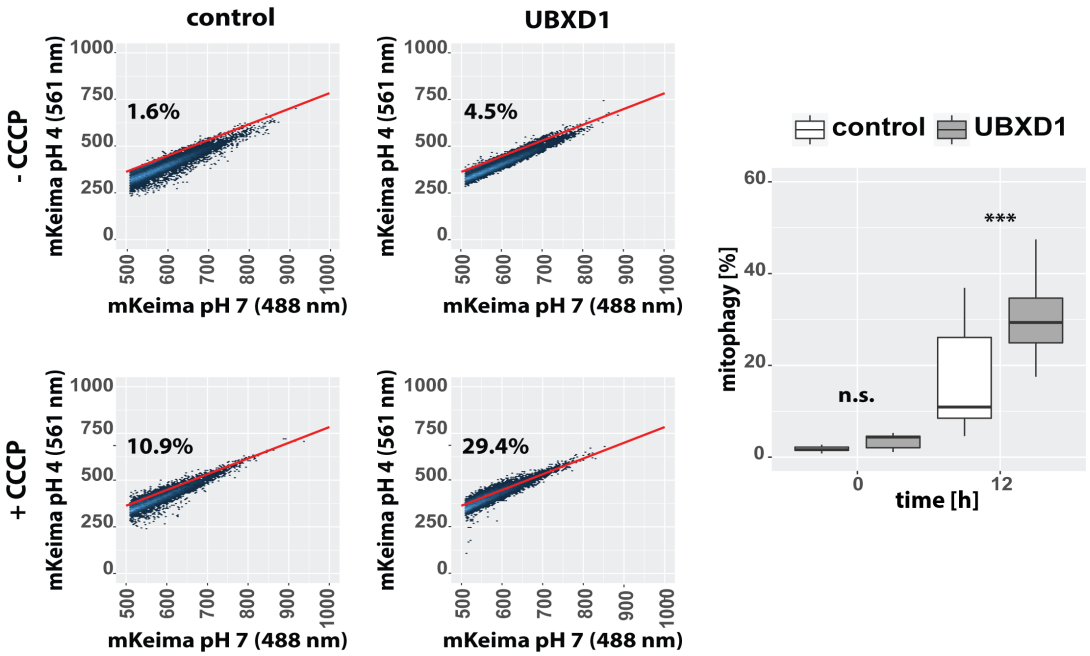

Figure 23: Increased mitophagy after ectopic expression of UBXD1. HeLa cells transfected with expression plasmids for UBXD1 or vector control and mKeima-T2A-^{3xmyc}Parkin were treated for 12 h with CCCP or left untreated and analyzed by flow cytometry. Shown are representative density plots (left panels). The box plot represents 6 independent experiments with in total 11 technical replicates. Statistical significance was assessed by ANOVA followed by Student's t-test using Bonferroni correction to account for multiple comparisons. *** marks p-values < 0.001, n.s. – no significant difference.

mKeima561nm/mKeima488nm is a measure for mitophagy [262]. In line with the observation of increased LC3-GFP positive vesicle formation (Figure 22), ectopic expression of ^{FLAG}UBXD1 significantly increased (p=0.0029) mitophagy following addition of CCCP. While 16.8 +/-11.6 % of CCCP treated control cells displayed mitophagy, CCCP treatment triggered mitophagy in 30.8 +/- 9.6 % of ^{FLAG}UBXD1-expressing cells (Figure 23). Expression of ^{FLAG}UBXD1 in the absence of CCCP treatment did not result in significant induction of mitophagy.

5.8.2 Diminished levels of UBXD1 promote mitophagy

To further assess whether UBXD1 indeed promotes mitophagy in CCCP treated cells, HeLa cells with diminished levels of UBXD1 were generated. To this end, CRISPR/Cas9 technology have been employed in this study [263]. An *UBXD1* specific gRNA under control of the human U6 promoter together with Cas9 and a plasmid containing a ex-

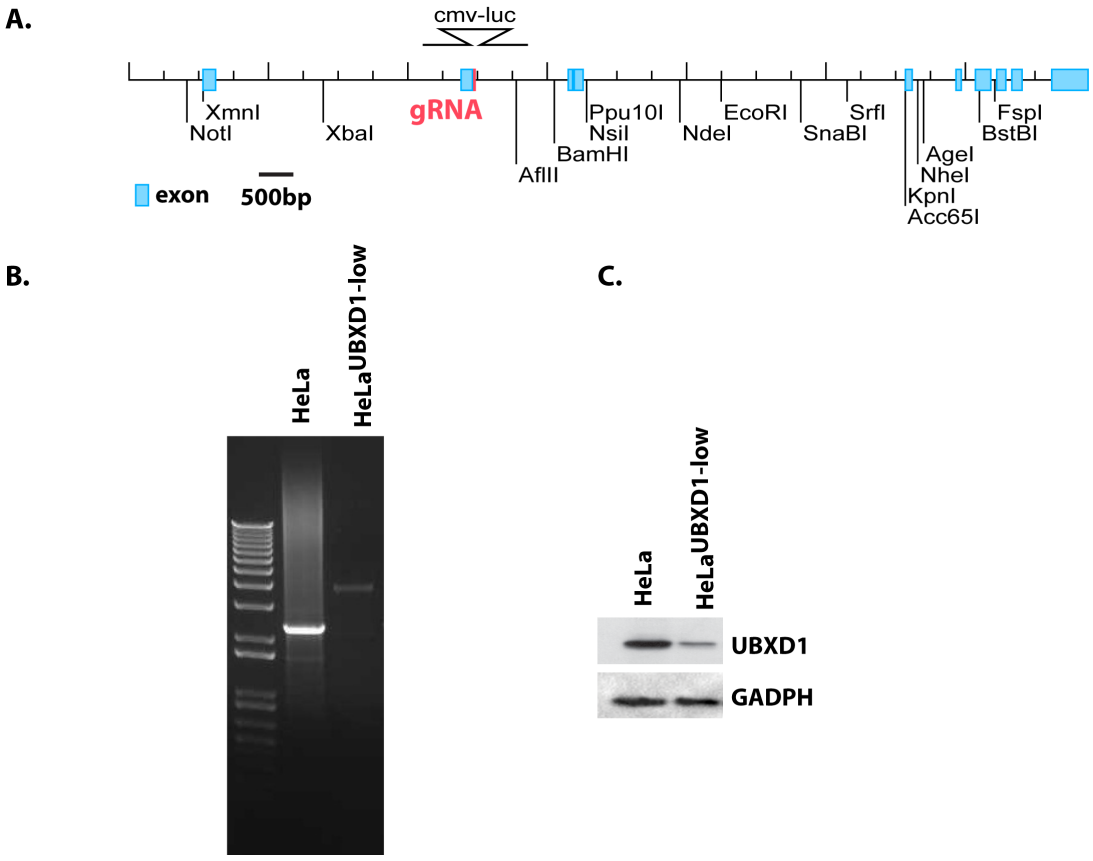

Figure 24: CRISPR/Cas9-mediated knock down of UBXD1. Using CRISPR/Cas9, UBXD1 was targeted in HeLa cells and several alleles of UBXD1 were replaced with a reporter cassette coding for secreted Gaussia luciferase. Shown are schematics of CRISPR/Cas9 strategy (A), PCR analysis of reporter integration, and levels of UBXD1 in HeLa and HeLa$^{\text{UBXD1-low}}$ (western blot, anti-UBXD1).

pression cassette for secreted Gaussia luciferase reporter flanked by UBXD1 sequences (Figure 24A) was transfected into HeLa cells. Following single cloning by dilution, luciferase activity was measured in the cell culture supernatant to identify cell clones with a potential deletion of UBXD1. Luciferase-positive single cell clones were expanded and integration of the Gaussia reporter in the UBXD1 as verified by PCR. In addition, detection of UBXD1 levels by Western blotting was performed. As shown in Figure 24B and C, PCR and Western blot analysis confirmed correct targeting of *UBXD1* and an about 80 % knockdown of UBXD1 protein levels. Interestingly, no complete knock-out of *UBXD1* could be identified.

These HeLa cells with diminished levels of UBXD1 were used to assess the impact of UBXD1 on mitophagic flux. To this end, HeLa and HeLa$^{\text{UBXD1-low}}$ cells were transfected

with mKeima-T2A-^{3xmyc}Parkin and treated with 10, 25 or 50 µM CCCP for 12 h before flow cytometric analysis. As shown in Figure 25, diminished levels of UBXD1 resulted in blunted mitophagic flux compared to wildtype control cells. While treatment of wildtype HeLa cells with 10, 25, or 50 µM CCCP resulted in 23.2 ± 16.3, 36.8 ± 9.6 and 29.9 ± 11.1 % mitophagic cells, respectively, the percentage of mitophagic HeLa$^{\text{UBXD1-low}}$ cells was significantly reduced by at least 50 % (10 µM: 10.1 ± 2.7, 25 µM: 12.8 ± 5.8, 50 µM 10.7 ± 2.8 %). This observation suggests that UBXD1 acts in a pro-mitophagic fashion with lowered levels of UBXD1 causing a diminished mitophagic flux. This is in line with the observation of increased mitophagic flux following ectopic expression of UBXD1 (Figure 23).

5.9 The UBXD1-interacting DUB YOD1

Papadopoulos and collegues reported about the DUB YOD1 which in collaboration with p97 and UBXD1 causes the clearance of ruptured lysosomes through lysophay [186]. Also YOD1 was shown to be involved in protein dislocation of proteins from the ER driven by p97 during ERAD [111]. Thus is seems conceivable, that YOD1 is not only involved in lysophagy and ERAD, but might also play a role in p97-dependent mitophagic processes.

5.9.1 YOD1 isoforms characterization

YOD1 belongs to the DUB subfamily characterized by an OTU domain [264]. Interestingly, alternative splicing of the *YOD1* gene results in two transcript variants. Protein domain structure analysis using InterPro [265] revealed the presence of an UBX, an OTU and a zinc finger domain in both isoforms (Figure 26). Due to the alternative splicing, the N-terminally located UBX domain differs in both isoforms. As the UBX domain is involved in protein-protein interactions, both YOD1 isoforms - YOD1.1 and YOD1.2 - were further analyzed.

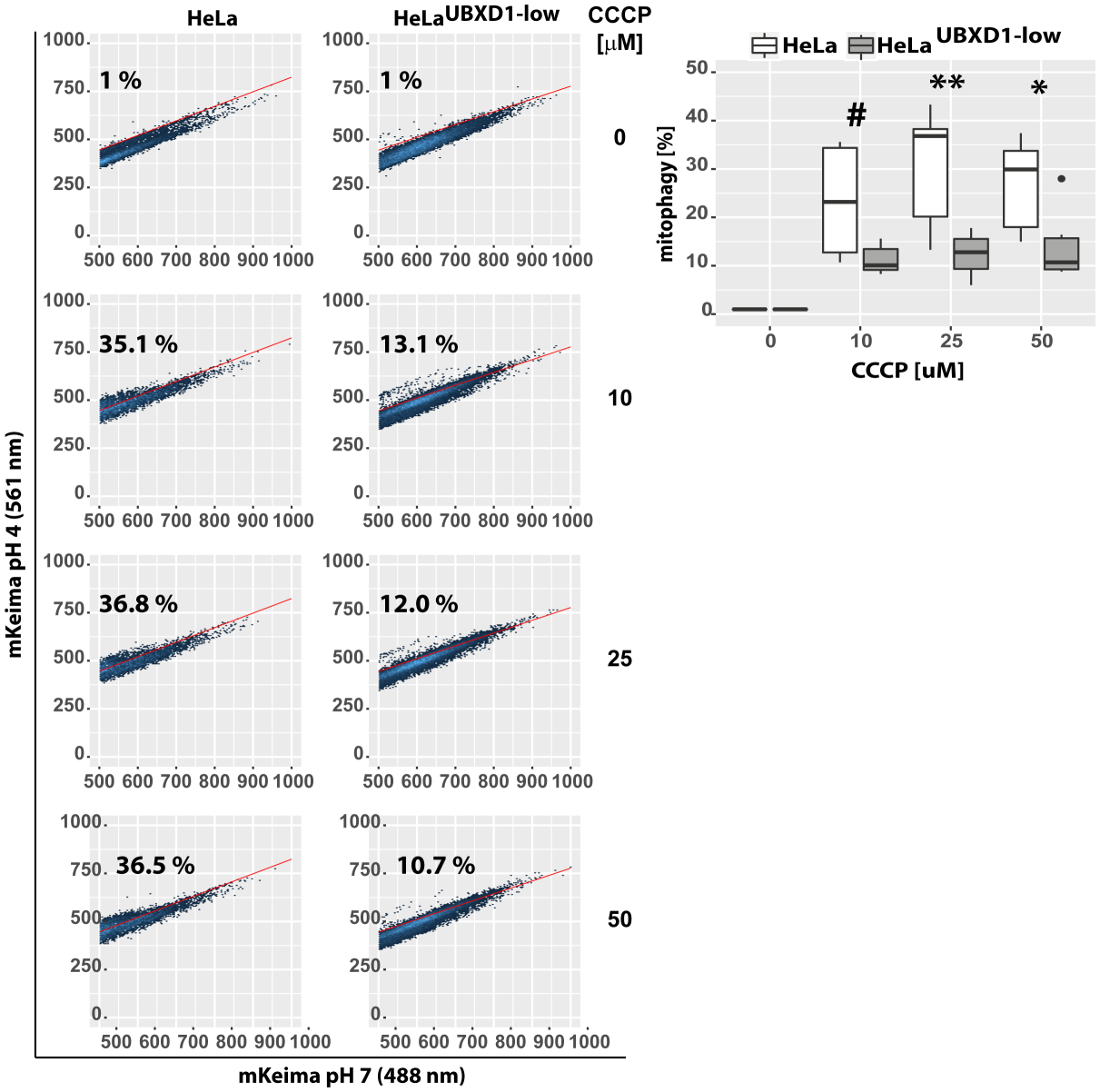

Figure 25: UBXD1 is a positive regulator of mitophagy.HeLa cells and HeLa$^{UBXD1\text{-}low}$ transfected with mKeima-T2A-^{3xmyc}Parkin were treated for 12 h with 10, 25 or 50 µM CCCP or left untreated as controls and were analyzed by flow cytometry. Shown are representative density plots. The box plot represents 5 independent experiments. Statistical significance was assessed by ANOVA followed by Student's t-test using correction to account for multiple comparisons according to Holm. * marks p-values < 0.05, ** < 0.01.

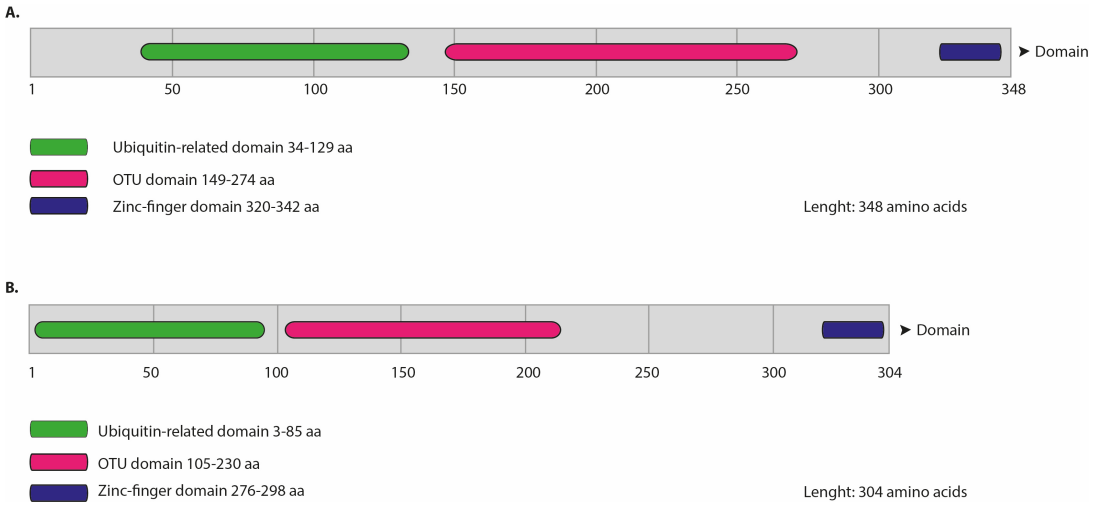

Figure 26: Domain structure of YOD1. Both YOD1 isoforms contain with UBX, OTU and Zn three protein-protein interaction domains. YOD1 isoform 2 has a distinct N-terminus and is shorter compared to isoform 1.

5.9.2 Physical interaction of YOD1 with UBXD1 and p97

To better characterize the two YOD1 isoforms in terms of their ability to interact with p97 and UBXD1, yeast two hybrid was employed. For that, a serial dilution of yeast strains containing GAL4BD-YOD1.1 or GAL4BD-YOD1.2 as bait and GAL4AD-p97 or GAL4AD-UBXD1 as prey was performed. Yeast strains containing GAL4BD-YOD1.1 and GAL4AD-p97 or GAL4AD-UBXD1 showed growth on plates selective for yeast two hybrid interaction consistent with a direct physical interaction between YOD1.1 and p97 or UBXD1. However, yeast strains containing GAL4BD-YOD1.2 grew only in the presence of GAL4AD-UBXD1, but not in the presence of GAL4AD-p97 indicative for a direct physical interaction between YOD1.2 with UBXD1 but not p97 (Figure 27). Thus, differences in the UBX domain between YOD1 isoform 1 and isoform 2 might contribute to a differential interaction pattern with p97.

5.9.3 Mitochondrial transloction of YOD1 during mitophagy

HeLa cells co-transfected with expression of mitoYPF-T2A-^{3xmyc}Parkin and ^{mcherry}YOD1.1 (Figure 28A) and ^{mcherry}YOD1.2 (Figure 28B) were treated with CCCP for 6 h to induce mitophagy. As shown in Figure 28 upon confocal microscopy

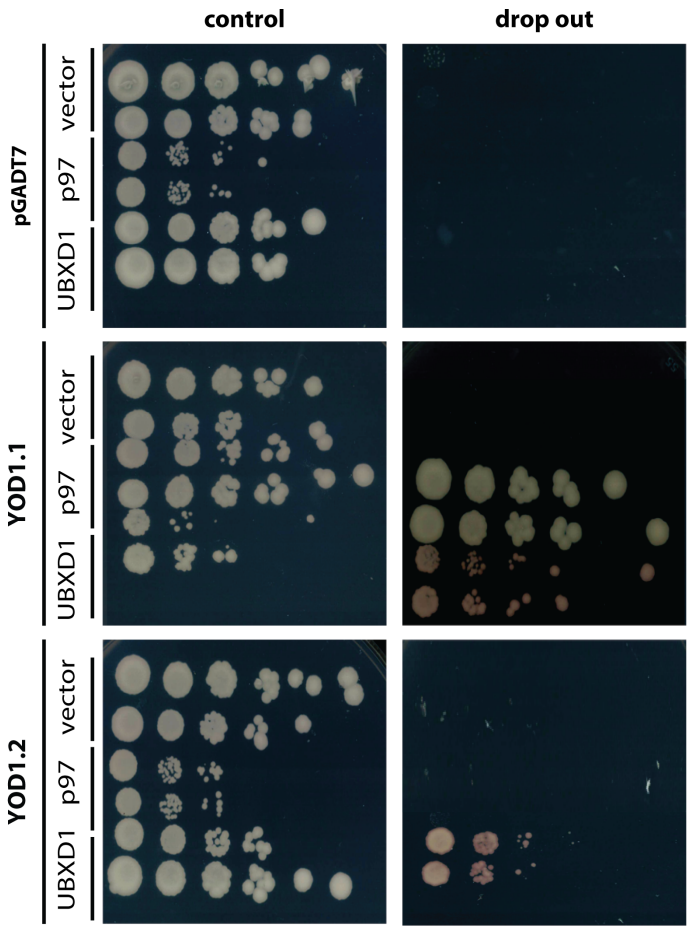

Figure 27: Physical interaction of YOD1 with p97 and UBXD1. Cells of yeast strain Y2HGold were transformed with expression constructs for fusion proteins between YOD1 isoform 1 and isoform 2 and the GAL4 DNA binding domain and p97 or UBXD1 and the GAL4 activation domain. Transformation with pGADT7 (empty vector with GAL4 activation domain – labeled vector) served as control. Yeast strains were serially diluted onto plates selecting for expression plasmids (control) and plates selecting for yeast two-hybrid interaction (drop-out).

analysis of both isoforms, only isoform 2 translocate to CCCP uncoupled mitochondria. However, this translocation was only observed in a small subset of cells.

5.9.4 YOD1.2 translocates to depolarized mitochondria in a UBXD1 and Parkin dependent manner

As YOD1.2 and UBXD1 physically interact, the dependence of mitochondrial translocation of YOD1.2 during mitophagic conditions on UBXD1 was assessed. To this end, HeLa cells co-transfected with expression plasmids for ^{FLAG}UBXD1, mitoYPF-T2A-^{3xmyc}Parkin and ^{mcherry}YOD1.2 were treated with 50 µM CCCP for 0 to 6 h. As shown in Figure 29, cells expressing mitoYPF-T2A-^{3xmyc}Parkin together with ^{FLAG}UBXD1 and YOD1.2 revealed YOD1.2 mitochondrial translocation after 6 h of CCCP treatment when UBXD1 is found in the cytosol. UBXD1 is found on mitochondria after 6 h of CCCP treatment when YOD1.2 is cytosolic and does not co-localize with either UBXD1 or mitoYPF-T2A-^{3xmyc}Parkin. These observations are consistent with UBXD1 recognizing depolarized, Parkin-containing mitochondria followed by increased recruitment of YOD1.2. The exclusive mitochondrial localization of UBXD1 and YOD1.2 under mitophagic conditions hints to a multi-step process where UBXD1 recognizes damaged mitochondria, recruits p97 and YOD1.2 and is released back into the cytosol.

5.9.5 Domain organization of YOD1.2 and its mutant derivatives

To study the role of the different protein domains in YOD1.2 and their impact on mitochondrial translocation, a variant lacking the N-terminal UBX and the OTU domain were generated (Figure 30).

5.9.6 Domain requirement for YOD1.2 mitochondrial translocation

HeLa cells co-expressing ^{FLAG}UBXD1 and ^{mcherry}YOD1.2 lacking UBX or OTU domain together with mitoYFP-T2A-^{3xmyc}Parkin were treated with CCCP or left untreated. As

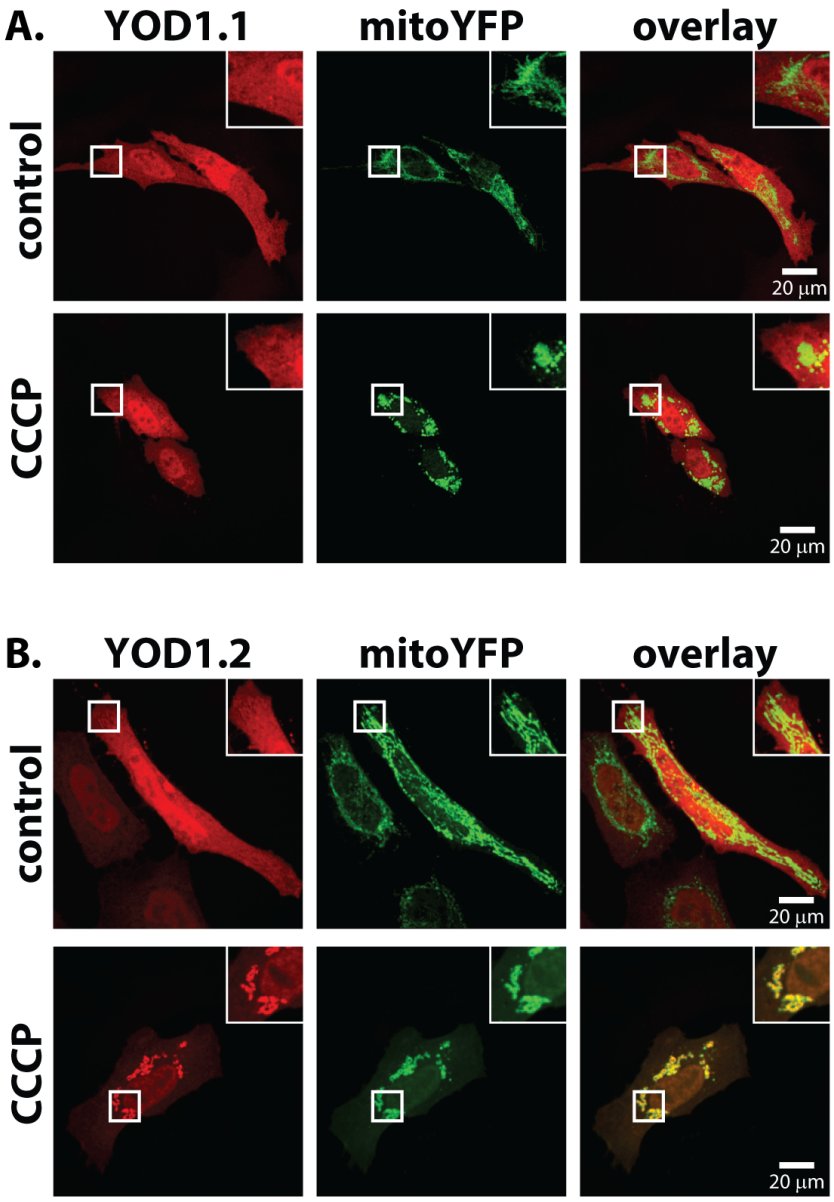

Figure 28: YOD1.2 translocates to depolarized mitochondria in a Parkin-dependent manner. HeLa cells transfected with YOD1 isoform 1 (A) or isoform 2 (B) and mitoYPF-T2A-^{3xmyc}Parkin were treated for 6 h with 50 µM CCCP, fixed and analyzed by fluorescence microscopy. Shown are representative images of three independent experiments.

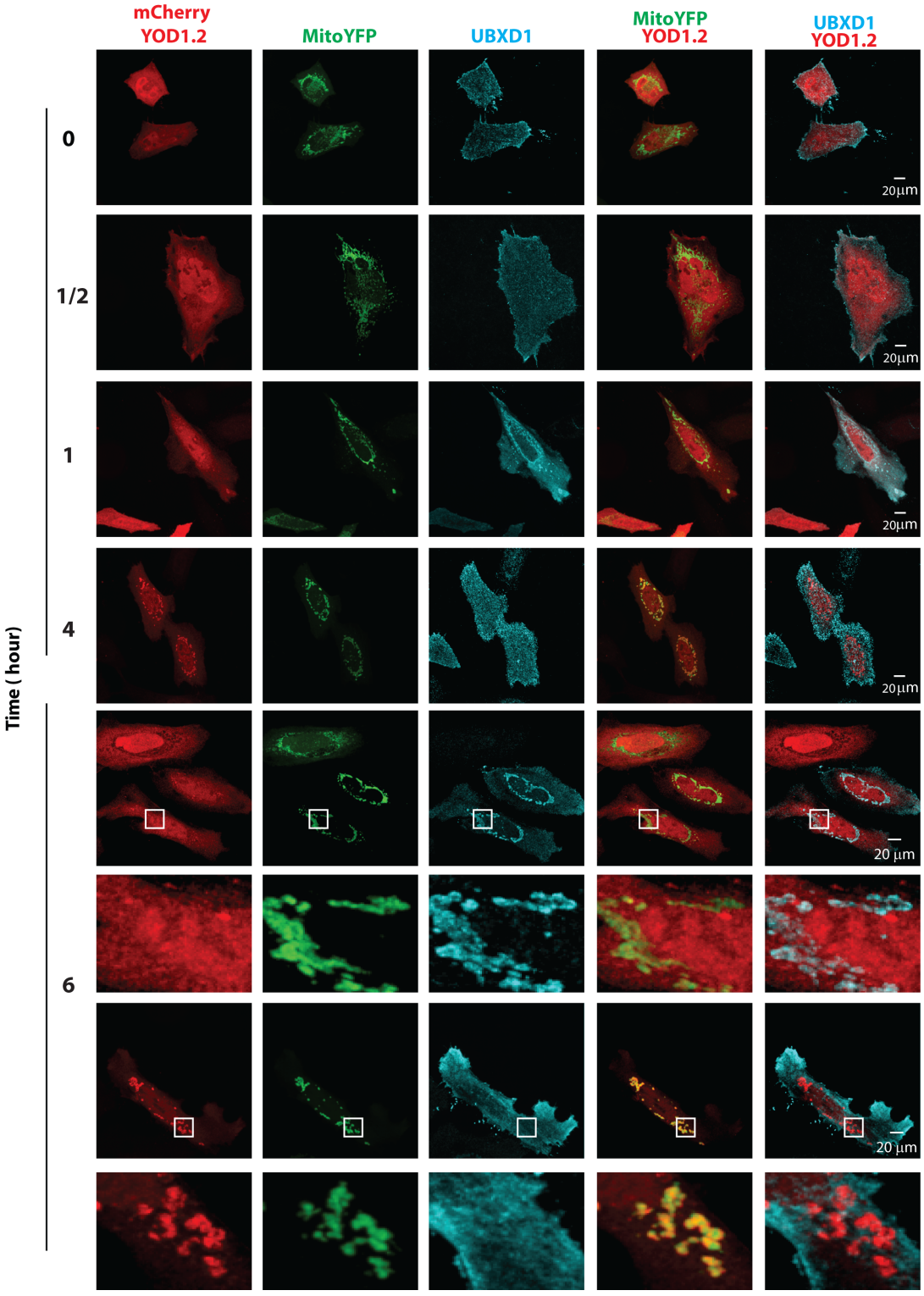

Figure 29: UBXD1 enhances mitochondrial translocation of YOD1.2. HeLa cells transfected with YOD1.2 isoform and mitoYPF-T2A-^{3xmyc}Parkin were treated for 6 h with 50 µM CCCP, fixed, stained using mouse anti-Flag antibodies to detect ^{FLAG}UBXD1 and analyzed by fluorescence microscopy. Shown are representative images of two independent experiments.

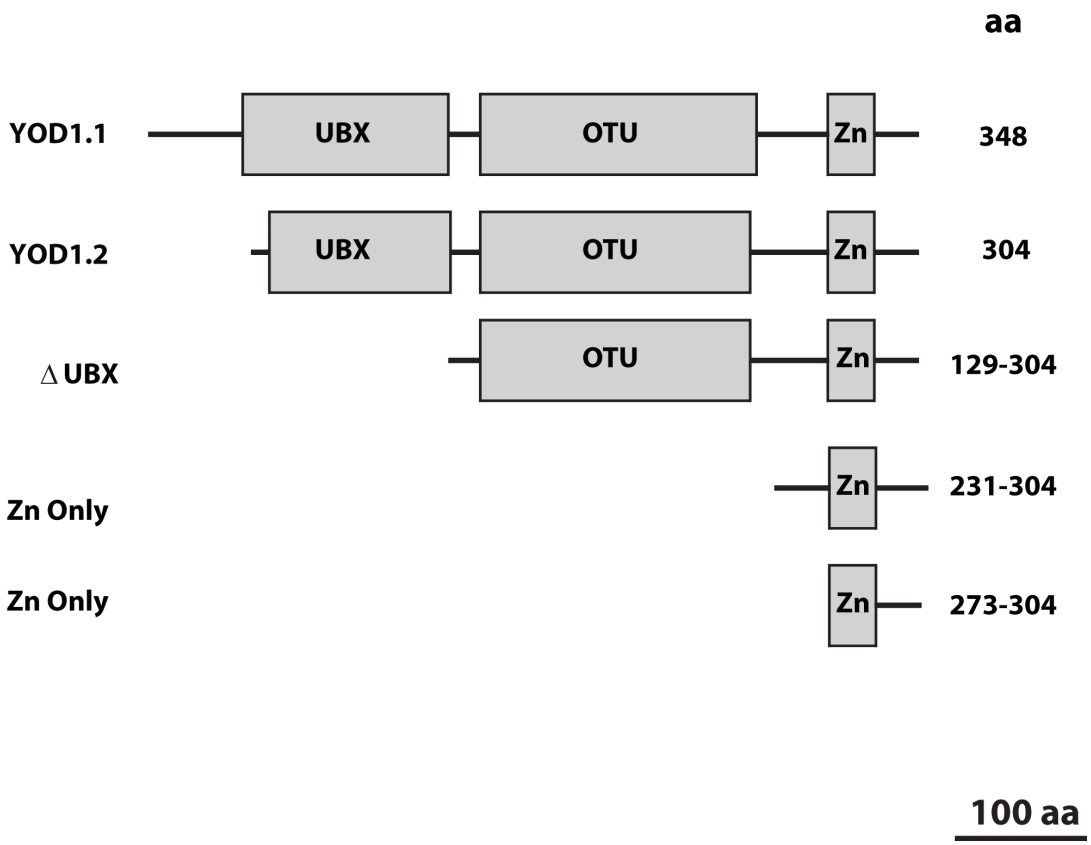

Figure 30: Schematic domain organization of YOD1.2 and YOD1.2 mutants. YOD1 contains with UBX, OTU and Zn three protein-protein interaction domains. Shown are drawn to scale schematic representation of YOD1 truncation mutants used in this study

shown in Figure 31A, YOD1.2 lacking UBX, or lacking UBX and OTU (Figure 31B,C) were not capable of mitochondrial translocation in UBXD1 dependent manner. This data suggests that the UBX domain of YOD1.2 is critical for its mitochondrial translocation.

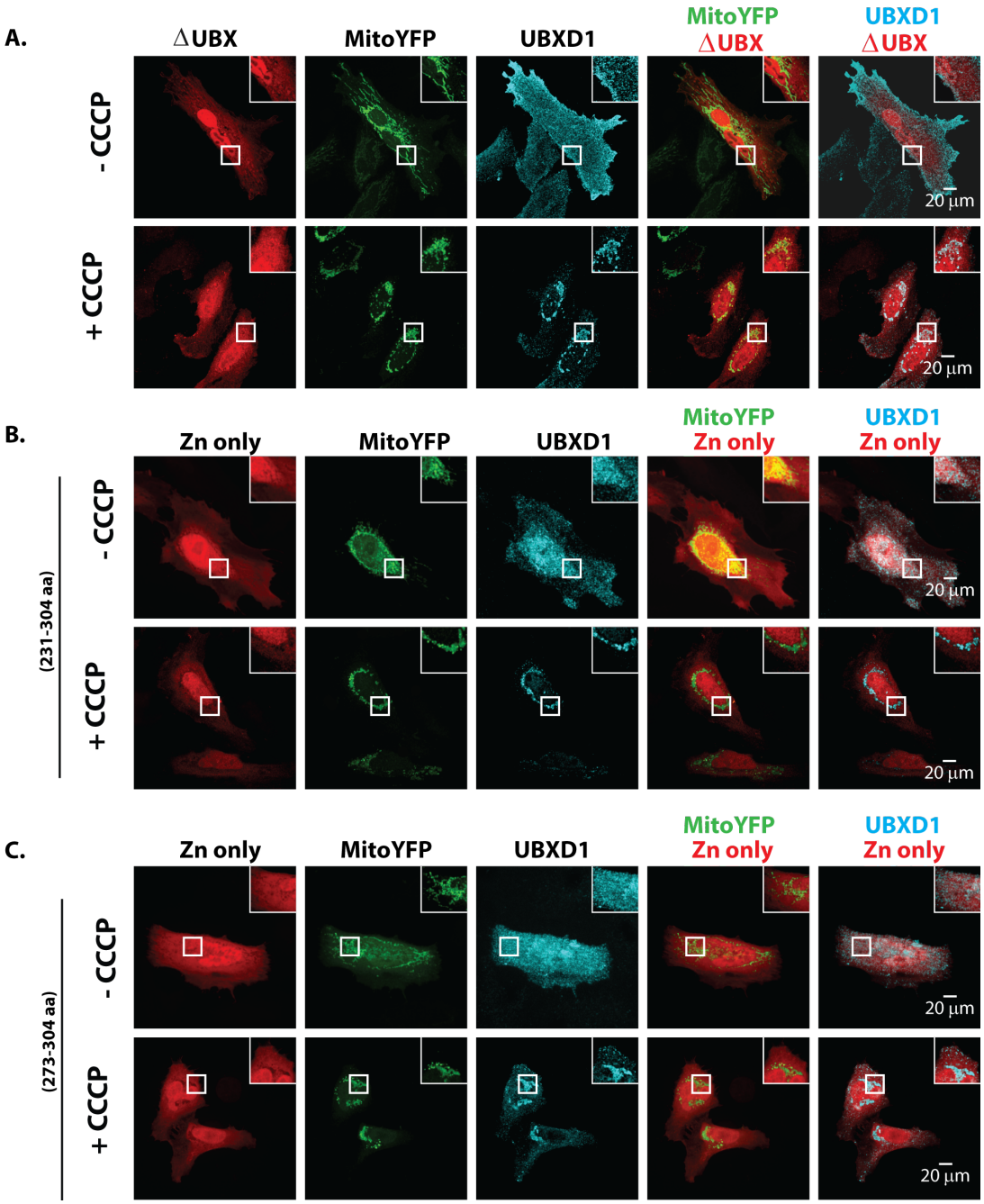

Figure 31: UBX (A) and Zn domains (B+C) are essential for YOD1.2 mitochondrial translocation. HeLa cells transfected with expression plasmids for ^{FLAG}UBXD1 or variants of YOD1.2 and mitoYFP-T2A-^{3xmyc}Parkin were treated with CCCP for 6 h or left untreated as control. Fixed cells were stained using mouse anti-FLAG antibodies and analyzed by confocal microscopy. Shown are representative images of two independent experiments.

6 Discussion

Mitochondrial dysfunction is central to virtually all neurodegenerative processes [266], with mitochondrial failure as consequence of accumulating damage to mitochondrial components over time. Therefore multiple mitochondrial quality control mechanisms are an essential part of maintaining cellular function to prevent aging and untimely death of neuronal cells. Keeping mitochondria in a healthy state is a complex process and has to be tightly regulated [267]. The aim of this work was to better understand the interplay between mitochondrial maintenance and the ubiquitin proteasome system with a special focus on p97 and its cofactors. The work presented here further establishes the role of p97 in mitochondrial quality control through mitophagic clearance of uncoupled mitochondria. Also, with UBXD1, YOD1.2, SAKS1 and Erasin, four novel partners for mitochondrial functions of p97 were identified and UBXD1 and YOD1 were characterized in more detail.

6.1 UBXD1 as mitochondrial recruitment factor for p97

UBXD1 contains with PUB and VIM two distinct p97 binding domains, enabling it to interact with p97 in a bipartite manner [268]. According to the literature [158], the N-terminal VIM and PUB domain are both sufficient to bind p97. Interestingly, upon ectopic expression, both domains are individually capable of recruiting p97 to mitochondria under mitophagic conditions. Based on results from quantitative yeast two-hybrid (Figure 21), both domains might provide additive binding strength. These observations point to additional functions of the bipartite, VIM/PUB-containing p97 binding motif in UBXD1. As suggested by Kern [183], VIM and PUB domain likely bind to different regions of p97 [183]. In accordance with our yeast-2-hybrid interaction data, this leads to a stronger binding between p97 and UBXD1. However, also a regulatory function for this binding pattern might be considered. It is conceivable, that UBXD1 not only recruits p97 via its VIM and PUB domain to mitochondria, but also regulates p97

activity additionally. Kern and colleagues [183] identified the VIM as direct competitor for binding between p97 and its cofactor p47. Whether such a mechanism is also involved in the mitophagy-related function of UBXD1 is unclear. While, p47 was connected to ER and Golgi biogenesis [269], no mitochondrial function for p47 is established until now. Nonetheless, that the bipartite p97 interaction motif consisting of the VIM and PUB domain might serve similar functions during mitophagy and not only recruits p97 to mitochondria but might also adjust cofactor binding of p97 under mitophagic conditions.

As for the UBX domain found in UBXD1, our data are consistent with UBXD1 recognizing depolarized mitochondria undergoing Parkin-dependent mitophagy and facilitating p97 recruitment. As shown in Figure 15, recognition of mitophagic mitochondria depends exclusively on the UBX domain contained in UBXD1, as evidenced by the complete lack of mitochondrial translocation of UBXD1 missing its UBX domain. The UBX domain does not contribute to p97 binding, although the UBX domain is generally considered to be a p97 interaction motif [270]. Our data points to a role for the UBX domain of UBXD1 as receptor for mitochondria undergoing mitophagy. It remains unclear what mitochondrial signal triggers UBXD1 translocation, however, it is likely that the UBX domain of UBXD1 recognizes a factor only present on mitochondria after mitophagic induction. A yeast-two-hybrid screen using the UBX domain of UBXD1 as bait and a cDNA library from CCCP-treated HeLa cells as prey did not reveal proteins with mitochondrial localization in mitophagic cells (Neutzner, personal communication).

Bringing UBXD1 fused to the ActA tail to mitochondria in the absence of Parkin and CCCP resulted in the recruitment of p97 (Figure 19). This suggests that UBXD1 is sufficient for p97 to recognize mitophagic mitochondria and additional signals are not necessary for this particular process. This observation further supports the notion that UBXD1 bridges mitochondria undergoing mitophagy with p97 and subsequently with the UPS.

6.2 Multiple connections between p97 and mitochondria

The work presented here strongly connects p97 via UBXD1 and potentially YOD1.2 to mitochondrial quality control. The identification of other p97 cofactors, namely SAKS1 and Erasin, hints to potentially additional roles for p97 in mitochondrial health. Depolarization of mitochondria in Parkin-expressing cells triggers likely a plethora of mechanisms all with the goal of removing mitochondrial subunits. With mitophagy being highly regulated and the general importance of ubiquitination, it is likely that several regulatory modules are in need for p97-mediated processing of ubiquitinated proteins. Also the different domain composition of the newly identified p97 cofactors points in the same direction. Especially interesting in this regard is Erasin. This cofactor contains a transmembrane domain anchoring the protein in the ER membrane. Upon mitophagic induction, Erasin seems to migrate towards ER-mitochondria contact sites (Neutzner, personal communication) suggesting a role for p97 at this important inter-organellar nexus during mitophagy. While further work is necessary to define the function of SAKS1, Erasin and YOD1.2, the identification of four novel accessory p97 proteins translocating to mitochondria under mitophagic conditions suggests an even more intricate relationship between the UPS and mitochondria as previously appreciated.

6.3 UBXD1 as pro-mitophagic factor

The translocation of UBXD1 after mitochondrial depolarization strongly suggests a role during mitophagy. Since p97 acts in a pro-mitophagic manner, it is resonable to expect that also UBXD1 is likely a pro-mitophagic factor. And indeed, ectopic expression of UBXD1 caused an increase in LC3-containing vesicles near mitochondria consistent with a positive regulatory function. In line with this observation, a significant decrease of mitophagy was observed in $HeLa^{UBXD1\text{-}low}$ cells (Figure 25). Increased mitophagy following ectopic expression of UBXD1 and decreased mitophagic flux under conditions of lowered UBXD1 levels are consistent with a pro-mitophagic role. While

it remains unclear how UBXD1 causes the observed increase in mitophagic flux, it is likely that removal of certain mitochondrial proteins by UBXD1 together with p97 is involved. It was previously described that p97-mediated removal of mitofusins promotes mitophagy. [255]. Interestingly, UBXD1 in concert with p97 and other cofactors was recently shown to promote the removal of K48-linked ubiquitin from ruptured lysosomes, thereby increasing the amount of K63-linked ubiquitin tipping the balance towards lysophagy. [186]. A similar mechanism might be at work during mitophagy. Here, Parkin is known to generate not only K48, but also K63-linked as well as other types of polyubiquitin on mitochondria. In analogy to the role of K48 and K63 ubiquitin chains in lysophagy, UBXD1 may also modulate the balance between these types of polyubiquitin on mitochondria promoting mitophagy.

6.4 UBXD1 and YOD1 in mitochondrial quality control

In order to maintain mitochondrial homeostasis, p97-mediated retrotranslocation of misfolded proteins is needed likely involving different cofactors and potentially deubiquitinating enzymes. Based on our data connecting UBXD1 to OMMAD and reports by Ernst and colleagues [111], we examined YOD1, an UBX-domain-containing member of the otubain family of DUBs. According to the literature, YOD1 is a p97-associated deubiquitinting enzyme in association with ERAD [102, 111, 271, 272]. A dominant negative mutant of YOD1 (YOD1C160S) has been shown to stabilize ERAD substrates mostly in a non-ubiquitinated and glycosylated form. This accumulation of substrate proteins in the ER lumen might be a consequence of stalling molecules in the putative exit channel [102, 111]. As for p97-mediated retrotranslocation, deubiquitinating activity of YOD1 is also required for retrotranslocation [120, 111, 271].

YOD1 comes in two different isoforms - YOD1.1 and YOD1.2 - and is part of multiprotein complex containing p97 [111]. According to Pfam predictions [273], YOD1 comprises three domains, an N-terminal UBX domain, OTU domain, and a C-terminal zinc finger

domain. Interestingly, the N-terminal UBX domain differs between the two YOD1 isoforms. As shown in Figure 29 upon UBXD1 expression both domains, UBX and Zn are necessary for YOD1.2 mitochondrial recruitment, under mitophagic conditions.
In line with previous reports [186], YOD1 acts as an ubiquitin sensor and together with UBXD1 drives the clearance of ruptured lysosomes by autophagy. Such a mechanism might also be in play during mitophagy. Alternatively and based on our time course experiments (Figure 29), initial recognition of mitophagic mitochondria is performed by UBXD1 via its UBX domain. Following p97 mitochondrial recruitment through the VIM and PUB domain of UBXD1, YOD1.2 translocates to this complex. Based on our findings of direct interaction between UBXD1 and both isoforms of YOD1 and the differential interaction between p97 and YOD1 isoforms (Figure 27), mitochondrial translocation of YOD1.2 is likely triggered by binding to UBXD1 on mitochondria. Interestingly, YOD1.2 shows only very limited recruitment to mitophagic mitochondria in the absence of ectopically expressed UBXD1, and UBXD1 and YOD1.2 are not found on the same mitochondria together. This might be explained by a two-step mechanism. Upon recognition of mitophagic mitochondria by UBXD1 and YOD1.2 recruitment, the presence of YOD1.2 triggers the next step in the UBXD1-mediated mitophagic process. Due to the presence of DUB activity in YOD1.2 it is tempting to speculate that ubiquitinated mitochondrial proteins are deubiquitinated. The consequence of this hypothesized deubiquitination could be two-fold. Either mitophagy is damped by counteracting Parkin-mediated ubiquitination, or mitophagy might also be accelerated due to diminishing K48 and enriching K63 ubiquitination of mitochondria as observed during lysophagy [186]. Further work will be necessary to address these questions.

6.5 Potential connections between UBXD1 and neurodegenerative disease

Mutations in p97 are connected to the development of IBMPFD. Such disease-causing mutations of p97 were shown to alter interaction with UBXD1 connecting this cofactor

to a disease process [274]. Mutations in p97 causing myopathy and neurodegeneration were shown to hamper interaction with UBXD1, resulting in impaired degradation and subsequent accumulation of p97 client proteins [185]. Also, UBXD1 was recently connected to the degradation of mitochondrial MCL1 in the context of an *in vitro* model of Huntington's disease. [274]. Since impaired mitophagy is strongly linked to neurodegenerative diseases, it is tempting to speculate that, due to altered binding of mutant p97 to UBXD1, p97-linked myopathy and neurodegeneration might not only be a consequence of disrupted lysophagy, but might also result from impaired mitophagic clearance of damaged mitochondria.

6.6 Organelle-linked ubiquitination shares p97-mediated retrotranslocation

Ubiquitination plays an essential role in virtually all cellular processes, and especially in the quality control of proteins. Recently, the role of ubiquitination and ubiquitin-dependent protein degradation in mitochondrial physiology became clearer. For OMMAD, the special topology of mitochondria requires specialized protein degradation mechanisms. As the UPS is mainly cytosolic, ubiquitin-dependent degradation of mitochondrial proteins necessitates the presence of factors able to connect the UPS to mitochondria. OMM-anchored RING finger ubiquitin ligases such as MARCH5 [253], MULAN/MAPL [275] and IBRDC2 [191] might provide this interfacing function with the help of p97 [276, 277] and its cofactors. This is similar to (ERAD) [278]. There too, membrane-anchored ubiquitin ligases target organelle-resident proteins for proteasomal degradation, and there too, p97 and its cofactors are involved in the retrotranslocation of ubiquitinated protein. Interestingly, while both processes employ a different set of ubiquitin ligases relying on different mechanisms for selecting substrate proteins for ubiquitination, p97 seems to be a common component of OMMAD and ERAD linking organelle-specific recognition and ubiquitination to the shared downstream degradation machinery. Also for lysophagy, p97-mediated retrotranslocation of ubiquitinated proteins aids the autophagic

process [184, 185, 186, 274]. These mechanisms do not only share p97, but also cofactors. In this study, the recruitment of UBXD1 and YOD1.2 to mitochondria was established. Interestingly, both p97 cofactors are also connected to ERAD and lysophagy. Although protein retrotranslocation from lysosomes, mitochondria, and the ER certainly serves different functions and a varied machinery is involved in substrate targeting, p97 and to some extent its cofactors are a common theme in ubiquitin-dependent organellar quality control pathways.

6.7 UBXD1 linking UPS and mitophagy

Under physiological conditions, mitochondria are exposed to different stressors leading to different levels of damage. While initial low level damage is likely dealt with OMMAD through the removal of ubiquitinated proteins from mitochondria, mitophagic processes come in play once more extensive damage accumulates despite OMMAD activity. Our data supports a new role for p97-retrotranslocation mechanism in association with UBXD1 (Figure 32). In addition, our findings may connect the potential OMMAD mechanism with the clearance of damaged mitochondria through mitophagy. OMMAD may therefore provide an initial mitochondrial quality control for the clearance of misfolded proteins and help to keep mitochondria in a healthy state during constant low level of stress conditions. However, if mitochondrial damage levels exceed the capacity of OMMAD, mitophagic processes are initiated. P97 together with UBXD1 and YOD1.2 might be part of the regulatory mechanisms helping to switch from OMMAD to mitophagic quality control mechanisms. Thus, UBXD1 might role for the UPS in the maintenance of mitochondrial homeostasis by regulating organelle dynamics, the proteasome and mitophagy.

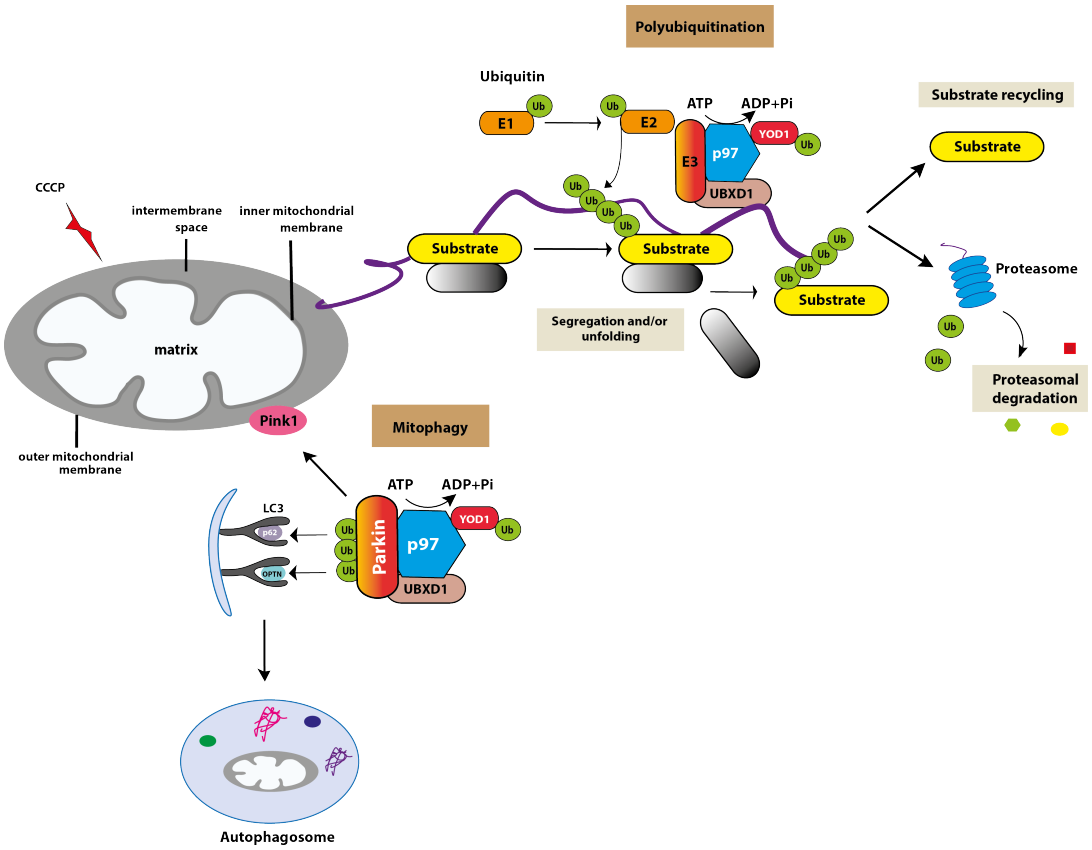

Figure 32: Model of UBXD1 in modulating the mitochondria quality control. Polyubiquitination of mitochondrial proteins by the catalyzed reaction of E1, E2 and E3 enzymes in this depiction leads to the recruitment of the P97/VCP complex by UBXD1 to the OMM. P97/VCP can extract an ubiquitinated protein in an ATP-dependent process that facilitates its proteasomal degradation with the help of DUBs such YOD1. On the other hand, the UPS is also needed for the autophagic degradation of damaged mitochondria, a process known as mitophagy.

7 Appendix

List of Figures

List of Tables

7.1 Acknowledgments

This thesis would not have been possible without the help and support of many people who always believed in my vision and endorsed me throughout all this years.

I would like to express my gratitude to *PD Dr. Albert Neutzner* for giving me the chance to work in the Laboratory Ocular Pharmacology. Thanks for guiding and supporting me through all these years. I want to thank his guidance, patience and willingness to discuss and share scientific ideas. I could learn a lot from his scientific expertise. His optimism and strength have taught me to never give up and always try to find the best solutions and alternatives to face the problems.

Many thanks to the members of my thesis committee, *Professor Mrsic-Flogel* and *Professor Christoph Handschin* for accepting to be part of my PhD committee and for the helpful advice on my project.

I want to thank *Dr. Michael Abanto*, *Mr. Beat Erne* from Microscopy Core Facility of our department, and *Mr. Emmanuel Traunecker* from FACS Core Facility. They helped me to study and perfect my knowledge of certain techniques, which contributed extensively into my project.

I want to thank the IT department of the DBM who was always supportive and capable in solving any IT problem I encountered.

A special thank goes to all my lab members of the Ocular Pharmacology. It was a pleasure working with all of them in the laboratory. Therefore, big thanks go to *Corina* and *Claudia* for supporting me so much in different experiments. Also special thanks go to *Chantal*, *Cavit*, *Lei*, *Charles*, *Esther*, *Tina*, *Tatjana*, *Marie Appoline*, *Marie Salat*, *Roy* and *Reto* for supporting me with good advise during my thesis.

Furthermore, I would like to thank *Professor Stephan Frank*, *Lisa* and *Lara* for their collaboration with ideas and scientific support.

Thanks for being there for me *Flussi* and *Xingui*. We always supported each other in the long evenings and weekends in the lab! Gynaecology lab: You all contributed to a nice working atmosphere in the lab.

I want to thank my lovely friends: *Lina*, *Esther*, *Cristian*, *Alexis*, *Ruben*, *Marlenita* and *Nubia* – we all shared a lot of great and unforgettable moments. Thank you for these years full of laughs, nice dinners, concerts, trips, parties and funny moments. You could always cheer me up when I was down, especially in the last times, and I am happy to call you my friends today.

I want to thank all the other nice people I met and with whom I spent a lot of joyful moments beside science: *Moni*, *Nadia*, *Daniela*, *Lara*, *Emma*, *Šime*, *Wiki* and of course the Portuguese connection: *Sofia*, *Anabela*, *Sandra*, *Antonio* and *João*.

I want to thank *Joana B.* and *Mariana* for the support among of those years.
Existem sentimentos e amizades que nenhuma palavra ou atitude consegue apagar.

Very last but not least: My deepest gratitude goes to my family; the most important piece in my life. Thank you very much for all the support, power and strength to continue the scientific way throughout the whole PhD.
Muito obrigada e desculpem me todas as ausências.
Adoro-vos incodicionalmente.

“ Temos, todos que vivemos,

Uma vida que é vivida

E outra vida que é pensada,

E a única vida que temos

É essa que é dividida

Entre a verdadeira e a errada.

Qual porém é a verdadeira

E qual errada, ninguém

Nos saberá explicar;

E vivemos de maneira

Que a vida que a gente tem

É a que tem que pensar.” FP

References

[1] Donald D Newmeyer and Shelagh Ferguson-Miller. Mitochondria: releasing power for life and unleashing the machineries of death. *Cell*, (4):481–90, 2003.

[2] Jodi Nunnari and Anu Suomalainen. Mitochondria: in sickness and in health. *Cell*, (6):1145–59, 2012.

[3] Takashi Tatsuta, Melanie Scharwey, and Thomas Langer. Mitochondrial lipid trafficking. *Trends Cell Biol*, (1):44–52, 2014.

[4] Rosario Rizzuto, Diego De Stefani, Anna Raffaello, and Cristina Mammucari. Mitochondria as sensors and regulators of calcium signalling. *Nat Rev Mol Cell Biol*, (9):566–78, 2012.

[5] Jonathan R Friedman and Jodi Nunnari. Mitochondrial form and function. *Nature*, (7483):335–43, 2014.

[6] Oliver Stehling and Roland Lill. The role of mitochondria in cellular iron-sulfur protein biogenesis: mechanisms, connected processes, and diseases. *Cold Spring Harb Perspect Biol*, (8):a011312, 2013.

[7] Marc Liesa and Orian S Shirihai. Mitochondrial dynamics in the regulation of nutrient utilization and energy expenditure. *Cell Metab*, (4):491–506, 2013.

[8] Lena Pernas and Luca Scorrano. Mito-morphosis: Mitochondrial fusion, fission, and cristae remodeling as key mediators of cellular function. *Annu Rev Physiol*, (78):505–31, 2016.

[9] Sarah E Calvo, Karl R Clauser, and Vamsi K Mootha. Mitocarta2.0: an updated inventory of mammalian mitochondrial proteins. *Nucleic Acids Res*, (D1):D1251–7, 2016.

[10] B Martin Hallberg and Nils-Goran Larsson. Making proteins in the powerhouse. *Cell Metab*, (2):226–40, 2014.

[11] Robert N Lightowlers, Agata Rozanska, and Zofia M Chrzanowska-Lightowlers. Mitochondrial protein synthesis: figuring the fundamentals, complexities and complications, of mammalian mitochondrial translation. *FEBS Lett*, (15):2496–503, 2014.

[12] Michael J Baker, Takashi Tatsuta, and Thomas Langer. Quality control of mitochondrial proteostasis. *Cold Spring Harb Perspect Biol*, (7):2011, 2011.

[13] Randal J Kaufman and Jyoti D Malhotra. Calcium trafficking integrates endoplasmic reticulum function with mitochondrial bioenergetics. *Biochim Biophys Acta*, (10):2233–9, 2014.

[14] Anna Karnkowska, Vojtech Vacek, Zuzana Zubacova, Sebastian C Treitli, Romana Petrzelkova, Laura Eme, Lukas Novak, Vojtech Zarsky, Lael D Barlow, Emily K Herman, Petr Soukal, Miluse Hroudova, Pavel Dolezal, Courtney W Stairs, Andrew J Roger, Marek Elias, Joel B Dacks, Cestmir Vlcek, and Vladimir Hampl. A eukaryote without a mitochondrial organelle. *Curr Biol*, (10):1274–84, 2016.

[15] Nadine S Anderson, Indrani Mukherjee, Christine M Bentivoglio, and Charles Barlowe. The golgin protein coy1 functions in intra-golgi retrograde transport and interacts with the cog complex and golgi snares. *Mol Biol Cell*, (2017):2017, 2017.

[16] T G Frey and C A Mannella. The internal structure of mitochondria. *Trends Biochem Sci*, (7):319–24, 2000.

[17] Johannes M Herrmann and Jan Riemer. The intermembrane space of mitochondria. *Antioxid Redox Signal*, (9):1341–58, 2010.

[18] Kaye N Truscott, Nils Wiedemann, Peter Rehling, Hanne Muller, Chris Meisinger, Nikolaus Pfanner, and Bernard Guiard. Mitochondrial import of the adp/atp carrier: the essential tim complex of the intermembrane space is required for precursor release from the tom complex. *Mol Cell Biol*, (22):7780–9, 2002.

[19] Hannah M Heath-Engel and Gordon C Shore. Mitochondrial membrane dynamics, cristae remodelling and apoptosis. *Biochim Biophys Acta*, (5-6):549–60, 2006.

[20] F N Gellerich, S Trumbeckaite, J R Opalka, E Seppet, H N Rasmussen, C Neuhoff, and S Zierz. Function of the mitochondrial outer membrane as a diffusion barrier in health and diseases. *Biochem Soc Trans*, (2):164–9, 2000.

[21] Thomas Becker, F-Nora Vogtle, Diana Stojanovski, and Chris Meisinger. Sorting and assembly of mitochondrial outer membrane proteins. *Biochim Biophys Acta*, (7-8):557–63, 2008.

[22] D Rapaport, K P Kunkele, M Dembowski, U Ahting, F E Nargang, W Neupert, and R Lill. Dynamics of the tom complex of mitochondria during binding and translocation of preproteins. *Mol Cell Biol*, (9):5256–62, 1998.

[23] Jean E Vance. Mam (mitochondria-associated membranes) in mammalian cells: lipids and beyond. *Biochim Biophys Acta*, (4):595–609, 2014.

[24] Teruo Hayashi, Rosario Rizzuto, Gyorgy Hajnoczky, and Tsung-Ping Su. Mam: more than just a housekeeper. *Trends Cell Biol*, (2):81–8, 2009.

[25] Rongbin Zhou, Amir S Yazdi, Philippe Menu, and Jurg Tschopp. A role for mitochondria in nlrp3 inflammasome activation. *Nature*, (7329):221–5, 2011.

[26] Saverio Marchi, Simone Patergnani, and Paolo Pinton. The endoplasmic reticulum-mitochondria connection: one touch, multiple functions. *Biochim Biophys Acta*, (4):461–9, 2014.

[27] Dusanka Milenkovic, James N Blaza, Nils-Goran Larsson, and Judy Hirst. The enigma of the respiratory chain supercomplex. *Cell Metab*, (4):765–776, 2017.

[28] Gabriele Giachin, Romain Bouverot, Samira Acajjaoui, Serena Pantalone, and Montserrat Soler-Lopez. Dynamics of human mitochondrial complex i assembly: Implications for neurodegenerative diseases. *Front Mol Biosci*, (3):43, 2016.

[29] Dmitry B Zorov, Magdalena Juhaszova, and Steven J Sollott. Mitochondrial reactive oxygen species (ros) and ros-induced ros release. *Physiol Rev*, (3):909–50, 2014.

[30] Hsiuchen Chen, Scott A Detmer, Andrew J Ewald, Erik E Griffin, Scott E Fraser, and David C Chan. Mitofusins mfn1 and mfn2 coordinately regulate mitochondrial fusion and are essential for embryonic development. *J Cell Biol*, (2):189–200, 2003.

[31] Zhiyin Song, Hsiuchen Chen, Maja Fiket, Christiane Alexander, and David C Chan. Opa1 processing controls mitochondrial fusion and is regulated by mrna splicing, membrane potential, and yme1l. *J Cell Biol*, (5):749–55, 2007.

[32] Suzanne Hoppins, Frank Edlich, Megan M Cleland, Soojay Banerjee, J Michael McCaffery, Richard J Youle, and Jodi Nunnari. The soluble form of bax regulates mitochondrial fusion via mfn2 homotypic complexes. *Mol Cell*, (2):150–60, 2011.

[33] Takumi Koshiba, Scott A Detmer, Jens T Kaiser, Hsiuchen Chen, J Michael McCaffery, and David C Chan. Structural basis of mitochondrial tethering by mitofusin complexes. *Science*, (5685):858–62, 2004.

[34] Zhiyin Song, Mariam Ghochani, J Michael McCaffery, Terrence G Frey, and David C Chan. Mitofusins and opa1 mediate sequential steps in mitochondrial membrane fusion. *Mol Biol Cell*, (15):3525–32, 2009.

[35] E Smirnova, L Griparic, D L Shurland, and A M van der Bliek. Dynamin-related protein drp1 is required for mitochondrial division in mammalian cells. *Mol Biol Cell*, (8):2245–56, 2001.

[36] Hidenori Otera, Chunxin Wang, Megan M Cleland, Kiyoko Setoguchi, Sadaki Yokota, Richard J Youle, and Katsuyoshi Mihara. Mff is an essential factor for mitochondrial recruitment of drp1 during mitochondrial fission in mammalian cells. *J Cell Biol*, (6):1141–58, 2010.

[37] Catherine S Palmer, Laura D Osellame, David Laine, Olga S Koutsopoulos, Ann E Frazier, and Michael T Ryan. Mid49 and mid51, new components of the mitochondrial fission machinery. *EMBO Rep*, (6):565–73, 2011.

[38] Yisang Yoon, Eugene W Krueger, Barbara J Oswald, and Mark A McNiven. The mitochondrial protein hfis1 regulates mitochondrial fission in mammalian cells through an interaction with the dynamin-like protein dlp1. *Mol Cell Biol*, (15):5409–20, 2003.

[39] A Santel and M T Fuller. Control of mitochondrial morphology by a human mitofusin. *J Cell Sci*, (Pt 5):867–74, 2001.

[40] A D Mozdy, J M McCaffery, and J M Shaw. Dnm1p gtpase-mediated mitochondrial fission is a multi-step process requiring the novel integral membrane component fis1p. *J Cell Biol*, (2):367–80, 2000.

[41] Oliver C Loson, Zhiyin Song, Hsiuchen Chen, and David C Chan. Fis1, mff, mid49, and mid51 mediate drp1 recruitment in mitochondrial fission. *Mol Biol Cell*, (5):659–67, 2013.

[42] Shilpa Gandre-Babbe and Alexander M van der Bliek. The novel tail-anchored membrane protein mff controls mitochondrial and peroxisomal fission in mammalian cells. *Mol Biol Cell*, (6):2402–12, 2008.

[43] Mariusz Karbowski and Albert Neutzner. Neurodegeneration as a consequence of failed mitochondrial maintenance. *Acta Neuropathol*, (2):157–71, 2012.

[44] Jill A Fahrner, Raymond Liu, Michael Scott Perry, Jessica Klein, and David C Chan. A novel de novo dominant negative mutation in dnm1l impairs mitochondrial fission and presents as childhood epileptic encephalopathy. *Am J Med Genet A*, (8):2002–11, 2016.

[45] Sylvie Gerber, Majida Charif, Arnaud Chevrollier, Tanguy Chaumette, Claire Angebault, Mariame Selma Kane, Aurelien Paris, Jennifer Alban, Melanie Quiles, Cecile Delettre, Dominique Bonneau, Vincent Procaccio, Patrizia Amati-Bonneau, Pascal Reynier, Stephanie Leruez, Raphael Calmon, Nathalie Boddaert, Benoit Funalot, Marlene Rio, Didier Bouccara, Isabelle Meunier, Hiromi Sesaki, Josseline Kaplan, Christian P Hamel, Jean-Michel Rozet, and Guy Lenaers. Mutations in dnm1l, as in opa1, result indominant optic atrophy despite opposite effectson mitochondrial fusion and fission. *Brain*, (10):2586–2596, 2017.

[46] Sergio Papa, Pietro Luca Martino, Giuseppe Capitanio, Antonio Gaballo, Domenico De Rasmo, Anna Signorile, and Vittoria Petruzzella. The oxidative phosphorylation system in mammalian mitochondria. *Adv Exp Med Biol*, (942):3–37, 2012.

[47] Rita V Chertkova, Nadezda A Brazhe, Tatiana V Bryantseva, Alexey N Nekrasov, Dmitry A Dolgikh, Alexander I Yusipovich, Olga Sosnovtseva, Georgy V Maksimov, Andrei B Rubin, and Mikhail P Kirpichnikov. New insight into the mechanism of mitochondrial cytochrome c function. *PLoS One*, (5):e0178280, 2017.

[48] Anna V Kudryavtseva, George S Krasnov, Alexey A Dmitriev, Boris Y Alekseev, Olga L Kardymon, Asiya F Sadritdinova, Maria S Fedorova, Anatoly V Pokrovsky, Nataliya V Melnikova, Andrey D Kaprin, Alexey A Moskalev, and Anastasiya V Snezhkina. Mitochondrial dysfunction and oxidative stress in aging and cancer. *Oncotarget*, (29):44879–44905, 2016.

[49] Ville R I Kaila, Marten Wikstrom, and Gerhard Hummer. Electrostatics, hydration, and proton transfer dynamics in the membrane domain of respiratory complex i. *Proc Natl Acad Sci U S A*, (19):6988–93, 2014.

[50] Lothar Kussmaul and Judy Hirst. The mechanism of superoxide production by nadh:ubiquinone oxidoreductase (complex i) from bovine heart mitochondria. *Proc Natl Acad Sci U S A*, (20):7607–12, 2006.

[51] Vera G Grivennikova, Darya V Serebryanaya, Elena P Isakova, Tatyana A Belozerskaya, and Andrei D Vinogradov. The transition between active and de-activated forms of nadh:ubiquinone oxidoreductase (complex i) in the mitochondrial membrane of neurospora crassa. *Biochem J*, (Pt 3):619–26, 2003.

[52] Elizabeth A Mazzio, Fran Close, and Karam F A Soliman. The biochemical and cellular basis for nutraceutical strategies to attenuate neurodegeneration in parkinson's disease. *Int J Mol Sci*, (1):506–69, 2011.

[53] Franco Zoccarato, Paola Toscano, and Adolfo Alexandre. Dopamine-derived dopaminochrome promotes h(2)o(2) release at mitochondrial complex i: stimulation by rotenone, control by ca(2+), and relevance to parkinson disease. *J Biol Chem*, (16):15587–94, 2005.

[54] Michael P Murphy. How mitochondria produce reactive oxygen species. *Biochem J*, (1):1–13, 2009.

[55] S Raha and B H Robinson. Mitochondria, oxygen free radicals, and apoptosis. *Am J Med Genet*, (1):62–70, 2001.

[56] S Raha and B H Robinson. Mitochondria, oxygen free radicals, disease and ageing. *Trends Biochem Sci*, (10):502–8, 2000.

[57] B CHANCE and G HOLLUNGER. The interaction of energy and electron transfer reactions in mitochondria. i. general properties and nature of the products of succinate-linked reduction of pyridine nucleotide. *J Biol Chem*, (236):1534–43, 1961.

[58] B CHANCE and G HOLLUNGER. The interaction of energy and electron transfer reactions in mitochondria. iv. the pathway of electron transfer. *J Biol Chem*, (236):1562–8, 1961.

[59] T V Votyakova and I J Reynolds. Deltapsi(m)-dependent and -independent production of reactive oxygen species by rat brain mitochondria. *J Neurochem*, (2):266–77, 2001.

[60] Vera G Grivennikova and Andrei D Vinogradov. Generation of superoxide by the mitochondrial complex i. *Biochim Biophys Acta*, (5-6):553–61, 2006.

[61] B L Trumpower. The protonmotive q cycle. energy transduction by coupling of proton translocation to electron transfer by the cytochrome bc1 complex. *J Biol Chem*, (20):11409–12, 1990.

[62] E Braunwald and R A Kloner. Myocardial reperfusion: a double-edged sword? *J Clin Invest*, (5):1713–9, 1985.

[63] Dieter G Brdiczka, Dmitry B Zorov, and Shey-Shing Sheu. Mitochondrial contact sites: their role in energy metabolism and apoptosis. *Biochim Biophys Acta*, (2):148–63, 2006.

[64] Andrej Musatov and Neal C Robinson. Susceptibility of mitochondrial electron-transport complexes to oxidative damage. focus on cytochrome c oxidase. *Free Radic Res*, (11):1313–26, 2012.

[65] K M Broekemeier, M E Dempsey, and D R Pfeiffer. Cyclosporin a is a potent inhibitor of the inner membrane permeability transition in liver mitochondria. *J Biol Chem*, (14):7826–30, 1989.

[66] K M Broekemeier, C K Klocek, and D R Pfeiffer. Proton selective substate of the mitochondrial permeability transition pore: regulation by the redox state of the electron transport chain. *Biochemistry*, (38):13059–65, 1998.

[67] Kimberly M Broekemeier, James R Iben, Emily G LeVan, Elliott D Crouser, and Douglas R Pfeiffer. Pore formation and uncoupling initiate a ca2+-independent degradation of mitochondrial phospholipids. *Biochemistry*, (24):7771–80, 2002.

[68] C B Thompson. Apoptosis in the pathogenesis and treatment of disease. *Science*, (5203):1456–62, 1995.

[69] D W Choi. Excitotoxic cell death. *J Neurobiol*, (9):1261–76, 1992.

[70] B Hoffman and D A Liebermann. Molecular controls of apoptosis: differentiation/growth arrest primary response genes, proto-oncogenes, and tumor suppressor genes as positive and negative modulators. *Oncogene*, (7):1807–12, 1994.

[71] R E Ellis, J Y Yuan, and H R Horvitz. Mechanisms and functions of cell death. *Annu Rev Cell Biol*, (7):663–98, 1991.

[72] H Y Chang and X Yang. Proteases for cell suicide: functions and regulation of caspases. *Microbiol Mol Biol Rev*, (4):821–46, 2000.

[73] Chunxin Wang and Richard J Youle. The role of mitochondria in apoptosis*. *Annu Rev Genet*, (43):95–118, 2009.

[74] Anne-Sophie Benischke, Charles Hemion, Josef Flammer, and Albert Neutzner. Proteasome-mediated quality control of s-nitrosylated mitochondrial proteins. *Mitochondrion*, (17):182–6, 2014.

[75] Hermann-Josef Meyer and Michael Rape. Enhanced protein degradation by branched ubiquitin chains. *Cell*, (4):910–21, 2014.

[76] D Voges, P Zwickl, and W Baumeister. The 26s proteasome: a molecular machine designed for controlled proteolysis. *Annu Rev Biochem*, (68):1015–68, 1999.

[77] Rina Rosenzweig, Vered Bronner, Daoning Zhang, David Fushman, and Michael H Glickman. Rpn1 and rpn2 coordinate ubiquitin processing factors at proteasome. *J Biol Chem*, (18):14659–71, 2012.

[78] Elena Koulich, Xiaohua Li, and George N DeMartino. Relative structural and functional roles of multiple deubiquitylating proteins associated with mammalian 26s proteasome. *Mol Biol Cell*, (3):1072–82, 2008.

[79] Y Saeki, A Toh-e, and H Yokosawa. Rapid isolation and characterization of the yeast proteasome regulatory complex. *Biochem Biophys Res Commun*, (2):509–15, 2000.

[80] B Ehring, T H Meyer, C Eckerskorn, F Lottspeich, and R Tampe. Effects of major-histocompatibility-complex-encoded subunits on the peptidase and proteolytic activities of human 20s proteasomes. cleavage of proteins and antigenic peptides. *Eur J Biochem*, (1-2):404–15, 1996.

[81] A K Nussbaum, T P Dick, W Keilholz, M Schirle, S Stevanovic, K Dietz, W Heinemeyer, M Groll, D H Wolf, R Huber, H G Rammensee, and H Schild. Cleavage motifs of the yeast 20s proteasome beta subunits deduced from digests of enolase 1. *Proc Natl Acad Sci U S A*, (21):12504–9, 1998.

[82] Kai-Uwe Kalies, Susanne Allan, Tatiana Sergeyenko, Heike Kroger, and Karin Romisch. The protein translocation channel binds proteasomes to the endoplasmic reticulum membrane. *EMBO J*, (13):2284–93, 2005.

[83] Waiyan Ng, Tatiana Sergeyenko, Naiyan Zeng, Jeremy D Brown, and Karin Romisch. Characterization of the proteasome interaction with the sec61 channel in the endoplasmic reticulum. *J Cell Sci*, (Pt 4):682–91, 2007.

[84] Nikhil Panicker, Valina L Dawson, and Ted M Dawson. Activation mechanisms of the e3 ubiquitin ligase parkin. *Biochem J*, (18):3075–3086, 2017.

[85] Rhesa Budhidarmo, Yoshio Nakatani, and Catherine L Day. Rings hold the key to ubiquitin transfer. *Trends Biochem Sci*, (2):58–65, 2012.

[86] Hyung Cheol Kim and Jon M Huibregtse. Polyubiquitination by hect e3s and the determinants of chain type specificity. *Mol Cell Biol*, (12):3307–18, 2009.

[87] Donald E Spratt, Helen Walden, and Gary S Shaw. Rbr e3 ubiquitin ligases: new structures, new insights, new questions. *Biochem J*, (3):421–37, 2014.

[88] Deepak Chhangani, Ajay Prakash Joshi, and Amit Mishra. E3 ubiquitin ligases in protein quality control mechanism. *Mol Neurobiol*, (3):571–85, 2012.

[89] Christopher E Berndsen and Cynthia Wolberger. New insights into ubiquitin e3 ligase mechanism. *Nat Struct Mol Biol*, (4):301–7, 2014.

[90] K L Lorick, J P Jensen, S Fang, A M Ong, S Hatakeyama, and A M Weissman. Ring fingers mediate ubiquitin-conjugating enzyme (e2)-dependent ubiquitination. *Proc Natl Acad Sci U S A*, (20):11364–9, 1999.

[91] J S Thrower, L Hoffman, M Rechsteiner, and C M Pickart. Recognition of the polyubiquitin proteolytic signal. *EMBO J*, (1):94–102, 2000.

[92] Eric B Dammer, Chan Hyun Na, Ping Xu, Nicholas T Seyfried, Duc M Duong, Dongmei Cheng, Marla Gearing, Howard Rees, James J Lah, Allan I Levey, John Rush, and Junmin Peng. Polyubiquitin linkage profiles in three models of proteolytic stress suggest the etiology of alzheimer disease. *J Biol Chem*, (12):10457–65, 2011.

[93] Lynn Bedford, Robert Layfield, R John Mayer, Junmin Peng, and Ping Xu. Diverse polyubiquitin chains accumulate following 26s proteasomal dysfunction in mammalian neurones. *Neurosci Lett*, (1):44–7, 2011.

[94] Donald S Kirkpatrick, Nathaniel A Hathaway, John Hanna, Suzanne Elsasser, John Rush, Daniel Finley, Randall W King, and Steven P Gygi. Quantitative analysis of in vitro ubiquitinated cyclin b1 reveals complex chain topology. *Nat Cell Biol*, (7):700–10, 2006.

[95] Junwu Yang, Yi Hong, Wenzong Wang, Weibing Wu, Yayun Chi, Hongliang Zong, Xiangfei Kong, Yuanyan Wei, Xiaojing Yun, Chunming Cheng, Kangli Chen, and Jianxin Gu. Hsp70 protects bcl2l12 and bcl2l12a from n-terminal ubiquitination-mediated proteasomal degradation. *FEBS Lett*, (9):1409–14, 2009.

[96] David Komander, Michael J Clague, and Sylvie Urbe. Breaking the chains: structure and function of the deubiquitinases. *Nat Rev Mol Cell Biol*, (8):550–63, 2009.

[97] Bernat Crosas, John Hanna, Donald S Kirkpatrick, Dan Phoebe Zhang, Yoshiko Tone, Nathaniel A Hathaway, Christa Buecker, David S Leggett, Marion Schmidt, Randall W King, Steven P Gygi, and Daniel Finley. Ubiquitin chains are remodeled at the proteasome by opposing ubiquitin ligase and deubiquitinating activities. *Cell*, (7):1401–13, 2006.

[98] Sebastian Rumpf and Stefan Jentsch. Functional division of substrate processing cofactors of the ubiquitin-selective cdc48 chaperone. *Mol Cell*, (2):261–9, 2006.

[99] Francisca E Reyes-Turcu, Karen H Ventii, and Keith D Wilkinson. Regulation and cellular roles of ubiquitin-specific deubiquitinating enzymes. *Annu Rev Biochem*, (78):363–97, 2009.

[100] Byung-Hoon Lee, Min Jae Lee, Soyeon Park, Dong-Chan Oh, Suzanne Elsasser, Ping-Chung Chen, Carlos Gartner, Nevena Dimova, John Hanna, Steven P Gygi, Scott M Wilson, Randall W King, and Daniel Finley. Enhancement of proteasome activity by a small-molecule inhibitor of usp14. *Nature*, (7312):179–84, 2010.

[101] Cecile M Pickart and Robert E Cohen. Proteasomes and their kin: proteases in the machine age. *Nat Rev Mol Cell Biol*, (3):177–87, 2004.

[102] Robert Ernst, Jasper H L Claessen, Britta Mueller, Sumana Sanyal, Eric Spooner, Annemarthe G van der Veen, Oktay Kirak, Christian D Schlieker, Wilhelm A Weihofen, and Hidde L Ploegh. Enzymatic blockade of the ubiquitin-proteasome pathway. *PLoS Biol*, (3):e1000605, 2011.

[103] Mathew E Sowa, Eric J Bennett, Steven P Gygi, and J Wade Harper. Defining the human deubiquitinating enzyme interaction landscape. *Cell*, (2):389–403, 2009.

[104] Y L Yang and X M Li. The iap family: endogenous caspase inhibitors with multiple biological activities. *Cell Res*, (3):169–77, 2000.

[105] Pooja Agrawal, Yu-Ting Chen, Birgit Schilling, Bradford W Gibson, and Robert E Hughes. Ubiquitin-specific peptidase 9, x-linked (usp9x) modulates activity of mammalian target of rapamycin (mtor). *J Biol Chem*, (25):21164–75, 2012.

[106] Robyn T Sussman, Timothy J Stanek, Paul Esteso, John D Gearhart, Karen E Knudsen, and Steven B McMahon. The epigenetic modifier ubiquitin-specific protease 22 (usp22) regulates embryonic stem cell differentiation via transcriptional repression of sex-determining region y-box 2 (sox2). *J Biol Chem*, (33):24234–46, 2013.

[107] Sarah G Hymowitz and Ingrid E Wertz. A20: from ubiquitin editing to tumour suppression. *Nat Rev Cancer*, (5):332–41, 2010.

[108] Hongbo Hu, George C Brittain, Jae-Hoon Chang, Nahum Puebla-Osorio, Jin Jin, Anna Zal, Yichuan Xiao, Xuhong Cheng, Mikyoung Chang, Yang-Xin Fu, Tomasz Zal, Chengming Zhu, and Shao-Cong Sun. Otud7b controls non-canonical nf-kappab activation through deubiquitination of traf3. *Nature*, (7437):371–4, 2013.

[109] Kirstin Keusekotten, Paul Ronald Elliott, Laura Glockner, Berthe Katrine Fiil, Rune Busk Damgaard, Yogesh Kulathu, Tobias Wauer, Manuela Kathrin Hospenthal, Mads Gyrd-Hansen, Daniel Krappmann, Kay Hofmann, and David Komander. Otulin antagonizes lubac signaling by specifically hydrolyzing met1-linked polyubiquitin. *Cell*, (6):1312–26, 2013.

[110] Nobuhiko Kayagaki, Qui Phung, Salina Chan, Ruchir Chaudhari, Casey Quan, Karen M O'Rourke, Michael Eby, Eric Pietras, Genhong Cheng, J Fernando Bazan, Zemin Zhang, David Arnott, and Vishva M Dixit. Duba: a deubiquitinase that regulates type i interferon production. *Science*, (5856):1628–32, 2007.

[111] Robert Ernst, Britta Mueller, Hidde L Ploegh, and Christian Schlieker. The otubain yod1 is a deubiquitinating enzyme that associates with p97 to facilitate protein dislocation from the er. *Mol Cell*, (1):28–38, 2009.

[112] Shinichiro Nakada, Ikue Tai, Stephanie Panier, Abdallah Al-Hakim, Shun-Ichiro Iemura, Yu-Chi Juang, Lara O'Donnell, Ayako Kumakubo, Meagan Munro, Frank Sicheri, Anne-Claude Gingras, Tohru Natsume, Toshio Suda, and Daniel Durocher. Non-canonical inhibition of dna damage-dependent ubiquitination by otub1. *Nature*, (7309):941–6, 2010.

[113] Guem Hee Baek, Haili Cheng, Vitnary Choe, Xin Bao, Jia Shao, Shiwen Luo, and Hai Rao. Cdc48: a swiss army knife of cell biology. *J Amino Acids*, (2013):183421, 2013.

[114] Delphine Fessart, Esther Marza, Said Taouji, Frederic Delom, and Eric Chevet. P97/cdc-48: proteostasis control in tumor cell biology. *Cancer Lett*, (1):26–34, 2013.

[115] Hemmo Meyer, Monika Bug, and Sebastian Bremer. Emerging functions of the vcp/p97 aaa-atpase in the ubiquitin system. *Nat Cell Biol*, (2):117–23, 2012.

[116] Dieter H Wolf and Alexandra Stolz. The cdc48 machine in endoplasmic reticulum associated protein degradation. *Biochim Biophys Acta*, (1):117–24, 2012.

[117] Efrat Rabinovich, Anat Kerem, Kai-Uwe Frohlich, Noam Diamant, and Shoshana Bar-Nun. Aaa-atpase p97/cdc48p, a cytosolic chaperone required for endoplasmic reticulum-associated protein degradation. *Mol Cell Biol*, (2):626–34, 2002.

[118] Yang Wang, Petek Ballar, Yongwang Zhong, Xuebao Zhang, Chao Liu, Ying-Jiu Zhang, Mervyn J Monteiro, Jun Li, and Shengyun Fang. Svip induces localization of p97/vcp to the plasma and lysosomal membranes and regulates autophagy. *PLoS One*, (8):e24478, 2011.

[119] Nico P Dantuma and Thorsten Hoppe. Growing sphere of influence: Cdc48/p97 orchestrates ubiquitin-dependent extraction from chromatin. *Trends Cell Biol*, (9):483–91, 2012.

[120] Kunitoshi Yamanaka, Yohei Sasagawa, and Teru Ogura. Recent advances in p97/vcp/cdc48 cellular functions. *Biochim Biophys Acta*, (1):130–7, 2012.

[121] Keiji Uchiyama, Go Totsukawa, Maija Puhka, Yayoi Kaneko, Eija Jokitalo, Ingrid Dreveny, Fabienne Beuron, Xiaodong Zhang, Paul Freemont, and Hisao Kondo. p37 is a p97 adaptor required for golgi and er biogenesis in interphase and at the end of mitosis. *Dev Cell*, (6):803–16, 2006.

[122] Emilie Tresse, Florian A Salomons, Jouni Vesa, Laura C Bott, Virginia Kimonis, Tso-Pang Yao, Nico P Dantuma, and J Paul Taylor. Vcp/p97 is essential for maturation of ubiquitin-containing autophagosomes and this function is impaired by mutations that cause ibmpfd. *Autophagy*, (2):217–27, 2010.

[123] Stefan Jentsch and Sebastian Rumpf. Cdc48 (p97): a.

[124] Catherine Dargemont and Batool Ossareh-Nazari. Cdc48/p97, a key actor in the interplay between autophagy and ubiquitin/proteasome catabolic pathways. *Biochim Biophys Acta*, (1):138–44, 2012.

[125] Harish N Ramanathan and Yihong Ye. Revoking the cellular license to replicate: yet another aaa assignment. *Mol Cell*, (1):3–4, 2011.

[126] Leo J Pallanck. Culling sick mitochondria from the herd. *J Cell Biol*, (7):1225–7, 2010.

[127] Masatoshi Esaki and Teru Ogura. Cdc48p/p97-mediated regulation of mitochondrial morphology is vms1p-independent. *J Struct Biol*, (2):112–20, 2012.

[128] Patrik Kloppsteck, Caroline A Ewens, Andreas Forster, Xiaodong Zhang, and Paul S Freemont. Regulation of p97 in the ubiquitin-proteasome system by the ubx protein-family. *Biochim Biophys Acta*, (1):125–9, 2012.

[129] Hemmo Meyer and Conrad C Weihl. The vcp/p97 system at a glance: connecting cellular function to disease pathogenesis. *J Cell Sci*, (Pt 18):3877–83, 2014.

[130] J M Peters, M J Walsh, and W W Franke. An abundant and ubiquitous homo-oligomeric ring-shaped atpase particle related to the putative vesicle fusion proteins sec18p and nsf. *EMBO J*, (6):1757–67, 1990.

[131] J M Peters, J R Harris, A Lustig, S Muller, A Engel, S Volker, and W W Franke. Ubiquitous soluble mg(2+)-atpase complex. a structural study. *J Mol Biol*, (2):557–71, 1992.

[132] Byron DeLaBarre and Axel T Brunger. Complete structure of p97/valosin-containing protein reveals communication between nucleotide domains. *Nat Struct Biol*, (10):856–63, 2003.

[133] Trevor Huyton, Valerie E Pye, Louise C Briggs, Terence C Flynn, Fabienne Beuron, Hisao Kondo, Jianpeng Ma, Xiaodong Zhang, and Paul S Freemont. The crystal structure of murine p97/vcp at 3.6a. *J Struct Biol*, (3):337–48, 2003.

[134] X Zhang, A Shaw, P A Bates, R H Newman, B Gowen, E Orlova, M A Gorman, H Kondo, P Dokurno, J Lally, G Leonard, H Meyer, M van Heel, and P S Freemont. Structure of the aaa atpase p97. *Mol Cell*, (6):1473–84, 2000.

[135] Soojay Banerjee, Alberto Bartesaghi, Alan Merk, Prashant Rao, Stacie L Bulfer, Yongzhao Yan, Neal Green, Barbara Mroczkowski, R Jeffrey Neitz, Peter Wipf, Veronica Falconieri, Raymond J Deshaies, Jacqueline L S Milne, Donna Huryn, Michelle Arkin, and Sriram Subramaniam. 2.3 a resolution cryo-em structure of human p97 and mechanism of allosteric inhibition. *Science*, (6275):871–5, 2016.

[136] Changcheng Song, Qing Wang, and Chou-Chi H Li. Atpase activity of p97-valosin-containing protein (vcp). d2 mediates the major enzyme activity, and d1 contributes to the heat-induced activity. *J Biol Chem*, (6):3648–55, 2003.

[137] Qing Wang, Changcheng Song, and Chou-Chi H Li. Hexamerization of p97-vcp is promoted by atp binding to the d1 domain and required for atpase and biological activities. *Biochem Biophys Res Commun*, (2):253–60, 2003.

[138] Wai Kwan Tang and Di Xia. Mutations in the human aaa+ chaperone p97 and related diseases. *Front Mol Biosci*, (3):79, 2016.

[139] Louise C Briggs, Geoff S Baldwin, Non Miyata, Hisao Kondo, Xiaodong Zhang, and Paul S Freemont. Analysis of nucleotide binding to p97 reveals the properties of a tandem aaa hexameric atpase. *J Biol Chem*, (20):13745–52, 2008.

[140] Petra Hanzelmann and Hermann Schindelin. Characterization of an additional binding surface on the p97 n-terminal domain involved in bipartite cofactor interactions. *Structure*, (1):140–147, 2016.

[141] Petra Hanzelmann and Hermann Schindelin. Structural basis of atp hydrolysis and intersubunit signaling in the aaa+ atpase p97. *Structure*, (1):127–139, 2016.

[142] Cezary Wojcik, Maga Rowicka, Andrzej Kudlicki, Dominika Nowis, Elizabeth McConnell, Marek Kujawa, and George N DeMartino. Valosin-containing protein (p97) is a regulator of endoplasmic reticulum stress and of the degradation of n-end rule and ubiquitin-fusion degradation pathway substrates in mammalian cells. *Mol Biol Cell*, (11):4606–18, 2006.

[143] Shruthi S Vembar and Jeffrey L Brodsky. One step at a time: endoplasmic reticulum-associated degradation. *Nat Rev Mol Cell Biol*, (12):944–57, 2008.

[144] Y Ye, H H Meyer, and T A Rapoport. The aaa atpase cdc48/p97 and its partners transport proteins from the er into the cytosol. *Nature*, (6864):652–6, 2001.

[145] Ikjin Kim, Jungmi Ahn, Chang Liu, Kaori Tanabe, Jennifer Apodaca, Tadashi Suzuki, and Hai Rao. The png1-rad23 complex regulates glycoprotein turnover. *J Cell Biol*, (2):211–9, 2006.

[146] M Koegl, T Hoppe, S Schlenker, H D Ulrich, T U Mayer, and S Jentsch. A novel ubiquitination factor, e4, is involved in multiubiquitin chain assembly. *Cell*, (5):635–44, 1999.

[147] Xiaoyan Zhong and Randall N Pittman. Ataxin-3 binds vcp/p97 and regulates retrotranslocation of erad substrates. *Hum Mol Genet*, (16):2409–20, 2006.

[148] Holger Richly, Michael Rape, Sigurd Braun, Sebastian Rumpf, Carsten Hoege, and Stefan Jentsch. A series of ubiquitin binding factors connects cdc48/p97 to substrate multiubiquitylation and proteasomal targeting. *Cell*, (1):73–84, 2005.

[149] Stefanie Bohm, Giorgia Lamberti, Vanesa Fernandez-Saiz, Christopher Stapf, and Alexander Buchberger. Cellular functions of ufd2 and ufd3 in proteasomal protein degradation depend on cdc48 binding. *Mol Cell Biol*, (7):1528–39, 2011.

[150] Changcheng Song, Qing Wang, Changzheng Song, and Thomas J Rogers. Valosin-containing protein (vcp/p97) is capable of unfolding polyubiquitinated proteins through its atpase domains. *Biochem Biophys Res Commun*, (3):453–7, 2015.

[151] Lisette G G C Verhoef, Christian Heinen, Alexandra Selivanova, Els F Halff, Florian A Salomons, and Nico P Dantuma. Minimal length requirement for proteasomal degradation of ubiquitin-dependent substrates. *FASEB J*, (1):123–33, 2009.

[152] Yihong Ye, Hemmo H Meyer, and Tom A Rapoport. Function of the p97-ufd1-npl4 complex in retrotranslocation from the er to the cytosol: dual recognition of nonubiquitinated polypeptide segments and polyubiquitin chains. *J Cell Biol*, (1):71–84, 2003.

[153] Qiuyan Wang, Lianyun Li, and Yihong Ye. Inhibition of p97-dependent protein degradation by eeyarestatin i. *J Biol Chem*, (12):7445–54, 2008.

[154] Yuki Murayama, Teru Ogura, and Kunitoshi Yamanaka. Characterization of c-terminal adaptors, ufd-2 and ufd-3, of cdc-48 on the polyglutamine aggregation in c. elegans. *Biochem Biophys Res Commun*, (1):154–60, 2015.

[155] Liyan Qiu, Natasha Pashkova, John R Walker, Stanley Winistorfer, Abdellah Allali-Hassani, Masato Akutsu, Robert Piper, and Sirano Dhe-Paganon. Structure and function of the plaa/ufd3-p97/cdc48 complex. *J Biol Chem*, (1):365–72, 2010.

[156] Veronique Schaeffer, Masato Akutsu, Michael H Olma, Ligia C Gomes, Masato Kawasaki, and Ivan Dikic. Binding of otulin to the pub domain of hoip controls nf-kappab signaling. *Mol Cell*, (3):349–61, 2014.

[157] Gang Zhao, Xiaoke Zhou, Liqun Wang, Guangtao Li, Hermann Schindelin, and William J Lennarz. Studies on peptide:n-glycanase-p97 interaction suggest that p97 phosphorylation modulates endoplasmic reticulum-associated degradation. *Proc Natl Acad Sci U S A*, (21):8785–90, 2007.

[158] Franziska Trusch, Anja Matena, Maja Vuk, Lisa Koerver, Helene Knaevelsrud, Paul S Freemont, Hemmo Meyer, and Peter Bayer. The n-terminal region of the ubiquitin regulatory x (ubx) domain-containing protein 1 (ubxd1) modulates interdomain communication within the valosin-containing protein p97. *J Biol Chem*, (49):29414–27, 2015.

[159] C Schuberth and A Buchberger. Ubx domain proteins: major regulators of the aaa atpase cdc48/p97. *Cell Mol Life Sci*, (15):2360–71, 2008.

[160] Christopher Stapf, Edward Cartwright, Mark Bycroft, Kay Hofmann, and Alexander Buchberger. The general definition of the p97/valosin-containing protein (vcp)-interacting motif (vim) delineates a new family of p97 cofactors. *J Biol Chem*, (44):38670–8, 2011.

[161] Annett Boeddrich, Sebastien Gaumer, Annette Haacke, Nikolay Tzvetkov, Mario Albrecht, Bernd O Evert, Eva C Muller, Rudi Lurz, Peter Breuer, Nancy Schugardt, Stephanie Plassmann, Kexiang Xu, John M Warrick, Jaana Suopanki, Ullrich Wullner, Ronald Frank, Ulrich F Hartl, Nancy M Bonini, and Erich E Wanker. An arginine/lysine-rich motif is crucial for vcp/p97-mediated modulation of ataxin-3 fibrillogenesis. *EMBO J*, (7):1547–58, 2006.

[162] Roland M Bruderer, Catherine Brasseur, and Hemmo H Meyer. The aaa atpase p97/vcp interacts with its alternative co-factors, ufd1-npl4 and p47, through a common bipartite binding mechanism. *J Biol Chem*, (48):49609–16, 2004.

[163] Petek Ballar, Yuxian Shen, Hui Yang, and Shengyun Fang. The role of a novel p97/valosin-containing protein-interacting motif of gp78 in endoplasmic reticulum-associated degradation. *J Biol Chem*, (46):35359–68, 2006.

[164] Petek Ballar, Yongwang Zhong, Masami Nagahama, Mitsuo Tagaya, Yuxian Shen, and Shengyun Fang. Identification of svip as an endogenous inhibitor of endoplasmic reticulum-associated degradation. *J Biol Chem*, (47):33908–14, 2007.

[165] Yihong Ye, Yoko Shibata, Chi Yun, David Ron, and Tom A Rapoport. A membrane protein complex mediates retro-translocation from the er lumen into the cytosol. *Nature*, (6994):841–7, 2004.

[166] H Kondo, C Rabouille, R Newman, T P Levine, D Pappin, P Freemont, and G Warren. p47 is a cofactor for p97-mediated membrane fusion. *Nature*, (6637):75–8, 1997.

[167] H H Meyer, J G Shorter, J Seemann, D Pappin, and G Warren. A complex of mammalian ufd1 and npl4 links the aaa-atpase, p97, to ubiquitin and nuclear transport pathways. *EMBO J*, (10):2181–92, 2000.

[168] Ethan J Greenblatt, James A Olzmann, and Ron R Kopito. Derlin-1 is a rhomboid pseudoprotease required for the dislocation of mutant alpha-1 antitrypsin from the endoplasmic reticulum. *Nat Struct Mol Biol*, (10):1147–52, 2011.

[169] Brendan N Lilley and Hidde L Ploegh. A membrane protein required for dislocation of misfolded proteins from the er. *Nature*, (6994):834–40, 2004.

[170] Petra Hanzelmann and Hermann Schindelin. The interplay of cofactor interactions and post-translational modifications in the regulation of the aaa+ atpase p97. *Front Mol Biosci*, (4):21, 2017.

[171] A Buchberger, M J Howard, M Proctor, and M Bycroft. The ubx domain: a widespread ubiquitin-like module. *J Mol Biol*, (1):17–24, 2001.

[172] James H Hurley, Sangho Lee, and Gali Prag. Ubiquitin-binding domains. *Biochem J*, (3):361–72, 2006.

[173] Gabriela Alexandru, Johannes Graumann, Geoffrey T Smith, Natalie J Kolawa, Ruihua Fang, and Raymond J Deshaies. Ubxd7 binds multiple ubiquitin ligases and implicates p97 in hif1alpha turnover. *Cell*, (5):804–16, 2008.

[174] Gabriela Alexandru. Exploring the role of p97 and its ubx-domain cofactors through identification of their interacting proteins. *Methods Mol Biol*, (832):305–12, 2012.

[175] Louise Madsen, Katrine M Andersen, Soren Prag, Torben Moos, Colin A Semple, Michael Seeger, and Rasmus Hartmann-Petersen. Ubxd1 is a novel co-factor of the human p97 atpase. *Int J Biochem Cell Biol*, (12):2927–42, 2008.

[176] Rasmus Hartmann-Petersen, Mairi Wallace, Kay Hofmann, Grete Koch, Anders H Johnsen, Klavs B Hendil, and Colin Gordon. The ubx2 and ubx3 cofactors direct cdc48 activity to proteolytic and nonproteolytic ubiquitin-dependent processes. *Curr Biol*, (9):824–8, 2004.

[177] Keiji Uchiyama, Eija Jokitalo, Fumi Kano, Masayuki Murata, Xiaodong Zhang, Benito Canas, Richard Newman, Catherine Rabouille, Darryl Pappin, Paul Freemont, and Hisao Kondo. Vcip135, a novel essential factor for p97/p47-mediated membrane fusion, is required for golgi and er assembly in vivo. *J Cell Biol*, (5):855–66, 2002.

[178] T Suzuki, H Park, E A Till, and W J Lennarz. The pub domain: a putative protein-protein interaction domain implicated in the ubiquitin-proteasome pathway. *Biochem Biophys Res Commun*, (5):1083–7, 2001.

[179] Tobias Doerks, Richard R Copley, Jorg Schultz, Chris P Ponting, and Peer Bork. Systematic identification of novel protein domain families associated with nuclear functions. *Genome Res*, (1):47–56, 2002.

[180] Mark D Allen, Alexander Buchberger, and Mark Bycroft. The pub domain functions as a p97 binding module in human peptide n-glycanase. *J Biol Chem*, (35):25502–8, 2006.

[181] N W Bays, S K Wilhovsky, A Goradia, K Hodgkiss-Harlow, and R Y Hampton. Hrd4/npl4 is required for the proteasomal processing of ubiquitinated er proteins. *Mol Biol Cell*, (12):4114–28, 2001.

[182] Shahri Raasi and Dieter H Wolf. Ubiquitin receptors and erad: a network of pathways to the proteasome. *Semin Cell Dev Biol*, (6):780–91, 2007.

[183] Maximilian Kern, Vanesa Fernandez-Saiz, Zasie Schafer, and Alexander Buchberger. Ubxd1 binds p97 through two independent binding sites. *Biochem Biophys Res Commun*, (2):303–7, 2009.

[184] Masami Nagahama, Machi Ohnishi, Yumiko Kawate, Takayuki Matsui, Hitomi Miyake, Keizo Yuasa, Katsuko Tani, Mitsuo Tagaya, and Akihiko Tsuji. Ubxd1 is a vcp-interacting protein that is involved in er-associated degradation. *Biochem Biophys Res Commun*, (2):303–8, 2009.

[185] Danilo Ritz, Maja Vuk, Philipp Kirchner, Monika Bug, Sabina Schutz, Arnold Hayer, Sebastian Bremer, Caleb Lusk, Robert H Baloh, Houkeun Lee, Timo Glatter, Matthias Gstaiger, Ruedi Aebersold, Conrad C Weihl, and Hemmo Meyer. Endolysosomal sorting of ubiquitylated caveolin-1 is regulated by vcp and ubxd1 and impaired by vcp disease mutations. *Nat Cell Biol*, (9):1116–23, 2011.

[186] Chrisovalantis Papadopoulos, Philipp Kirchner, Monika Bug, Daniel Grum, Lisa Koerver, Nina Schulze, Robert Poehler, Alina Dressler, Sven Fengler, Khalid Arhzaouy, Vanda Lux, Michael Ehrmann, Conrad C Weihl, and Hemmo Meyer. Vcp/p97 cooperates with yod1, ubxd1 and plaa to drive clearance of ruptured lysosomes by autophagy. *EMBO J*, (2):135–150, 2017.

[187] Alexandra Stolz and Dieter H Wolf. Endoplasmic reticulum associated protein degradation: a chaperone assisted journey to hell. *Biochim Biophys Acta*, (6):694–705, 2010.

[188] Albert Neutzner, Richard J Youle, and Mariusz Karbowski. Outer mitochondrial membrane protein degradation by the proteasome. *Novartis Found Symp*, (287):4–14; discussion 14–20, 2007.

[189] Qihua Ling and Paul Jarvis. Dynamic regulation of endosymbiotic organelles by ubiquitination. *Trends Cell Biol*, (8):399–408, 2013.

[190] Fei Tang, Bin Wang, Na Li, Yanfang Wu, Junying Jia, Talin Suo, Quan Chen, Yong-Jun Liu, and Jie Tang. Rnf185, a novel mitochondrial ubiquitin e3 ligase, regulates autophagy through interaction with bnip1. *PLoS One*, (9):e24367, 2011.

[191] Giovanni Benard, Albert Neutzner, Guihong Peng, Chunxin Wang, Ferenc Livak, Richard J Youle, and Mariusz Karbowski. Ibrdc2, an ibr-type e3 ubiquitin ligase, is a regulatory factor for bax and apoptosis activation. *EMBO J*, (8):1458–71, 2010.

[192] Eric B Taylor and Jared Rutter. Mitochondrial quality control by the ubiquitin-proteasome system. *Biochem Soc Trans*, (5):1509–13, 2011.

[193] Yong-Yea Park, Seungmin Lee, Mariusz Karbowski, Albert Neutzner, Richard J Youle, and Hyeseong Cho. Loss of march5 mitochondrial e3 ubiquitin ligase induces cellular senescence through dynamin-related protein 1 and mitofusin 1. *J Cell Sci*, (Pt 4):619–26, 2010.

[194] Konstanze F Winklhofer. Parkin and mitochondrial quality control: toward assembling the puzzle. *Trends Cell Biol*, (6):332–41, 2014.

[195] Junya Hasegawa, Ikuko Maejima, Ryo Iwamoto, and Tamotsu Yoshimori. Selective autophagy: lysophagy. *Methods*, (75):128–32, 2015.

[196] Wei Wang and Suresh Subramani. Role of pex5 ubiquitination in maintaining peroxisome dynamics and homeostasis. *Cell Cycle*, (1-9):1–9, 2017.

[197] Gabriele Zaffagnini and Sascha Martens. Mechanisms of selective autophagy. *J Mol Biol*, (9 Pt A):1714–24, 2016.

[198] Eric H Baehrecke. Autophagy: dual roles in life and death? *Nat Rev Mol Cell Biol*, (6):505–10, 2005.

[199] G Ashrafi and T L Schwarz. The pathways of mitophagy for quality control and clearance of mitochondria. *Cell Death Differ*, (1):31–42, 2013.

[200] Akinori Eiyama and Koji Okamoto. Pink1/parkin-mediated mitophagy in mammalian cells. *Curr Opin Cell Biol*, (33):95–101, 2015.

[201] Hector Sandoval, Perumal Thiagarajan, Swapan K Dasgupta, Armin Schumacher, Josef T Prchal, Min Chen, and Jin Wang. Essential role for nix in autophagic maturation of erythroid cells. *Nature*, (7201):232–5, 2008.

[202] Lei Liu, Du Feng, Guo Chen, Ming Chen, Qiaoxia Zheng, Pingping Song, Qi Ma, Chongzhuo Zhu, Rui Wang, Wanjun Qi, Lei Huang, Peng Xue, Baowei Li, Xiaohui Wang, Haijing Jin, Jun Wang, Fuquan Yang, Pingsheng Liu, Yushan Zhu, Senfang Sui, and Quan Chen. Mitochondrial outer-membrane protein fundc1 mediates hypoxia-induced mitophagy in mammalian cells. *Nat Cell Biol*, (2):177–85, 2012.

[203] F Strappazzon, F Nazio, M Corrado, V Cianfanelli, A Romagnoli, G M Fimia, S Campello, R Nardacci, M Piacentini, M Campanella, and F Cecconi. Ambra1 is able to induce mitophagy via lc3 binding, regardless of parkin and p62/sqstm1. *Cell Death Differ*, (3):517, 2015.

[204] Silvia Campello, Flavie Strappazzon, and Francesco Cecconi. Mitochondrial dismissal in mammals, from protein degradation to mitophagy. *Biochim Biophys Acta*, (4):451–60, 2014.

[205] Tae-Young Kim, Ding Wang, Allen K Kim, Edward Lau, Amanda J Lin, David A Liem, Jun Zhang, Nobel C Zong, Maggie P Y Lam, and Peipei Ping. Metabolic labeling reveals proteome dynamics of mouse mitochondria. *Mol Cell Proteomics*, (12):1586–94, 2012.

[206] Gilad Twig, Alvaro Elorza, Anthony J A Molina, Hibo Mohamed, Jakob D Wikstrom, Gil Walzer, Linsey Stiles, Sarah E Haigh, Steve Katz, Guy Las, Joseph Alroy, Min Wu, Benedicte F Py, Junying Yuan, Jude T Deeney, Barbara E Corkey, and Orian S Shirihai. Fission and selective fusion govern mitochondrial segregation and elimination by autophagy. *EMBO J*, (2):433–46, 2008.

[207] Joshua M Shulman, Philip L De Jager, and Mel B Feany. Parkinson's disease: genetics and pathogenesis. *Annu Rev Pathol*, (6):193–222, 2011.

[208] Amy K Reeve, Kim J Krishnan, and Doug Turnbull. Mitochondrial dna mutations in disease, aging, and neurodegeneration. *Ann N Y Acad Sci*, (1147):21–9, 2008.

[209] Antonio Federico, Elena Cardaioli, Paola Da Pozzo, Patrizia Formichi, Gian Nicola Gallus, and Elena Radi. Mitochondria, oxidative stress and neurodegeneration. *J Neurol Sci*, (1-2):254–62, 2012.

[210] Marta Di Carlo, Daniela Giacomazza, Pasquale Picone, Domenico Nuzzo, and Pier Luigi San Biagio. Are oxidative stress and mitochondrial dysfunction the key players in the neurodegenerative diseases? *Free Radic Res*, (11):1327–38, 2012.

[211] Sonia Gandhi and Andrey Y Abramov. Mechanism of oxidative stress in neurodegeneration. *Oxid Med Cell Longev*, (2012):428010, 2012.

[212] Giles D J Watts, Jill Wymer, Margaret J Kovach, Sarju G Mehta, Steven Mumm, Daniel Darvish, Alan Pestronk, Michael P Whyte, and Virginia E Kimonis. Inclusion body myopathy associated with paget disease of bone and frontotemporal dementia is caused by mutant valosin-containing protein. *Nat Genet*, (4):377–81, 2004.

[213] Hajime Niwa, Caroline A Ewens, Chun Tsang, Heidi O Yeung, Xiaodong Zhang, and Paul S Freemont. The role of the n-domain in the atpase activity of the mammalian aaa atpase p97/vcp. *J Biol Chem*, (11):8561–70, 2012.

[214] Vanesa Fernandez-Saiz and Alexander Buchberger. Imbalances in p97 co-factor interactions in human proteinopathy. *EMBO Rep*, (6):479–85, 2010.

[215] Conrad C Weihl, Alan Pestronk, and Virginia E Kimonis. Valosin-containing protein disease: inclusion body myopathy with paget's disease of the bone and fronto-temporal dementia. *Neuromuscul Disord*, (5):308–15, 2009.

[216] C Minetti, F Sotgia, C Bruno, P Scartezzini, P Broda, M Bado, E Masetti, M Mazzocco, A Egeo, M A Donati, D Volonte, F Galbiati, G Cordone, F D Bricarelli, M P Lisanti, and F Zara. Mutations in the caveolin-3 gene cause autosomal dominant limb-girdle muscular dystrophy. *Nat Genet*, (4):365–8, 1998.

[217] Marta Martinez-Vicente, Zsolt Talloczy, Esther Wong, Guomei Tang, Hiroshi Koga, Susmita Kaushik, Rosa de Vries, Esperanza Arias, Spike Harris, David Sulzer, and Ana Maria Cuervo. Cargo recognition failure is responsible for inefficient autophagy in huntington's disease. *Nat Neurosci*, (5):567–76, 2010.

[218] Yvette C Wong and Erika L F Holzbaur. The regulation of autophagosome dynamics by huntingtin and hap1 is disrupted by expression of mutant huntingtin, leading to defective cargo degradation. *J Neurosci*, (4):1293–305, 2014.

[219] Yan-Ning Rui, Zhen Xu, Bindi Patel, Ana Maria Cuervo, and Sheng Zhang. Htt/huntingtin in selective autophagy and huntington disease: A foe or a friend within? *Autophagy*, (5):858–60, 2015.

[220] B Khalil, N El Fissi, A Aouane, M-J Cabirol-Pol, T Rival, and J-C Lievens. Pink1-induced mitophagy promotes neuroprotection in huntington's disease. *Cell Death Dis*, (6):e1617, 2015.

[221] Madeleine Diedrich, Tohru Kitada, Grit Nebrich, Andrea Koppelstaetter, Jie Shen, Claus Zabel, Joachim Klose, and Lei Mao. Brain region specific mitophagy capacity could contribute to selective neuronal vulnerability in parkinson's disease. *Proteome Sci*, (9):59, 2011.

[222] Heng Du, Lan Guo, Fang Fang, Doris Chen, Alexander A Sosunov, Guy M McKhann, Yilin Yan, Chunyu Wang, Hong Zhang, Jeffery D Molkentin, Frank J Gunn-Moore, Jean Paul Vonsattel, Ottavio Arancio, John Xi Chen, and Shi Du Yan. Cyclophilin d deficiency attenuates mitochondrial and neuronal perturbation and ameliorates learning and memory in alzheimer's disease. *Nat Med*, (10):1097–105, 2008.

[223] Maria Manczak and P Hemachandra Reddy. Abnormal interaction of vdac1 with amyloid beta and phosphorylated tau causes mitochondrial dysfunction in alzheimer's disease. *Hum Mol Genet*, (23):5131–46, 2012.

[224] Marcus J Calkins, Maria Manczak, Peizhong Mao, Ulziibat Shirendeb, and P Hemachandra Reddy. Impaired mitochondrial biogenesis, defective axonal transport of mitochondria, abnormal mitochondrial dynamics and synaptic degeneration in a mouse model of alzheimer's disease. *Hum Mol Genet*, (23):4515–29, 2011.

[225] Ralph A Nixon. The role of autophagy in neurodegenerative disease. *Nat Med*, (8):983–97, 2013.

[226] Matteo Bordi, Martin J Berg, Panaiyur S Mohan, Corrinne M Peterhoff, Melissa J Alldred, Shaoli Che, Stephen D Ginsberg, and Ralph A Nixon. Autophagy flux in ca1 neurons of alzheimer hippocampus: Increased induction overburdens failing lysosomes to propel neuritic dystrophy. *Autophagy*, (12):2467–2483, 2016.

[227] Preeti J Khandelwal, Alexander M Herman, Hyang-Sook Hoe, G William Rebeck, and Charbel E-H Moussa. Parkin mediates beclin-dependent autophagic clearance of defective mitochondria and ubiquitinated abeta in ad models. *Hum Mol Genet*, (11):2091–102, 2011.

[228] V Corsetti, F Florenzano, A Atlante, A Bobba, M T Ciotti, F Natale, F Della Valle, A Borreca, A Manca, G Meli, C Ferraina, M Feligioni, S D'Aguanno, R Bussani, M Ammassari-Teule, V Nicolin, P Calissano, and G Amadoro. Nh2-truncated human tau induces deregulated mitophagy in neurons by aberrant recruitment of parkin and uchl-1: implications in alzheimer's disease. *Hum Mol Genet*, (11):3058–81, 2015.

[229] T Kitada, S Asakawa, N Hattori, H Matsumine, Y Yamamura, S Minoshima, M Yokochi, Y Mizuno, and N Shimizu. Mutations in the parkin gene cause autosomal recessive juvenile parkinsonism. *Nature*, (6676):605–8, 1998.

[230] E M Valente, A R Bentivoglio, P H Dixon, A Ferraris, T Ialongo, M Frontali, A Albanese, and N W Wood. Localization of a novel locus for autosomal recessive early-onset parkinsonism, park6, on human chromosome 1p35-p36. *Am J Hum Genet*, (4):895–900, 2001.

[231] Alicia M Pickrell and Richard J Youle. The roles of pink1, parkin, and mitochondrial fidelity in parkinson's disease. *Neuron*, (2):257–73, 2015.

[232] Andrew W Greene, Karl Grenier, Miguel A Aguileta, Stephanie Muise, Rasoul Farazifard, M Emdadul Haque, Heidi M McBride, David S Park, and Edward A Fon. Mitochondrial processing peptidase regulates pink1 processing, import and parkin recruitment. *EMBO Rep*, (4):378–85, 2012.

[233] Derek P Narendra, Seok Min Jin, Atsushi Tanaka, Der-Fen Suen, Clement A Gautier, Jie Shen, Mark R Cookson, and Richard J Youle. Pink1 is selectively stabilized on impaired mitochondria to activate parkin. *PLoS Biol*, (1):e1000298, 2010.

[234] Thomas M Durcan and Edward A Fon. The three 'p's of mitophagy: Parkin, pink1, and post-translational modifications. *Genes Dev*, (10):989–99, 2015.

[235] Matthew E Gegg, J Mark Cooper, Kai-Yin Chau, Manuel Rojo, Anthony H V Schapira, and Jan-Willem Taanman. Mitofusin 1 and mitofusin 2 are ubiquitinated in a pink1/parkin-dependent manner upon induction of mitophagy. *Hum Mol Genet*, (24):4861–70, 2010.

[236] Yvette C Wong and Erika L F Holzbaur. Optineurin is an autophagy receptor for damaged mitochondria in parkin-mediated mitophagy that is disrupted by an als-linked mutation. *Proc Natl Acad Sci U S A*, (42):E4439–48, 2014.

[237] Eisuke Itakura, Chieko Kishi-Itakura, Ikuko Koyama-Honda, and Noboru Mizushima. Structures containing atg9a and the ulk1 complex independently target depolarized mitochondria at initial stages of parkin-mediated mitophagy. *J Cell Sci*, (Pt 6):1488–99, 2012.

[238] Ghazaleh Ashrafi, Julia S Schlehe, Matthew J LaVoie, and Thomas L Schwarz. Mitophagy of damaged mitochondria occurs locally in distal neuronal axons and requires pink1 and parkin. *J Cell Biol*, (5):655–70, 2014.

[239] Aaron C Pawlyk, Benoit I Giasson, Deepak M Sampathu, Francisco A Perez, Kah Leong Lim, Valina L Dawson, Ted M Dawson, Richard D Palmiter, John Q Trojanowski, and Virginia M-Y Lee. Novel monoclonal antibodies demonstrate biochemical variation of brain parkin with age. *J Biol Chem*, (48):48120–8, 2003.

[240] Cheng Wang, Han Seok Ko, Bobby Thomas, Fai Tsang, Katherine C M Chew, Shiam-Peng Tay, Michelle W L Ho, Tit-Meng Lim, Tuck-Wah Soong, Olga Pletnikova, Juan Troncoso, Valina L Dawson, Ted M Dawson, and Kah-Leong Lim. Stress-induced alterations in parkin solubility promote parkin aggregation and compromise parkin's protective function. *Hum Mol Genet*, (24):3885–97, 2005.

[241] Baris Bingol, Joy S Tea, Lilian Phu, Mike Reichelt, Corey E Bakalarski, Qinghua Song, Oded Foreman, Donald S Kirkpatrick, and Morgan Sheng. The mitochondrial deubiquitinase usp30 opposes parkin-mediated mitophagy. *Nature*, (7505):370–5, 2014.

[242] Tom Cornelissen, Dominik Haddad, Fieke Wauters, Cindy Van Humbeeck, Wim Mandemakers, Brianada Koentjoro, Carolyn Sue, Kris Gevaert, Bart De Strooper, Patrik Verstreken, and Wim Vandenberghe. The deubiquitinase usp15 antagonizes parkin-mediated mitochondrial ubiquitination and mitophagy. *Hum Mol Genet*, (19):5227–42, 2014.

[243] Thomas M Durcan, Matthew Y Tang, Joelle R Perusse, Eman A Dashti, Miguel A Aguileta, Gian-Luca McLelland, Priti Gros, Thomas A Shaler, Denis Faubert, Benoit Coulombe, and Edward A Fon. Usp8 regulates mitophagy by removing k6-linked ubiquitin conjugates from parkin. *EMBO J*, (21):2473–91, 2014.

[244] Cindy Van Humbeeck, Tom Cornelissen, Hilde Hofkens, Wim Mandemakers, Kris Gevaert, Bart De Strooper, and Wim Vandenberghe. Parkin interacts with ambra1 to induce mitophagy. *J Neurosci*, (28):10249–61, 2011.

[245] Michael Lazarou, Danielle A Sliter, Lesley A Kane, Shireen A Sarraf, Chunxin Wang, Jonathon L Burman, Dionisia P Sideris, Adam I Fogel, and Richard J Youle. The ubiquitin kinase pink1 recruits autophagy receptors to induce mitophagy. *Nature*, (7565):309–314, 2015.

[246] Fredrik H Sterky, Seungmin Lee, Rolf Wibom, Lars Olson, and Nils-Goran Larsson. Impaired mitochondrial transport and parkin-independent degeneration of respiratory chain-deficient dopamine neurons in vivo. *Proc Natl Acad Sci U S A*, (31):12937–42, 2011.

[247] Cheng-Wu Zhang, Liting Hang, Tso-Pang Yao, and Kah-Leong Lim. Parkin regulation and neurodegenerative disorders. *Front Aging Neurosci*, (7):248, 2015.

[248] K Mullis, F Faloona, S Scharf, R Saiki, G Horn, and H Erlich. Specific enzymatic amplification of dna in vitro: the polymerase chain reaction. *Cold Spring Harb Symp Quant Biol*, (51 Pt 1):263–73, 1986.

[249] Behrooz Moosavi, Bibimaryam Mousavi, Wen-Chao Yang, and Guang-Fu Yang. Yeast-based assays for detecting protein-protein/drug interactions and their inhibitors. *Eur J Cell Biol*, (6):529–541, 2017.

[250] Yasunori Fukumoto, Yuuki Obata, Kenichi Ishibashi, Naoki Tamura, Ikue Kikuchi, Kazumasa Aoyama, Yasuyuki Hattori, Kunihiko Tsuda, Yuji Nakayama, and Naoto Yamaguchi. Cost-effective gene transfection by dna compaction at ph 4.0 using acidified, long shelf-life polyethylenimine. *Cytotechnology*, (1):73–82, 2010.

[251] Johannes Schindelin, Ignacio Arganda-Carreras, Erwin Frise, Verena Kaynig, Mark Longair, Tobias Pietzsch, Stephan Preibisch, Curtis Rueden, Stephan Saalfeld, Benjamin Schmid, Jean-Yves Tinevez, Daniel James White, Volker Hartenstein, Kevin Eliceiri, Pavel Tomancak, and Albert Cardona. Fiji: an open-source platform for biological-image analysis. *Nat Methods*, (7):676–82, 2012.

[252] Albert Neutzner and Richard J Youle. Instability of the mitofusin fzo1 regulates mitochondrial morphology during the mating response of the yeast saccharomyces cerevisiae. *J Biol Chem*, (19):18598–603, 2005.

[253] Mariusz Karbowski, Albert Neutzner, and Richard J Youle. The mitochondrial e3 ubiquitin ligase march5 is required for drp1 dependent mitochondrial division. *J Cell Biol*, (1):71–84, 2007.

[254] Shan Xu, Guihong Peng, Yang Wang, Shengyun Fang, and Mariusz Karbowski. The aaa-atpase p97 is essential for outer mitochondrial membrane protein turnover. *Mol Biol Cell*, (3):291–300, 2011.

[255] Atsushi Tanaka, Megan M Cleland, Shan Xu, Derek P Narendra, Der-Fen Suen, Mariusz Karbowski, and Richard J Youle. Proteasome and p97 mediate mitophagy and degradation of mitofusins induced by parkin. *J Cell Biol*, (7):1367–80, 2010.

[256] Yoko Kimura, Junpei Fukushi, Seiji Hori, Noriyuki Matsuda, Kei Okatsu, Yukie Kakiyama, Junko Kawawaki, Akira Kakizuka, and Keiji Tanaka. Different dynamic movements of wild-type and pathogenic vcps and their cofactors to damaged mitochondria in a parkin-mediated mitochondrial quality control system. *Genes Cells*, (12):1131–43, 2013.

[257] Pablo de Felipe, Garry A Luke, Jeremy D Brown, and Martin D Ryan. Inhibition of 2a-mediated 'cleavage' of certain artificial polyproteins bearing n-terminal signal sequences. *Biotechnol J*, (2):213–23, 2010.

[258] Jin Hee Kim, Sang-Rok Lee, Li-Hua Li, Hye-Jeong Park, Jeong-Hoh Park, Kwang Youl Lee, Myeong-Kyu Kim, Boo Ahn Shin, and Seok-Yong Choi. High cleavage efficiency of a 2a peptide derived from porcine teschovirus-1 in human cell lines, zebrafish and mice. *PLoS One*, (4):e18556, 2011.

[259] I Lasa, E Gouin, M Goethals, K Vancompernolle, V David, J Vandekerckhove, and P Cossart. Identification of two regions in the n-terminal domain of acta involved in the actin comet tail formation by listeria monocytogenes. *EMBO J*, (7):1531–40, 1997.

[260] S Pistor, T Chakraborty, K Niebuhr, E Domann, and J Wehland. The acta protein of listeria monocytogenes acts as a nucleator inducing reorganization of the actin cytoskeleton. *EMBO J*, (4):758–63, 1994.

[261] Carlo Rodolfo, Silvia Campello, and Francesco Cecconi. Mitophagy in neurodegenerative diseases. *Neurochem Int*, pages S0197–0186(17)30087–6, 2017.

[262] Daniel J Klionsky, Fabio C Abdalla, Hagai Abeliovich, Robert T Abraham, Abraham Acevedo-Arozena, Khosrow Adeli, Lotta Agholme, Maria Agnello, Patrizia Agostinis, Julio A Aguirre-Ghiso, Hyung Jun Ahn, Ouardia Ait-Mohamed, Slimane Ait-Si-Ali, Takahiko Akematsu, Shizuo Akira, Hesham M Al-Younes, Munir A Al-Zeer, Matthew L Albert, Roger L Albin, Javier Alegre-Abarrategui, Maria Francesca Aleo, Mehrdad Alirezaei, Alexandru Almasan, Maylin Almonte-Becerril, Atsuo Amano, Ravi Amaravadi, Shoba Amarnath, Amal O Amer, Nathalie Andrieu-Abadie, Vellareddy Anantharam, David K Ann, Shailendra Anoopkumar-Dukie, Hiroshi Aoki, Nadezda Apostolova, Giuseppe Arancia, John P Aris, Katsuhiko Asanuma, Nana Y O Asare, Hisashi Ashida, Valerie Askanas, David S Askew, Patrick Auberger, Misuzu Baba, Steven K Backues, Eric H Baehrecke, Ben A Bahr, Xue-Yuan Bai,

Yannick Bailly, Robert Baiocchi, Giulia Baldini, Walter Balduini, Andrea Ballabio, Bruce A Bamber, Edward T W Bampton, Gabor Banhegyi, Clinton R Bartholomew, Diane C Bassham, Robert C Jr Bast, Henri Batoko, Boon-Huat Bay, Isabelle Beau, Daniel M Bechet, Thomas J Begley, Christian Behl, Christian Behrends, Soumeya Bekri, Bryan Bellaire, Linda J Bendall, Luca Benetti, Laura Berliocchi, Henri Bernardi, Francesca Bernassola, Sebastien Besteiro, Ingrid Bhatia-Kissova, Xiaoning Bi, Martine Biard-Piechaczyk, Janice S Blum, Lawrence H Boise, Paolo Bonaldo, David L Boone, Beat C Bornhauser, Karina R Bortoluci, Ioannis Bossis, Frederic Bost, Jean-Pierre Bourquin, Patricia Boya, Michael Boyer-Guittaut, Peter V Bozhkov, Nathan R Brady, Claudio Brancolini, Andreas Brech, Jay E Brenman, Ana Brennand, Emery H Bresnick, Patrick Brest, Dave Bridges, Molly L Bristol, Paul S Brookes, Eric J Brown, John H Brumell, Nicola Brunetti-Pierri, Ulf T Brunk, Dennis E Bulman, Scott J Bultman, Geert Bultynck, Lena F Burbulla, Wilfried Bursch, Jonathan P Butchar, Wanda Buzgariu, Sergio P Bydlowski, Ken Cadwell, Monika Cahova, Dongsheng Cai, Jiyang Cai, Qian Cai, Bruno Calabretta, Javier Calvo-Garrido, Nadine Camougrand, Michelangelo Campanella, Jenny Campos-Salinas, Eleonora Candi, Lizhi Cao, Allan B Caplan, Simon R Carding, Sandra M Cardoso, Jennifer S Carew, Cathleen R Carlin, Virginie Carmignac, Leticia A M Carneiro, Serena Carra, Rosario A Caruso, Giorgio Casari, Caty Casas, Roberta Castino, Eduardo Cebollero, Francesco Cecconi, Jean Celli, Hassan Chaachouay, Han-Jung Chae, Chee-Yin Chai, David C Chan, Edmond Y Chan, Raymond Chuen-Chung Chang, Chi-Ming Che, Ching-Chow Chen, Guang-Chao Chen, Guo-Qiang Chen, Min Chen, Quan Chen, Steve S-L Chen, WenLi Chen, Xi Chen, Xiangmei Chen, Xiequn Chen, Ye-Guang Chen, Yingyu Chen, Yongqiang Chen, Yu-Jen Chen, Zhixiang Chen, Alan Cheng, Christopher H K Cheng, Yan Cheng, Heesun Cheong, Jae-Ho Cheong, Sara Cherry, Russ Chess-Williams, Zelda H Cheung, Eric Chevet, Hui-Ling Chiang, Roberto Chiarelli, Tomoki Chiba, Lih-Shen Chin, Shih-Hwa Chiou, Francis V Chisari, Chi Hin Cho, Dong-Hyung Cho, Augustine M K Choi, DooSeok Choi, Kyeong Sook Choi, Mary E Choi, Salem Chouaib, Divaker Choubey, Vinay Choubey, Charleen T Chu, Tsung-Hsien Chuang, Sheau-Huei Chueh, Taehoon Chun, Yong-Joon Chwae, Mee-Len Chye, Roberto Ciarcia, Maria R Ciriolo, Michael J Clague, Robert S B Clark, Peter G H Clarke, Robert Clarke, Patrice Codogno, Hilary A Coller, Maria I Colombo, Sergio Comincini, Maria Condello, Fabrizio Condorelli, Mark R Cookson, Graham H Coombs, Isabelle Coppens, Ramon Corbalan, Pascale Cossart, Paola Costelli, Safia Costes, Ana Coto-Montes, Eduardo Couve, Fraser P Coxon, James M Cregg, Jose L Crespo, Marianne J Cronje, Ana Maria Cuervo, Joseph J Cullen, Mark J Czaja, Marcello D'Amelio, Arlette Darfeuille-Michaud, Lester M Davids, Faith E Davies, Massimo De Felici, John F de Groot, Cornelis A M de Haan, Luisa De Martino, Angelo De Milito, Vincenzo De Tata, Jayanta Debnath, Alexei Degterev, Benjamin Dehay, Lea M D Delbridge, Francesca Demarchi, Yi Zhen Deng, Jorn Dengjel, Paul Dent, Donna Denton, Vojo Deretic, Shyamal D Desai, Rodney J Devenish, Mario Di Gioacchino, Gilbert Di Paolo, Chiara Di Pietro, Guillermo Diaz-Araya, Ines Diaz-Laviada, Maria T Diaz-Meco, Javier Diaz-Nido, Ivan Dikic, Savithramma P Dinesh-Kumar, Wen-Xing Ding, Clark W Distelhorst, Abhinav Diwan, Mojgan Djavaheri-Mergny, Svetlana Dokudovskaya, Zheng Dong, Frank C Dorsey, Victor Dosenko, James J Dowling, Stephen Doxsey, Marlene Dreux, Mark E Drew, Qiuhong Duan, Michel A Duchosal, Karen Duff, Isabelle Dugail, Madeleine Durbeej, Michael Duszenko, Charles L Edelstein, Aimee L Edinger, Gustavo Egea, Ludwig Eichinger, N Tony Eissa, Suhendan Ekmekcioglu, Wafik S El-Deiry, Zvulun Elazar, Mohamed Elgendy, Lisa M Ellerby, Kai Er Eng, Anna-Mart Engelbrecht, Simone Engelender, Jekaterina Erenpreisa, Ricardo Escalante, Audrey Esclatine, Eeva-Liisa Eskelinen, Lucile Espert, Virginia Espina, Huizhou Fan, Jia Fan, Qi-Wen Fan, Zhen Fan, Shengyun Fang, Yongqi Fang, Manolis Fanto, Alessandro Fanzani, Thomas Farkas, Jean-Claude Farr. Guidelines for the use and interpretation of assays for monitoring autophagy. *Autophagy*, (4):445–544, 2012.

[263] Prashant Mali, Luhan Yang, Kevin M Esvelt, John Aach, Marc Guell, James E DiCarlo, Julie E Norville, and George M Church. Rna-guided human genome engineering via cas9. *Science*, (6121):823–6, 2013.

[264] Luo-Qiao Wang, Yue Zhang, Huan Yan, Kai-Jiang Liu, and Shu Zhang. Microrna-373 functions as an oncogene and targets yod1 gene in cervical cancer. *Biochem Biophys Res Commun*, (3):515–20, 2015.

[265] Alex Mitchell, Hsin-Yu Chang, Louise Daugherty, Matthew Fraser, Sarah Hunter, Rodrigo Lopez, Craig McAnulla, Conor McMenamin, Gift Nuka, Sebastien Pesseat, Amaia Sangrador-Vegas, Maxim Scheremetjew, Claudia Rato, Siew-Yit Yong, Alex Bateman, Marco Punta, Teresa K Attwood, Christian J A Sigrist, Nicole Redaschi, Catherine Rivoire, Ioannis Xenarios, Daniel Kahn, Dominique Guyot, Peer Bork, Ivica Letunic, Julian Gough, Matt Oates, Daniel Haft, Hongzhan Huang, Darren A Natale, Cathy H Wu, Christine Orengo, Ian Sillitoe, Huaiyu Mi, Paul D Thomas, and Robert D Finn. The interpro protein families database: the classification resource after 15 years. *Nucleic Acids Res*, (Database issue):D213–21, 2015.

[266] V Cavallucci, A Nobili, and M D'Amelio. Emerging role of mitochondria dysfunction in the onset of neurodegenerative diseases. *J Biol Regul Homeost Agents*, (2 Suppl):1–9, 2013.

[267] Heinz D Osiewacz and Dominik Bernhardt. Mitochondrial quality control: impact on aging and life span - a mini-review. *Gerontology*, (5):413–20, 2013.

[268] Alexander Buchberger, Hermann Schindelin, and Petra Hanzelmann. Control of p97 function by cofactor binding. *FEBS Lett*, (19 Pt A):2578–89, 2015.

[269] Eun Sil Park, Yung Joon Yoo, and Muthukumar Elangovan. The opposite role of two uba-ubx containing proteins, p47 and saks1 in the degradation of a single erad substrate, alpha-tcr. *Mol Cell Biochem*, (1-2):37–45, 2017.

[270] L Carim-Todd, M Escarceller, X Estivill, and L Sumoy. Identification and characterization of ubxd1, a novel ubx domain-containing gene on human chromosome 19p13, and its mouse ortholog. *Biochim Biophys Acta*, (2):298–301, 2001.

[271] Sumana Sanyal, Jasper H L Claessen, and Hidde L Ploegh. A viral deubiquitylating enzyme restores dislocation of substrates from the endoplasmic reticulum (er) in semi-intact cells. *J Biol Chem*, (28):23594–603, 2012.

[272] Kaleena M Bernardi, Jeffrey M Williams, Takamasa Inoue, Aric Schultz, and Billy Tsai. A deubiquitinase negatively regulates retro-translocation of nonubiquitinated substrates. *Mol Biol Cell*, (22):3545–56, 2013.

[273] Robert D Finn, John Tate, Jaina Mistry, Penny C Coggill, Stephen John Sammut, Hans-Rudolf Hotz, Goran Ceric, Kristoffer Forslund, Sean R Eddy, Erik L L Sonnhammer, and Alex Bateman. The pfam protein families database. *Nucleic Acids Res*, (Database issue):D281–8, 2008.

[274] Xing Guo and Xin Qi. Vcp cooperates with ubxd1 to degrade mitochondrial outer membrane protein mcl1 in model of huntington's disease. *Biochim Biophys Acta*, (2):552–559, 2017.

[275] Wei Li, Mario H Bengtson, Axel Ulbrich, Akio Matsuda, Venkateshwar A Reddy, Anthony Orth, Sumit K Chanda, Serge Batalov, and Claudio A P Joazeiro. Genome-wide and functional annotation of human e3 ubiquitin ligases identifies mulan, a mitochondrial e3 that regulates the organelle's dynamics and signaling. *PLoS One*, (1):e1487, 2008.

[276] Luc Farout and Bertrand Friguet. Proteasome function in aging and oxidative stress: implications in protein maintenance failure. *Antioxid Redox Signal*, (1-2):205–16, 2006.

[277] I Juranek and S Bezek. Controversy of free radical hypothesis: reactive oxygen species–cause or consequence of tissue injury? *Gen Physiol Biophys*, (3):263–78, 2005.

[278] Melanie H Smith, Hidde L Ploegh, and Jonathan S Weissman. Road to ruin: targeting proteins for degradation in the endoplasmic reticulum. *Science*, (6059):1086–90, 2011.